Crystallography and Shape of Nanoparticles and Clusters

José Luis Rodríguez-López

Crystallography and Shape of Nanoparticles and Clusters

J. M. Montejano

Instituto de Física, Universidad Autónoma de San Luis Potosí, Mexico

J. L. Rodríguez

Instituto Potosino de Investigación Científica y Tecnológica, Mexico

C. Gutierrez-Wing

Instituto Nacional de Investigaciones Nucleares, Mexico, and Texas Materials Institute, University of Texas at Austin, Austin, TX, USA

M. Miki

Texas Materials Institute, University of Texas at Austin, Austin, TX, USA, and Centro de Investigación en Materiales Avanzados, Mexico

M. Jose-Yacaman

Texas Materials Institute, University of Texas at Austin, Austin, TX, USA, and Chemical Engineering Department, University of Texas at Austin, Austin, TX, USA, and Instituto de Física, UNAM, Mexico

CONTENTS

1. INTRODUCTION

Nanotechnology is a leading interdisciplinary science that is emerging as a distinctive field of research. Its advances and applications will result in technical capabilities that will allow the development of novel nanomaterials with applications that will revolutionize the industry in many areas [1, 2]. It is now well established that dimensionality plays a critical role in determining the properties of materials, and its study has produced important results in chemistry and physics [3].

Nanoparticles are one of the cornerstones of nanotechnology. Indeed, even though the research in this field has been underway for a long time, many present and future applications are based on nanoparticles. For instance, the electron tunneling through quantum dots has led to the possibility of fabricating single-electron transistors [4–9]. One concept particularly appealing is a new three-dimensional periodic table based on the possibility of generating artificial atoms from clusters of all of the elements [10]. This idea is based on the fact that several properties of nanoparticles show large fluctuations, which can be interpreted as electronic or shell-closing properties with the appearance of magic numbers. Therefore, it is conceivable to tailor artificial superatoms with given properties by controlling the number of shells on a nanoparticle.

The development of nanotechnology can be approached from several directions; mesoscopic physics, microelectronics, materials nanotechnology, and cluster science. The different fields are now coming together, and a completely new area is emerging [11, 12]. Figure 1 illustrates how the different approaches are converging; it exhibits the domains of clusters and nanoparticles with different structures that result from an increase in the number of atoms. The different possible structures include nanorods, nanoparticles, fullerenes, nanotubes, and layered materials.

One of the most remarkable advances in this field has been the synthesis of ligand-capped metallic clusters. In a seminal contribution, Brust et al. [13] used the classical two-phase Faraday colloid separation combined with contemporary phase-transfer chemistry to produce small gold nanoclusters coated with alkanethiolate monolayers. Several groups have pursued this technique [14–21], and have introduced improvements and modifications to the original technique. Whetten and his group [15, 16] made important contributions to this technique.

A significant property of ligand-capped clusters is that they can be repeatedly isolated from and redissolved in common organic solvents without irreversible aggregation or decomposition. The properties of the monolayer-protected nanoparticles (MPNs and MPANs) allow handling in ways that are familiar to the molecular chemist since they are stable in air conditions. The MPNs of some metals such as Pt [22], Ag [23], Rh, and Pd [24] have been synthesized.

2. GEOMETRIC CONSIDERATIONS

2.1. Clusters and Nanoparticles

Since the pioneering work of Ino and Ogawa [25, 26], it was clear that, in most cases, the structure of nanoparticles cannot be described by the bulk crystallography of the used material. The concept of multiple twins was used to explain many of the structures, such as the icosahedron and the decahedron. This concept was directly imported from the macroscopic metallurgical studies, and was certainly very useful for a first understanding of the structure of nanoparticles. Another related research field was the study of clusters formed by few atoms. From that field, we learned that structures are formed by shells, and the concept of a magic number was introduced [27]. Nanoparticles referred to sizes of ∼5–10 nm, and clusters referred to sizes of ∼1 nm. In recent times, the computational tools for study

Figure 1. Domains of nanoparticles and clusters with different structures.

clusters allow the analysis of a large number of atoms, and the methods to study nanoparticles allow interrogating smaller nanoparticles. The two fields are merging into one. In this chapter, we will use the term particle and cluster indistinctly.

2.2. Clusters with Cubic Symmetry

When considering atom clusters of nanometric dimensions, it can be supposed that they correspond to some symmetry group. In previous works, small clusters (up to tens of atoms) of diverse forms (tetrahedron, hexahedron, octahedron, decahedron, dodecaheltahedron, trigonal, trigonal prism, and hexagonal antiprism, with and without a central site) have already been studied [28]. Partially and totally capped clusters were also considered (clusters to which a site has been added to each face of the polyhedron, equidistant to every site of the face), in order to vary the number of sites for all of the polyhedrons, and thus allowing the comparison as a function of the number of sites.

Geometric characteristics of the clusters formed by concentric layers can be considered, as formed by equivalent sites: sites located at the same distance from the origin, which occupy the same geometric place and have the same environment, that is, the same number and type of neighbors. These layers can be arranged in such a way that they group in shells forming clusters of different sizes, retaining the original geometric structure. The number of shells in the cluster is called the order of the cluster, and is represented by the letter v. The studied structures were: the icosahedron, the face-centered cubic structure fcc (the cubooctahedron), the body-centered cubic bcc, and the simple cubic sc.

In order to determine the stability of the structures from an energetic point of view, a study of the cubooctahedral and icosahedral structure was performed using the embedded atom method (EAM) for the transition metals Cu, Pd, Ag, Ni [29]. It was determined that, for sizes smaller than 2000 atoms, the icosahedron is the most stable structure, and for larger sizes, it is the cubooctahedron (CO). For this study, the advantage of having equivalent sites in the clusters was used to reduce the computation time. In a latter study, based upon the same metals, small clusters of fewer than 100 atoms with regular polyhedron geometries were used, and to change the cluster size, partially and totally capped clusters were considered. Tetrahedral clusters showed the highest stability for sizes of fewer than 18 atoms, and icosahedrons for larger sizes.

In this work, the structural stability competition among different regular structures of the concentric shell type is searched. Here, the studied geometries are reproduced, considering some other arrays of the layers in shells, which give rise to other geometries. The fcc structure considers many structures, which are divided into two groups: (1) with a central site, and (2) without a central site. Among the centered ones, the cubooctahedron, octahedron, and truncated octahedron are considered. For the ones not centered, the octahedron and the truncated octahedron are considered. The bcc structure has the dodecahedron. The sc structure does not allow a study like the one presented here because, when a truncation is tried, second neighbor distances are obtained. Once the geometric properties of the structures
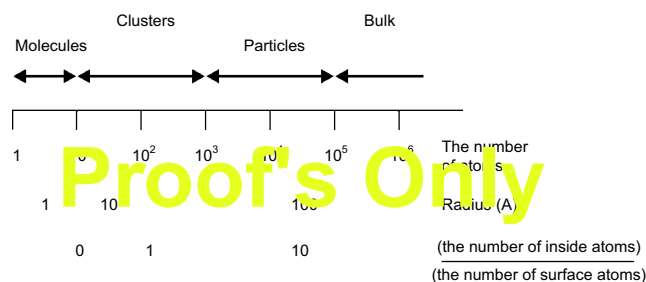
are determined, the EAM is applied to them, and their stability is discussed.

2.3. Geometric Characterization

The following procedure was used to determine the geometric characteristics of the structures. (1) First, identify the structures, that is, their geometric shape; (2) the nature of the site coordinates which conform the structures; and (3) their neighbors with surrounding layers, in order to identify the equivalent sites and generate the concentric shell-type structures. Once this previous stage is completed, the geometric properties to be determined are defined, the structures are presented, and the geometric properties of each structure are numbered. Afterwards, based on the geometric characteristics of each structure, the analytic expressions are deducted as a function only of the cluster order for the defined properties.

An example of the concentric shell-type structures is shown in Figure 2, which presents the cubooctahedron in three different sizes. In this figure, a central site surrounded by 12 sites forming a cubooctahedron with one first shell can be seen; Figure 2(a). Then it is covered with another shell of sites distributed in three layers of equivalent sites, as will be seen later, but retaining the original geometric shape; Figure 2(b). And finally, Figure 2(c) presents a three-shell cubooctahedron.

The structures considered are the face-centered cubic fcc [Fig. 3(a)] and the body-centered cubic bcc [Fig. 3(d) and (e)]. Although both are cubic, in Figure 3(a), the fcc does not seem to be cubic, but the face-centered cubic structure with a central site fccc [Fig. 3(b)] and the face-centered cubic structure without a central site fccs [Fig. 3(c)] show that they do have a cubic shape: 8 vertexes, 6 square faces, and 12 edges. The bcc structure has a central site, while the fcc structure can be considered with and without a central site. Truncating each one of them in a certain direction, noncubic structures are obtained; they have, besides vertexes (V), edges (A), and square faces (C), faces of different shapes: a triangular face (T), a hexagonal face (H), and a rombohedral face (R). The resulting structures are: the cubooctahedron [Fig. 4(a)], the octahedron [Fig. 4(b)], the truncated octahedron [Fig. 4(c)], and the dodecahedron [Fig. 4(d)]. For the fccc, the obtained structures are the cubooctahedron CO, the octahedron OCTAC, and the truncated octahedron OCTTC; for the fccs, the structures obtained are the octahedron OCTAS and the truncated octahedron OCTTS; and for the bcc, only the decahedron is obtained, DODE.
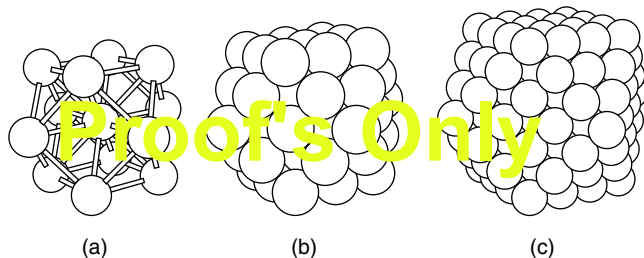

Figure 2. Cubooctahedrons formed by a central site and (a) one layer, (b) two layers, and (c) three layers.
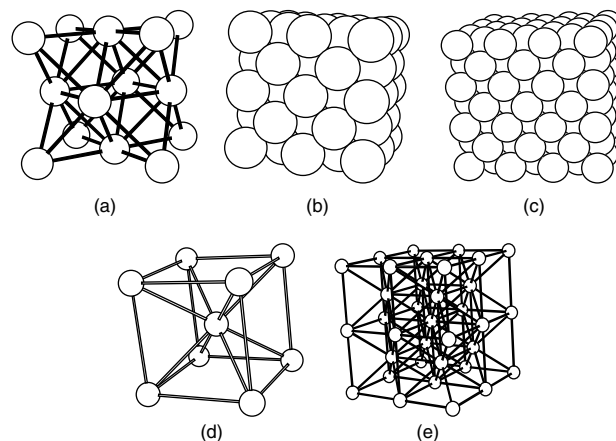

Figure 3. Structures (a) face-centered cubic fcc, (b) face-centered cubic with central site fccc, (c) face-centered cubic without central site fccs, and (d), (e) body-centered cubic bcc.

Table 1 presents the number of characteristic sites of each structure, in such a way that each structure is read as: the structure is formed by V vertexes attached by A edges forming X faces of different types, where $X = C, T, H, R$, as it corresponds. The icosahedron is included [Fig. 4(e)] because it can be obtained by an adequate distortion of the CO, and it is useful as a reference for a comparison of results. ICO, the fccc and its derivates, as well as the bcc and the DODE, present a central site. The OCTTC is centered over an octahedron with a central site of 19 sites, and the OCTTS over a regular octahedron of 6 sites.

2.3.1. Standard Coordinates

Each of the structures studied here, except the ICO, corresponds to a well-defined crystalline structure, fcc or bcc, so that the coordinates of the geometric sites which compose them are characteristic of each one of them. In each structure, the standard coordinates are described by triads (a, b, c); a, b and c are integers, where the total number of sites is obtained by doing permutations and commutations of the positive and negative values of a, b, and c. Table 2 presents the characteristics of standard coordinates for each structure as a function of the cluster order v for each structure.

2.3.2. First Neighbors

There will be different types of equivalent sites, depending on the geometric structure, and each type will occupy a geometric position which will be of type vertex (V), edge (A),
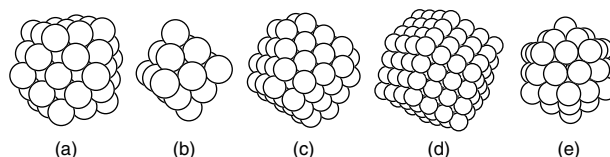

Figure 4. Polyhedrons resulting from truncation of fcc and bcc structures. (a) Cubooctahedron, (b) octahedron, (c) truncated octahedron, and (d) dodecahedron. As a result of an adequate distortion of the cubooctahedron, the icosahedron is obtained.

Table 1. Number of geometric sites corresponding to the structures of the first column. Last column presents the number of central sites of the structure.

	V	A	C	T	H	R	Central site
ICO	12	30	—	20	—	—	1
fccc	8	12	6	—	—	—	1
CO	12	24	6	8	—	—	1
OCTAC	6	12	—	8	—	—	1
OCTTC	24	36	6	—	8	—	19
fccs	8	12	6	—	—	—	—
OCTAS	6	12	—	8	—	—	—
OCTTS	24	36	6	—	8	—	6
bcc	8	12	6	—	—	—	1
DODE	14	24	—	—	—	12	1

square face (C), triangular face (T), hexagonal face (H), and it will have a total number of neighbors, coordination z, which will correspond to the structure, but the number of neighbors with layers of its same shell, with interior and exterior shells, will be characteristic of each site. Table 3 presents the different types of sites in the studied structures, as well as the number of first neighbors with layers of interior shells ($\downarrow$), in the same shell ($\leftrightarrow$), and with exterior shells ($\uparrow$). Also, total coordination z in the structure is presented. The truncated octahedron with a central site presents two types of edges, the edges between squared and hexagonal faces with coordination (2, 5, 5), and the edges between hexagonal faces with coordination (1, 6, 5), while all of the other structures have only one. It should be noticed that, in order to obtain structures of the concentric shell type in the fccc and fccs structures, two shells will be needed, as shown in Figure 5 for fccc (similarly for fccs); Figure 5(a) presents the fccc cube of 13 sites; Figure 5(b) shows the fccc of 63 sites, which will be a complete shell of 62 sites ($12 + 50$) over the central site; Figure 5(c) and (d) present the fccc of 171 sites and the fccc of 365 sites; the latter is the one with two shells, one with 62 sites and the other with 302 sites. The surface sites in the fccc of 13 sites become internal when adding 50 to complete the fccc of 63 sites; the same happens for that one of the 171 sites when covering it to complete the one with 365. From Figure 5(b), it is observed that there will exist 1×12 A sites, 5×6 C and 8 V, but looking carefully, it will be noticed that the C sites are not equivalent because the one in the center of the squared face has a coordination of 4 with the surface sites, while the other has a coordination of 6, but both have a coordination of 4 toward external layers. It is also observed that in Figure 5(c) the four sites of type C at the center of the face have a coordination of 4 with the surface sites, and the other eight sites of type C have a coordination of 5 with surface layers, but all of them have 4 toward external layers, while in Figure 5(d), it is observed that the C sites near the vertexes have a coordination of 6 with sites over the same surface shell, and the ones close to sites A have a coordination of 5; this is why in Table 3 the coordination for C sites can be of three types, but all of them with a coordination of 4 toward external layers. That is why in fccc and fccs there are shells composed of two subshells, one that will contain the surface sites, and the other that will remain internal. Surface sites will interact

with the internal sites, and these internal ones with those of the cluster and the surface ones.

2.3.3. Definition of Geometric Properties

Table 4 presents definitions and their mathematical expressions for the general geometric characteristics, which can be expressed analytically as a function of only the order of the cluster v, for each structure or geometric array. The upper section of Table 4 refers to the geometric characteristics of the cluster, the middle section to the bonds, and it relates Table 3 and the superior part of Table 4, and the lower section of Table 4 to the average coordination based on the rest of Table 4.

The cluster can be defined as a nucleus and a surface over the nucleus. The number of I sites, the number of types of I sites and what refers to dispersions is over the surface, and the average number of bonds and coordination is over the involved sites of the cluster. In the expressions for N_{CC} and N_{SS}, $(\uparrow)_I$ means the number of I-site bonds in the internal layer (the nucleus surface) with sites in the external layer (the cluster surface), $(\downarrow)_I$ means the number of I-site bonds in the external layer (the cluster surface) with sites in the internal layer (the nucleus surface), and $(\leftrightarrow)_I$ means the number of I-site bonds in the surface of the cluster with sites in the same surface. It must be clear that, due to the fact that there are many ways to coordinate C sites in the surface for fccc and fccs structures, the formula for N_{CC} must only be used as $\sum_I (\uparrow)_I \times N_I(v-1)$, and only for these two structures, the proposed equity does not apply.

2.4. fcc Structure

An fcc structure is that in which the unit cell is a cube with sites in the vertexes and in the center of squared faces; this means that there are 14 sites on a cube, 8 vertexes, and 6 squared faces [Fig. 3(a)]; also, it can be seen as a completely capped octahedron. When attaching many of these arrays with common or shared sites in faces and vertexes, clusters are obtained with sites in vertexes, edges, and squared faces. The origin of coordinates can be chosen to be at the center of the cube or on a vertex, obtaining structures with and without a central site, respectively.

2.4.1. fcc Structure with a Central Site

In the fcc structure with a central site, the cubic cluster of order 1 is a cube with 63 sites, distributed in 5 layers around a central site [Fig. 5(b)]; it can be seen that it is an array of 6 unit cells with common sites. The order 2 cluster is obtained when covering the one of order 1 with 302 sites distributed in 13 layers to obtain a total of 365 sites [Fig. 5(d)], and so on. Layers of equivalent sites can be identified (Table 1): squared face (C), edges (A), and vertexes (V). Table 2 presents the standard coordinates and its characteristics; it can be seen that the sum of the standard coordinates a, b, and c is an even number, and in Table 3, the coordination of each site. From Figure 5(a)–(d), it can be seen that a shell is composed of two subshells. Table 5 lists the geometric characteristics of the fccc structure, separating each shell into subshells to allow the calculus of surface dispersions and the number of bonds as defined in Table 4,

Table 2. Standard coordinate characteristics for each of the structures.

	Site	a	b	c	$b+c$	$a+b+c$
fccc						even
	S	$[2v-1, 2v]$	$[0, 2v-1]$			$[2v, 6v-2]$
	E		$[2v-1, 2]$	$[0, 2v-2]$ (even)		$[2v, 6v-2]$
	V		$2v$			$6v$
						even
CO	S	v	$[0, v-2]$		$[v-2]$	$[v, 2v-2]$
	T		$[1, v)$			$2v$
	E	v	$[1, v]$		v	$2v$
	V		v	0		$2v$
OCTAC	T		$[1, 2v-2]$			$2v$
	E		$[1, 2v-1)$	0		$2v$
	V	$2v$	0	0		$2v$
OCTTC	S	$v+2$	$[0, v-2]$	$[0, (v-2)/2], v$ even $[0, (v-3)/2], v$ odd		$[v+2, 2v]$
	H	$[v-2, v+1]$	$[(v/2)+1, v], v$ even $[(v+1)/2, v], v$ odd	$[1, (v/2)+2], v$ even $[1, (v+3)/2], v$ odd		$2v+2$
	ES	$v+2$		$[1, v]$	v	$2v+2$
	EH		$v+1$	0		$2v+2$
	V	$v+2$	v	0		$2v+2$
						odd
fccs	S	$[2v-2, 2v-1]$	$[0, 2v-2]$			$[2v-1, 6v-5]$
	E		$[2v-2, 2v-1]$	$[1, 2v-1]$ (odd)		$[4v-3, 6v-3]$
	V		$2v-1$			$6v-3$
OCTAS	T		$[1, v-1]$			$2v-1$
	E		$[1, 2v-1]$	0		$2v-1$
	V	$2v-1$	0	0		$2v-1$
OCTTS	S	$v+1$	$[0, v-2]$	$[0, v/2], v$ even $[0, (v-1)/2], v$ odd	$[v-4, v-2]$	
	H		$[1, v]$			$2v+1$
	E	$v+1$	$[v/2, v)$ $[(v-1)/2, v)$	$[1, v/2]$ $[1, (v-1)/2]$		$2v+1$
	V	$v+1$	v	0		$2v+1$
						even, v even odd, v odd
bcc	S	v	$[0, v-2]$			$[v, 3v-4]$
	E		v	$[0, v-2]$ (even) $[1, v-2]$ (odd)		$[2v, 3v-2]$ $[2v+1, 3v-2]$
	V		v			$3v$
DODE	R		$[1, v-1]$			$2v-1$
	E		$[0, 2v/-2]$	0		$2v-1$
	V	$2v-1$	0	0		$2v-1$

and for each shell. General expressions for the geometric characteristics of Table 4 are presented in Table 6. These are shown when they are being considered as shells or sub-shells; in both columns corresponding to subshells, the first one is for the internal, and the second one is for the external or surface. N_σ represents the number of sites added to the cluster of order $v-1$, N_{sup} is the number of sites forming the surface, and it is the same for either of the considered cases because the internal shell does not form part of the surface. Besides this, the distinction is made among the different types of sites C forming the surface. In the calculus of the number of bonds between the two sublayers, the coordination from inside to outside was considered because all

of the types of C sites have a coordination of 4 with the exterior shell.

When grouping the layers of equivalent sites in shells in a different manner than the one given in fccc, geometries that present, besides squared faces, triangular and hexagonal faces will rise. Here, the cubooctahedron, octahedron, and truncated octahedron are considered.

2.4.2. Cubooctahedron

The cubooctahedron can be obtained by truncating an fcc structure in direction (111); this is shown in Figure 6(b), where a cubooctahedron of 55 sites is presented, and is the result of removing the 8 corners of a cube of 63 sites. It is

Table 3. Number of first neighbors with shell on external layers ↑ (internal ↓) and with layers in the same shell ↔ for the different types of sites of the structures fcc, icosahedral, and bcc. The total coordination z is given by $(\uparrow) + (\downarrow) + (\leftrightarrow)$.

		Faces						z
		C	T	H	R	A	V	
↑		↑	↑	↑	↑	↑	↑	
↔		□	△	H	◇	\	•	
↓		↓	↓	↓	↓	↓	↓	
		4	4	4	—	7	9	
		4	5	6	—	4	3	12
		4	3	2	—	1	0	
fcc	CO	4	3	—	—	5	7	
		4	6	—	—	5	4	12
		4	3	—	—	2	1	
	OCTAC	—	3	—	—	5	8	
		—	6	—	—	6	4	12
		—	3	—	—	1	0	
	OCTTC	4	—	3	5	5	6	
		4	—	6	5	6	5	12
		4	—	3	2	1	1	
		4	4	4	—	7	9	
		4	5	6	—	4	3	12
		4	3	2	—	1	0	
fccs	OCTAS	—	3	—	—	5	8	
		—	6	—	—	6	4	12
		—	3	—	—	1	0	
	OCTTS	4	—	3	—	5	6	
		4	—	6	—	5	5	12
		4	—	3	—	2	1	
	ICO	—	3	—	—	4	6	
		—	6	—	—	6	5	12
		—	3	—	—	2	1	
bcc		4	—	—	—	6	7	
		0	—	—	—	0	0	8
		4	—	—	—	2	1	
	DODE	—	—	—	2	3	4	
		—	—	—	4	4	4	8
		—	—	—	2	1	0	

has a central site and a first shell with one single layer of 12 vertices; Figure 6(a). The CO of order 2 is formed by adding one shell formed by 42 sites in order to complete 55 [Fig. 6(b)], distributed in three layers: one layer of 6 C sites, another of 24 A sites, and a third one of 12 V sites. When adding a third shell of 92 sites, the third order CO of 147 sites is completed [Fig. 6(c)]; sites are distributed in four layers: one of 24 C sites, another of 8 T sites, one more of 48 A sites, and a fourth one of 12 V sites. Successively, complete shells are added this way, forming clusters of order v.

The standard coordinates for the cubooctahedron are listed in Table 2, the number of neighbors for each site can be found in Table 3, and the geometric characteristics of the CO are listed in Table 7; from this table, it is possible to obtain the general expressions for the geometric characteristics of the cubooctahedron defined in Table 4. These expressions are presented in Table 11 for the cubooctahedron and all of the other structures to be studies.

Figure 6(e) presents an icosahedron of 923 sites of order 6. When comparing with the CO, which has the same number of sites, from Figure 6(d), the distortion made to obtain the ICO can be observed. Table 3 shows the number of neighbors for each site, and Table 8 reproduces the geometric characteristics corresponding to the icosahedron, which have been reported previously. A great similarity can be noticed between Tables 7 and 8, in the columns referring to the types of sites or layers by shell (columns for T, A, V), and in the sites at the surface, in the total (the two last columns of tables N_σ and N), and in the expressions for both in Table 11. Based on these latter, it is possible to obtain the dispersions due to the surface sites of both structures obtaining the graphic in Figure 7. Surface and vertex dispersion is exactly the same for both structures; they start close to 1 and in 1, respectively, and then they decrease. Dispersion in triangular faces, for both structures, shows a very similar behavior; they start in the same value, and increase with the size of the cluster, but D_T in the ICO increases faster. Similarly for the edges, they increase rapidly from zero to a maximum value, and decrease slowly almost parallel. The predominance of D_T and D_C for large sizes has to be noticed for ICO and CO, respectively.

2.4.3. Octahedron with a Central Site

The octahedron with a central site has 6 vertices (V), 12 edges (A), and 8 triangular faces (T); Figure 8. In this figure, the sides of the triangular faces have a length of $2v d_{NN}$, an even number times the distance to first neighbors; this means that the triangular faces do not present a central site, and the number of sites for each edge is odd. The number of neighbors for each site with sites in other layers can be found in Table 3, the standard coordinates in Table 2, and the geometric characteristics for the octahedron with a central site are listed in Table 9. From this latter, the general expressions of the geometric characteristics for the octahedron with a central site (OCTAC) can be deduced, and are presented in Table 11. Figure 9 shows an octahedron of 891 sites with a central site.

With the same method applied for the CO and the ICO, the dispersions due to surface sites can be calculated from Table 5, and the results are presented in the graphic of

formed by 8 triangular faces and 6 squared ones, attached by 24 edges and 12 vertices; see Table 1. Consequently, the surface sites are localized in squared faces (C), triangular faces (T), edges (A), and vertexes. The CO of order 1
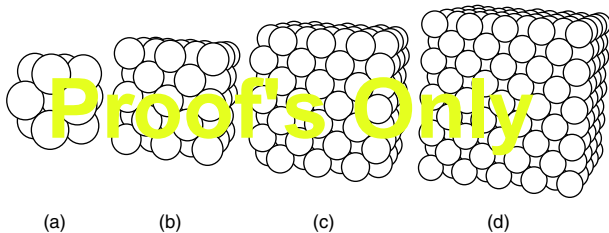

Figure 5. fcc polyhedrons of (a) 13 sites (central site plus a sublayer of 12 sites), (b) 63 sites (a complete layer of 62 sites), (c) 171 sites (a sublayer of 108 sites over the order 1 fccc), and (d) 365 sites (two complete layers).

Table 4. General definitions of geometric parameters for different structures.

Symbol	Definition	Mathematical expression
N	Total number of atoms in a cluster of order v	
N_σ	Number of atoms in a crust or on the surface	
$\mathscr{D}$	Dispersion;	N_σ/N
N_I	Number of surface atoms on site I, $I = S, T, H, R, E, V$	
R_I^a	Number of shells in which are contained the I sites (a = even, odd)	
$\mathscr{D}_I$	Dispersion due to surface I sites	N_I/N_σ
$\mathscr{N}_{CO}$	Number of internal bonds in a cluster of order v	$\frac{1}{2} \times z \times N(v-1)$
$\mathscr{N}_{OO}$	Number of bonds between two adjacent crusts ($v-1$) and v	$\sum_I(\uparrow)_I \times N_I(v-1) = \sum_I(\downarrow)_I \times N_I(v)$
	Number of bonds between the core and the surface	
$\mathscr{N}_{SS}$	Number of bonds on the surface of a cluster of order v	$\frac{1}{2}\sum_I(\leftrightarrow)_I \times N_I(v)$
$\mathscr{N}_C$	Number of bonds in a cluster of order v	$\mathscr{N}_{CO} + \mathscr{N}_{CS} + \mathscr{N}_{SS}$
$\overline{Z}$	cluster average coordination	$2\mathscr{N}_C(v)/N(v)$
$\overline{Z}_{CO}$	Core average coordination	$2\mathscr{N}_{CO}(v)/N(v-1)$
$\overline{Z}_{CS}$	Core–surface average coordination	$\mathscr{N}_{CC}(v)/N_\sigma(v-1)$
$\overline{Z}_{SC}$	Surface–core average coordination	$\mathscr{N}_{CC}(v)/N_\sigma(v)$
$\overline{Z}_{SS}$	Surface average coordination	$2\mathscr{N}_{SS}(v)/N_\sigma(v)$

Figure 10. It can be observed that the surface dispersion and dispersions due to edges and vertexes decrease, while the one due to the triangular faces starts from zero and increases rapidly, being predominant for larger sizes.

2.4.4. Truncated Octahedron with a Central Site

A truncated octahedron is a structure centered over an octahedron of 18 sites (2 layers) with a central site (layer 0), and has 24 vertexes (V) 36 edges (A), 6 squared faces (C), and 8 hexagonal faces (H); Figure 11. Edges are of two types: 24 between squared and hexagonal faces (AC), and 12 between hexagonal faces (AH); the number of AH sites N_{AH} is always equal to 12, one site in each edge (AH), while the one in AC sites N_{AC} depends on the order of the cluster; this means that the length of the edges AC is variable, and the one of AH edges is $2d_{NN}$. And so, the hexagonal faces are irregular, except when the number of AC sites is 24 and the number of AH sites is 12, which occurs in the cluster of order 2. The number of first neighbors for each site can be found in Table 3, standard coordinates are in Table 2, and Table 10 presents the geometric characteristics of each structure. Figure 12 shows the truncated octahedron of 711 sites with a central site.

Table 5. Geometrical characteristics for the face-centered cubic and with central site fccc.

	Sites at			Layers at					Sites at	
v	C	A	V	C	A	V	v	Total	v	Total
1	0	12	0	0	1	0	1	2	12	13
	30	12	8	2	1	1	4	6	50	63
	30	24	8	2	2	1	5	6	62	63
2	72	36	0	2	2	0	4	10	108	181
	150	36	8	6	2	1	9	19	194	365
	222	72	8	8	4	1	13	19	302	365
3	240	60	0	6	3	0	9	28	300	665
	366	60	8	12	3	1	16	44	434	1099
	606	120	8	18	6	1	25	44	734	1099

From Table 10, it can be observed that the number of AH sites is 12 and of V sites is 24 for all v; besides this, it is possible to obtain the general expressions of the geometric characteristics for the truncated octahedron with a central site, as presented in Table 11.

Figure 13 presents the dispersions for the truncated octahedron and with a central site, derived from the data of Table 10. The predominance of the dispersion due to the sites in hexagonal and squared faces for large sizes can be observed. Dispersions due to other sites and the surface one decrease with the size of the cluster.

With support from Tables 4 and 6–10, it is possible to obtain the characteristics defined in the middle and lower parts of Table 4 for each and every studied structure. Characteristics in the middle part of Table 4 are presented in Table 11, and Figures 14–17 present the obtained graphics of the dependence of the number of bonds at the surface N_{SS}, the number of bonds between the surface and the internal cluster N_{SC}, the number of bonds in the internal cluster N_C, and of the total number of bonds in the cluster N, respectively, for all of the structures studied here; the curves for the ICO and CO practically coincide, so that just the curve of CO will be presented, except for N_C. It is observed that, for the structures with a central site, and taking as reference the CO and the ICO, the OCTAC has a larger number of surface bonds and the OCTTC has fewer. But for N_{SC}, the CO and ICO surpass the OCTAC and the OCTTC. For N_C, the OCTAC and the OCTTC surpass the CO. For N, there are some crossings for smaller sizes, while for larger sizes, the OCTAC and OCTTC surpass the CO.

2.4.5. EAM Applied to fcc Structures

The embedded atom method is applied, in the Foiles version and with the parameters of copper, to clusters with central site fcc structures in order to calculate the cohesion energy per atom, determining in this way the stability of the clusters. The results are compared with the ones from the icosahedrons and cubooctahedrons previously reported [28]. Figure 18 presents the cohesive energy graphic as a function

Table 6. Particular expressions of the geometrical characteristics for the fcc with central site fccc, and without central site fccs structures.

	fccc			fccs		
	Shells	Subshells		Shells	Subshells	
N		$32v^3 + 24v^2 + 6v + 1$			$32v^3 - 24v^2 + 6v$	
N_σ	$96v^2 - 48v + 4$	$48v^2 - 48v + 12$	$48v^2 + 2$	$96v^2 - 144v + 62$	$48(v-1)^2$	$48v^2 - 48v + 14$
N		$48v^2 + 2$			$48v^2 - 48v + 14$	
$\mathcal{D}$		$\dfrac{48v^2 + 2}{32v^3 + 24v^2 + 6v + 1}$			$\dfrac{48v^2 - 48v + 14}{32v^3 + 24v^2 + 6v + 1}$	
N	24	—	24	24	—	24
R	1	—	1	1	—	1
N	$48(v-1)$	—	$48(v-1)$	$24(2v-3)$	—	$24(2v-3)$
R	$v-1$	—	$v-1$	$v-1$	—	$v-1$
N	$24[(2v-1)^2 + (2v-2)^2]$	—	$24[(2v-1)^2 + (2v-2)^2]$	$6[(2v-2)^2 + (2v-3)^2]$	—	$6[(2v-2)^2 + (2v-3)^2]$
R	v^2	—	v^2	$v(v-1)$	—	$v(v-1)$
N_E	$24(2v-1)$	$12(2v-1)$		$48(v-1)$	$24(v-1)$	
R_E^p	$2v$	v		$2(v-1)$	$v-1$	
N_V	8	0	8	8	0	8
R_V	1	0	1	1	0	1
$\mathcal{N}_C$		$6(32v^3 - 24v^2 + 6v - 13)$			$12(16v^3 - 36v^2 + 27v - 7)$	
$\mathcal{N}_{CC}$		$12(16v^2 - 10v + 1)$			$24(8v^2 - 13v + 5)$	
$\mathcal{N}_{SS}$		$48v(4v + 48)$			$24(8v^2 - 6v + 1)$	
$\mathcal{N}$		$4(48v^3 + 60v^2 - 9v - 14)$			$12(16v^3 - 4v^2 - 11v + 5)$	

of $N^{1/3}$ for the octahedron and truncated octahedron clusters of fcc with central site type, for sizes from 300 to 3400 atoms. From Figure 18, it can be seen that the truncated octahedrons (Δ) have a higher stability than the icosahedrons ($\bullet$) and cubooctahedrons ($\square$), while the octahedrons ($\Diamond$) have sizes larger than 900 atoms.

In a previous work, it was found that the CO presented a higher stability than the ICO for larger sizes; when analyzing the number of bonds in the clusters, it is found that this condition is present when the number of bonds of CO surpasses the ICO ones. The competition among fcc structures with a central site and the icosahedron observed in the graphic of Figure 18 must have the same origin.

2.5. fcc Structure without Central Site

In the fcc structure without a central site, the cubic cluster of order 1 has the same unit cell as the fcc structure of Figure 5(a), a cube with 14 sites, 8 in vertexes and 6 in the center of the squared faces. The second order cluster has 172 sites [Fig. 15(c)], which results from covering the first-order cluster with one shell of 158 sites, distributed in 8 layers; the second-order cluster is an array of 9 cubes attached by faces and common sites. The next cubic cluster is formed by the second-order one and a shell of 494 sites in 18 layers covering it, and so on. Equivalent sites layers can
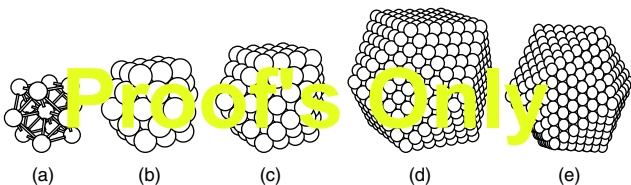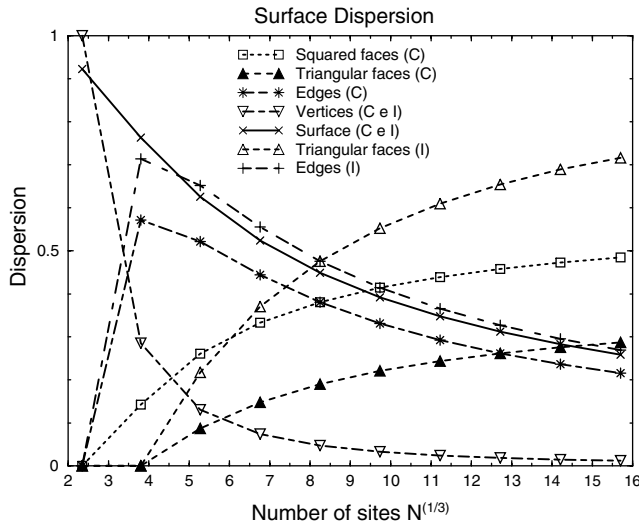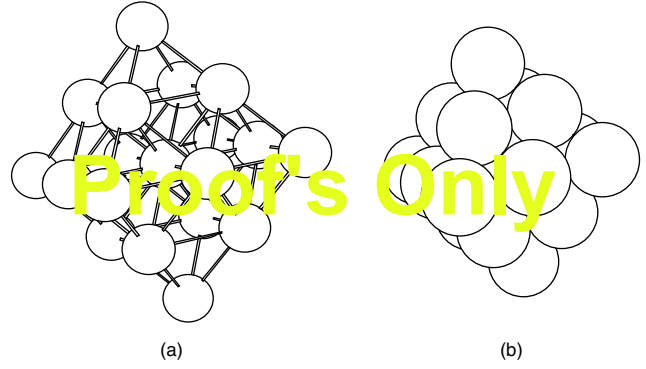
Figure 6. Cubooctahedron of (a) order 1 of 13 sites, (b) order 2 of 55 sites, (c) order 3 of 147 sites, and (d) order 6 of 923 sites. Observe the distortion of CO (d) to obtain (e) an icosahedron of order 6 of 923 sites.

be identified: Table 1: squared face (C), edges (A), and vertexes (V). As in the fccc structure, each shell is composed of two subshells. Table 12 lists the geometric characteristics of the fccs structures, and the separation of subshells for each shell is done in order to allow the calculus of the number of bonds as defined in Table 2, and for each shell also. General expressions for the geometric characteristics of Table 4 are presented in Table 10. Table 2 presents the standard coordinates and their characteristics; it can be seen that the sum of the standard coordinates a, b, and c is an odd number, and in Table 3, the coordination of each site is presented.

When grouping the layers of equivalent sites in shells, in a different way than for fccs, the geometries presented are given: besides the squared faces, triangular and hexagonal faces are included. Here, the cubooctahedron, octahedron, and truncated octahedron will be considered.

2.5.1. Octahedron without Central Site

The octahedron is formed by 6 vertexes, 12 edges, and 8 triangular faces. Figure 19 shows the octahedrons of 44 and 146 sites, without a central site. In these figures, it can be

Table 7. Geometrical characteristics for the cubooctahedron.

	Sites at				Layers at				Layers at		Sites at	
v	C	T	A	V	C	T	A	V	v	Total	v	Total
1	0	0	0	12	0	0	0	1	1	1	12	13
2	6	0	24	12	1	0	1	1	3	4	42	55
3	24	8	48	12	1	1	1	1	4	8	92	147
4	54	24	72	12	3	1	2	1	7	15	162	309
5	96	48	96	12	3	2	2	1	8	23	252	561
6	150	80	120	12	6	3	3	1	13	36	362	923
7	216	120	144	12	6	4	3	1	14	50	492	1415
8	294	168	168	12	10	5	4	1	20	70	642	2057
9	384	224	192	12	10	7	4	1	22	92	812	2869
10	486	288	216	12	15	8	5	1	29	121	1002	3871

Table 8. Geometrical characteristics for the icosahedron.

	Sites at			Layers at			Layers at		Sites at	
v	T	A	V	T	A	V	v	Total	v	Total
1	0	0	12	0	0	1	1	1	12	13
2	0	30	12	0	1	1	2	3	42	55
3	20	60	12	1	1	1	3	6	92	147
4	60	90	12	1	2	1	4	10	162	309
5	120	120	12	2	2	1	5	15	252	561
6	200	150	12	3	3	1	7	22	362	923
7	300	180	12	4	3	1	8	30	492	1415
8	420	210	12	5	4	1	10	40	642	2057
9	560	240	12	7	4	1	12	52	812	2869
10	720	270	12	8	5	1	14	66	1002	3871

seen that there are sites in vertexes (V), edges (A), and in triangular faces (T). In this structure, the sides of the triangular faces have a length of $(2v-1)d_{NN}$, an odd number times the distance to first neighbors d_{NN}; this means that the triangular faces can present a central site, and the number of sites in each edge is even. The number of first neighbors is presented in Table 3, the standard coordinates in Table 2, and the geometric characteristics for the octahedron without a central site are listed in Table 13. Figure 20 shows the octahedron of 1156 sites without a central site.

The number of V sites N_V is equal to 6 for all v, and they are of just one type. From Table 13, it is possible to determine, for the octahedron without a central site, the dependence of the geometric characteristics on the order of the cluster v, and it is reported in Table 15. This same procedure is applied for the truncated octahedron, and without a central site and with the ones from the dodecahedron, which will be studied afterwards. The surface dispersion and the one due to each surface site also can be obtained from Table 13, and are presented in the graphic of Figure 21. The strong predominance of the sites of triangular faces and the fast decrease of the dispersions due to the vertexes and edges can be observed.

Figure 8. Octahedron of 19 atoms with central site. Smaller atoms are presented in (a) to allow observation of first neighbor bonds and central site in (b).

Table 9. Geometrical characteristics for the octahedron with central site.

	Sites at			Layers at			Layers at		Sites at	
v	T	A	V	T	A	V	v	Total	v	Total
1	0	12	6	0	1	1	2	2	18	19
2	24	36	6	1	2	1	4	6	66	85
3	80	60	6	3	3	1	7	13	146	231
4	168	84	6	5	4	1	10	23	258	489
5	288	108	6	8	5	1	14	37	402	891
6	440	132	6	12	6	1	19	56	578	1469
7	624	156	6	16	7	1	24	80	786	2255
8	840	180	6	21	8	1	30	110	1026	3281
9	1088	204	6	27	9	1	37	147	1298	4579
10	1368	228	6	33	10	1	44	191	1602	6181

Figure 7. Dispersions due to surface sites of the cubooctahedron (C) and icosahedron (I) as a function of the cubic root of the number of sites.
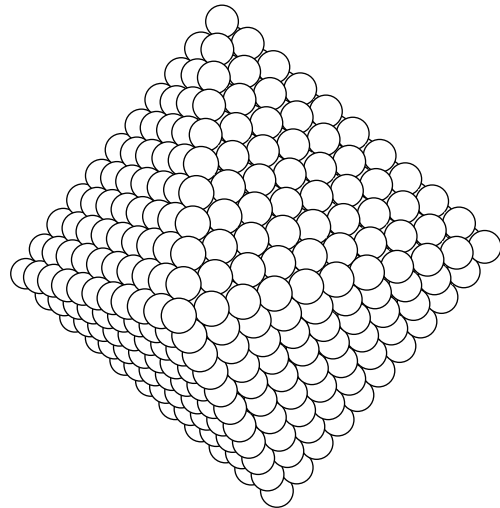
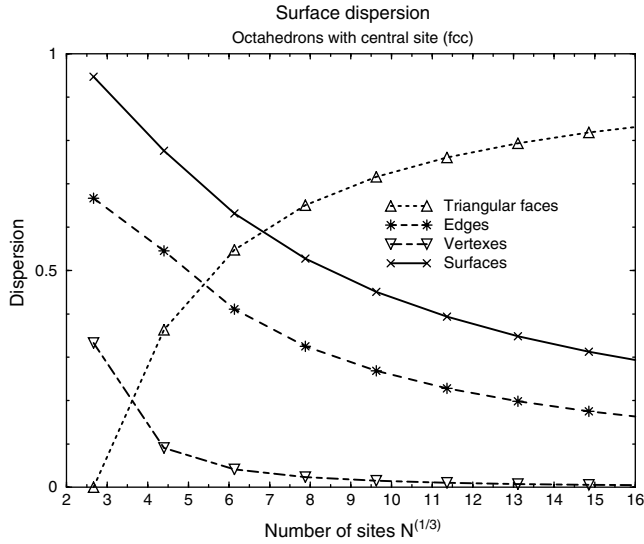**Figure 9.** Octahedron of 891 atoms, order 5, and with central site.

Figure 10. Dispersions due to surface sites of the octahedron, with a central site.
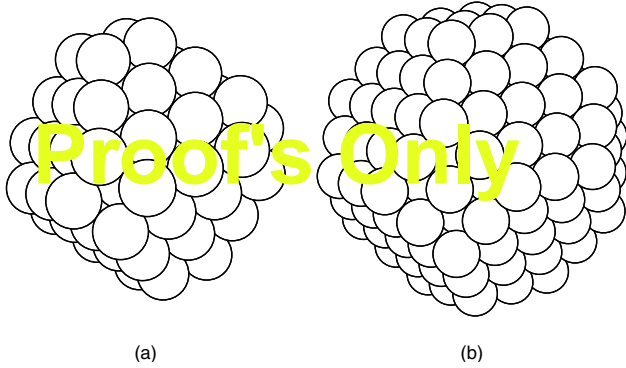

Figure 11. Truncated octahedron with central site of (a) order 1 and 79 atoms, and (b) order 2 and 201 atoms.
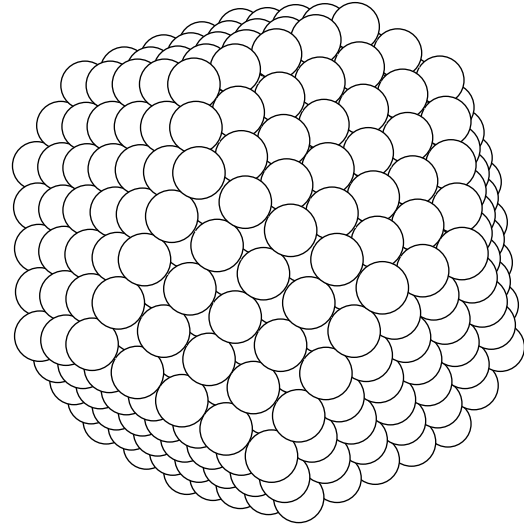

Figure 12. Truncated octahedron of 711 atoms, order 4, with central site.

2.5.2. Truncated Octahedron without Central Site

The truncated octahedron without a central site, Figure 22, is formed by a central octahedron surrounded by 6 squared faces and 8 irregular hexagonal faces (3 sides of length 1 and 3 of length equal to the order of the cluster v, in units of d_{NN}, alternated) attached by 24 vertexes and 36 edges, so the edges are of two types: 24 between squared and hexagonal faces and 12 between hexagonal faces; the first ones are length dependent on the cluster order, and the second ones on length $1d_{NN}$; this means that there is not a single site in them, so the first 24 are simply called A. The number of first neighbors of each site is presented in Table 3, the standard coordinates in Table 2, and the geometric characteristics for the truncated octahedron without a central site are listed in Table 12. Figure 23 shows the truncated octahedron of 1288 without a central site.

The number of V sites N_V is equal to 24 for all v, and they are of just one type. From Table 14, the expressions for the geometric characteristics for the truncated octahedron without a central site can be determined, and are presented in Table 15. Also, the surface dispersions can be determined,

Table 10. Geometric characteristics for the truncated octahedron with central site.

Order	Sites at					Layers at					Layers		Sites	
v	C	H	AC	AH	V	C	H	AC	AH	V	en v	Total	en v	Total
1	0	24	0	12	24	0	1	0	1	1	3	5	60	79
2	6	56	24	12	24	1	3	1	1	1	6	11	122	201
3	24	96	48	12	24	1	3	1	1	1	7	18	204	405
4	54	144	72	12	24	3	4	2	1	1	11	30	306	711
5	96	200	96	12	24	3	6	2	1	1	13	43	428	1139
6	150	264	120	12	24	6	7	3	1	1	18	61	570	1709
7	216	336	144	12	24	6	9	3	1	1	20	81	732	2441
8	294	416	168	12	24	10	11	4	1	1	27	108	914	3355
9	384	504	192	12	24	10	13	4	1	1	29	137	1116	4471
10	486	600	216	12	24	15	15	5	1	1	37	174	1338	5809

Table 11. Particular expressions of the geometrical characteristics for the icosahedral and fcc with central site structures.

	CO	ICO	OCTAC	OCTTC
N	$(10/3)v^3 + 5v^2 + (11/3)v + 1$		$(16/3)v^3 + 8v^2 + (14/3)v + 1$	$(10/3)v^3 + 21v^2 + (107/3)v + 19$
N_σ	$10v^2 + 2$		$16v^2 - 48v + 2$	$10v^2 + 32v + 18$
$\mathscr{D}$	$(30v^2 + 6)/(10v^3 + 15v^3 + 11v + 3)$		$3(v^2 - 48v + 2)/(16v^3 + 24v^2 + 14v + 3)$	$3(10v^2 + 32v + 18)/(10v^3 + 63v^2 + 107v + 57)$
N_S	$6(v-1)^2$	—	—	$6(v-1)^2$
R_S^p	$v(v+2)/8$	—	—	$v(v+2)/8$
R_S^i	$(v^2-1)/8$	—	—	$(v^2-1)/8$
N_T	$4(v-1)(v-2)$	$10(v-1)(v-2)$	$8(v-1)(2v-1)$	$4v^2 + 20v$
R_T^m	A	B	—	
N_H	—	—	—	$4v^2 + 20v$
R_H^m	—	—	—	C
N_E	$24(v-1)$	$30(v-1)$	$12(2v-1)$	$24(v-1)$
R_E^p	$v/2$		$v-1$	$v/2$
R_E^i	$(v-1)/2$		$v-1$	$(v-1)/2$
$\mathscr{N}_{CO}$	$4v(5v^2 + 3v + 1)$	$20v^3 + 15v^2 + 7v$	$32v^3 - 48v^2 + 28v + 11$	$20v^3 + 66v^2 + 22v + 6$
$\mathscr{N}_{CC}$	$12(3v^2 - 3/v + 1)$	$6(5v^2 - 5/v + 2)$	$12(4v^2 - 4v + 1)$	$12(3v^2 + 5v + 1)$
$\mathscr{N}_{SS}$	$24v^3$	$30v^2$	$48v^2$	$24(v^2 + 4v + 2)$
$\mathscr{N}_C$	$4(5v^3 - 12v^2 + 10v - 3)$	$20v^3 - 45v^2 + 37v - 12$	$2(16v^2 + 24v^2 - 10v + 3)$	$2(10v^3 + 63v^2 + 89v + 33)$

$$A = \begin{cases} \sum_{\alpha=1}^{m/2}(3\alpha + a) + \sum_{\alpha=1}^{(m/2)-1} 3\alpha; & m \\ & \begin{cases} v = 3m + a \\ a = -1, 0, 1 \end{cases} \\ \dfrac{1+a}{1+|a|} + \sum_{\alpha=1}^{(m-1)/2}(6\alpha + a); & m \end{cases}$$

$$B = \begin{cases} \sum_{\alpha=1}^{m/2}(3\alpha + a) + \sum_{\alpha=1}^{(m/2)-1} 3\alpha; & m \\ & \begin{cases} 2v = 3m + a \\ a = -1, 0, 1 \end{cases} \\ \dfrac{1+a}{1+|a|} + \sum_{\alpha=1}^{(m-1)/2}(6\alpha + a); & m \end{cases}$$

$$A = \begin{cases} \sum_{\alpha=1}^{m/2}(3\alpha + a) + \sum_{\alpha=1}^{(m/2)-1} 3\alpha + \sum_{1}^{b} 1; & m \\ & \begin{cases} v = 3m + a \\ a = -1, 0, 1 \end{cases} \\ \dfrac{1+a}{1+|a|} + \sum_{\alpha=1}^{(m-1)/2}(6\alpha + a) + \sum_{1}^{b} 1; & m \end{cases}$$

where b is the integer of $(v + m + |a| + 1)/2$

and are presented in the graphic of Figure 24. A not so strong predominance of the sites in squared and hexagonal faces can be observed, while the other dispersions decrease as the cluster size increases.

With support from Tables 4 and 13, it is possible to obtain expressions for the number of bonds for the different types of bonds in the truncated octahedron without a central site, which are presented in Table 14, and whose graphics are shown in Figures 16–19.
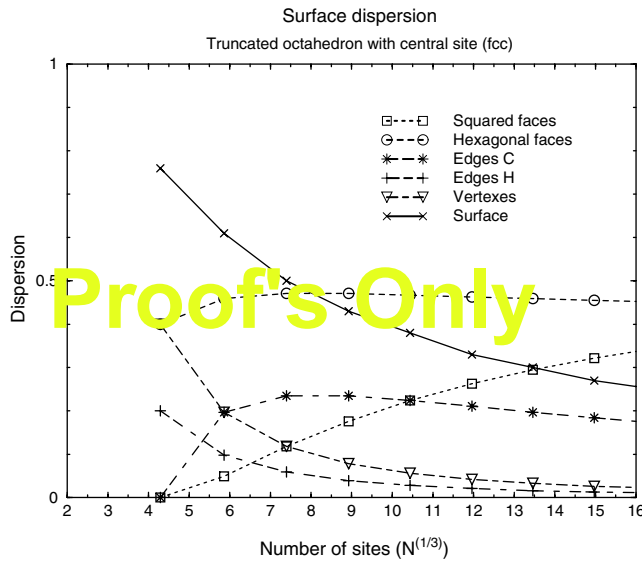
Figure 13. Dispersions due to surface sites of truncated octahedron with central site.
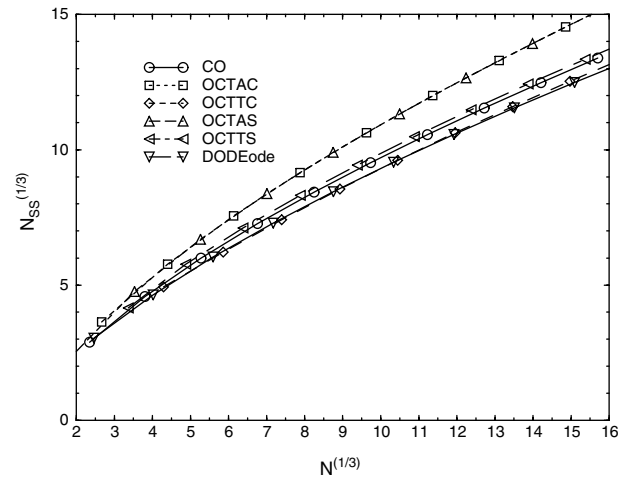
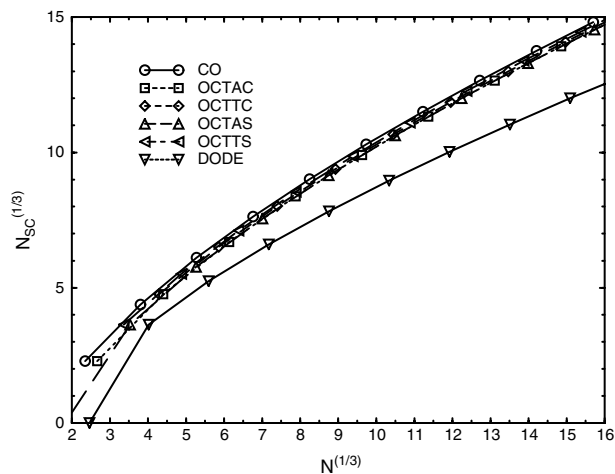**Figure 14.** Number of surface bonds as a function of the number of sites.

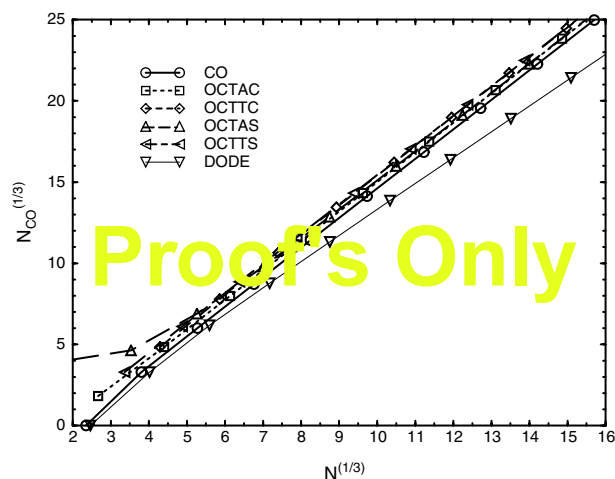**Figure 15.** Number of bonds between the surface and the internal cluster as a function of the number of sites.

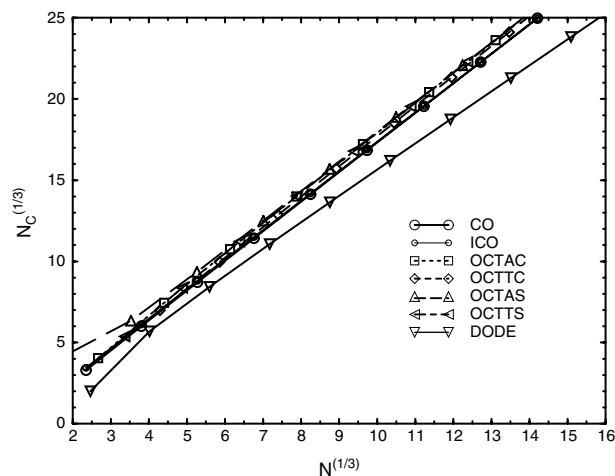**Figure 16.** Number of internal bonds as a function of the number of sites.

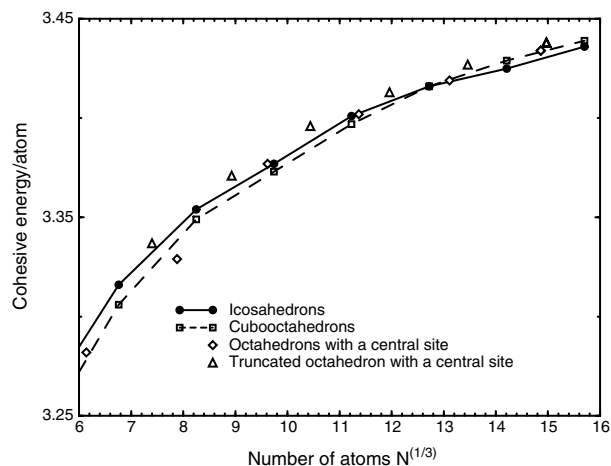**Figure 17.** Total numbers of bonds as a function of the number of sites.

Figure 18. Cohesive energy per atom as a function of the cubic root of the number of atoms in the cluster for the octahedrons and truncated octahedrons type fcc with a central site.

Table 12. Geometric characteristics for the face-centered cubic structure and without central site, fccs.

v	Sites at			Layers at			Layers at		Sites at	
	C	A	V	C	A	V	v	Total	v	Total
1	0	0	0	0	0	0	0	0	0	0
	6	0	8	1	0	1	2	2	14	14
	6	0	8	1	0	1	2	2	14	14
2	24	24	0	1	1	0	2	4	48	62
	78	24	8	4	1	1	6	10	110	172
	102	48	8	5	2	1	8	10	158	172
3	144	48	0	4	2	0	6	16	192	364
	246	48	8	9	2	1	12	28	302	666
	390	96	8	13	4	1	18	28	494	666
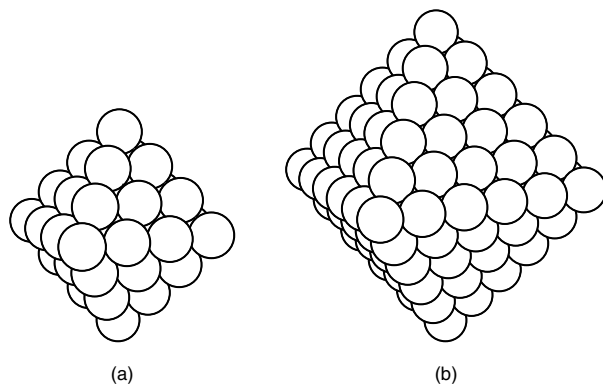
Figure 19. Octahedron without central site of (a) order 2 with 44 sites, and (b) order 3 with 146 sites.

Table 13. Geometric characteristics for the octahedron without central site.

	Sites at			Layers at			Layers		Sites	
v	T	A	V	T	A	V	v	Total	v	Total
1	0	0	6	0	0	1	1	1	6	6
2	8	24	6	1	1	1	3	4	38	44
3	48	48	6	2	2	1	5	9	102	146
4	120	72	6	4	3	1	8	17	198	344
5	224	96	6	7	4	1	12	29	326	670
6	360	120	6	10	5	1	16	45	486	1156
7	528	144	6	14	6	1	21	66	678	1834
8	728	168	6	19	7	1	27	93	902	2736
9	960	192	6	24	8	1	33	126	1158	3894
10	1224	216	6	30	9	1	40	166	1446	5340

Figure 22. Truncated octahedron without a central site of order 3 with 260 sites.

2.5.3. EAM Applied to fcc Structures without Central Site

The embedded atom method is applied, in the Foiles version and with the parameters of copper, to clusters with fcc structures without a central site to calculate the cohesion energy per atom, determining in this way the stability of the clusters. The results are compared with the ones from the icosahedrons and cubooctahedrons previously reported [28]. Figure 28 presents the cohesive energy graphic as a function of $N^{1/3}$ for the octahedron and truncated octahedron clusters of fcc without central site type, for sizes from 300 to 3400 atoms. From Figure 28, it can be seen that the truncated octahedrons (Δ) as well as the octahedrons ($\diamond$) compete in stability with the icosahedrons ($\bullet$) and cubooctahedrons ($\blacksquare$). And most of all, the truncated octahedrons show a higher stability than the octahedrons.
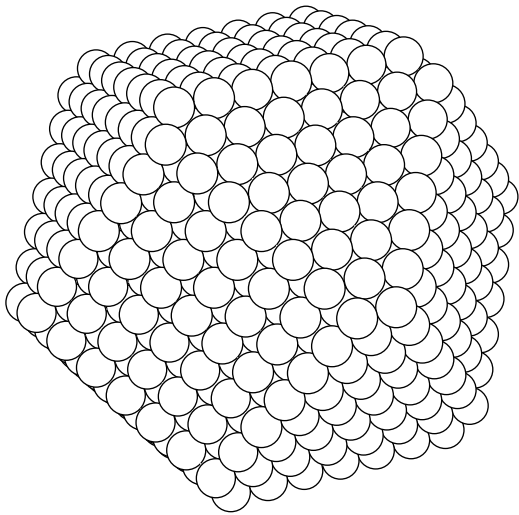
Figure 20. Octahedron of order 6 of 1156 atoms without a central site.

Surface Dispersion

Octahedron without central sites (fcc)

Triangular faces
Edges
Vertexes
Surfaces

Dispersion

Number of sites ($N^{(1/3)}$)
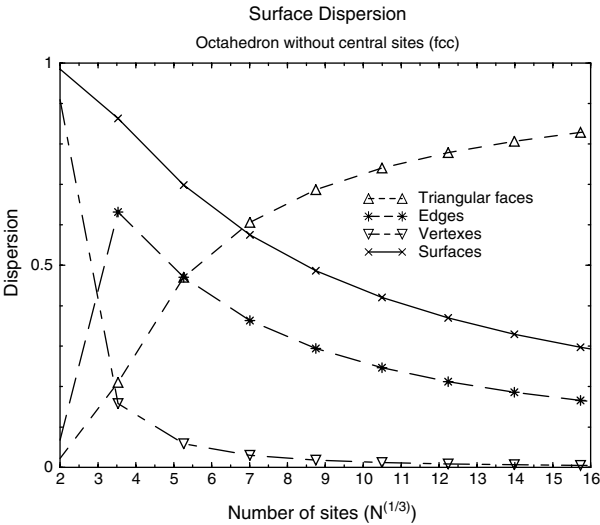
Figure 21. Dispersions caused by surface sites of octahedron without a central site as a function of the cluster size.

Figure 23. Truncated octahedron without a central site of order 6 with 1288 sites.

**Table 14.** Geometric characteristics for the truncated octahedron without central site.

	Sites at				Layers at				Layers at		Sites at	
v	C	H	A	V	C	H	A	V	v	Total	v	Total
1	0	8	0	24	0	1	0	1	2	3	32	38
2	6	24	24	24	1	1	1	1	4	7	78	116
3	24	48	48	24	1	2	1	1	5	12	144	260
4	54	80	72	24	3	3	2	1	9	21	230	490
5	96	120	96	24	3	4	2	1	10	31	336	826
6	150	168	120	24	6	5	3	1	15	46	462	1288
7	216	224	144	24	6	7	3	1	17	63	608	1896
8	294	288	168	24	10	8	4	1	23	86	774	2670
9	384	360	192	24	10	10	4	1	25	111	960	3630
10	486	440	216	24	15	12	5	1	33	144	1166	4796

2.6. bcc Structure

The body-centered cubic structure is a cube with sites in the vertexes and in the center of the cube, that is, there are 9 sites over a cube, 8 in vertexes, and 1 in the center of it; this is a cluster of order 1 with cubic arrays [Fig. 29(a)]. When attaching many of these arrays, clusters with sites in vertexes, edges, and squared faces are obtained. The cubic cluster of second order consists of an array of 8 cubes, which results from covering the first cube with a shell of sites distributed in three layers: 6 in squared face (C), 12 in edge (A), and 8 in vertexes (V) [Fig. 29(b)]. The next cluster has 56 sites distributed in 3 layers, and so on. From here, it is deduced that it is possible to identify layers of equivalent sites; these layers can be grouped into shells yielding noncubic geometries which present sites in vertexes, edges, and in rombohedral faces, such as in the dodecahedron.

2.6.1. Dodecahedron

The dodecahedron is formed by a central site, 14 vertexes of two types ($V1$ and $V2$), 24 edges (A), and 12 rombohedral faces (R); Figure 30. The two types of vertexes are: (1) 6
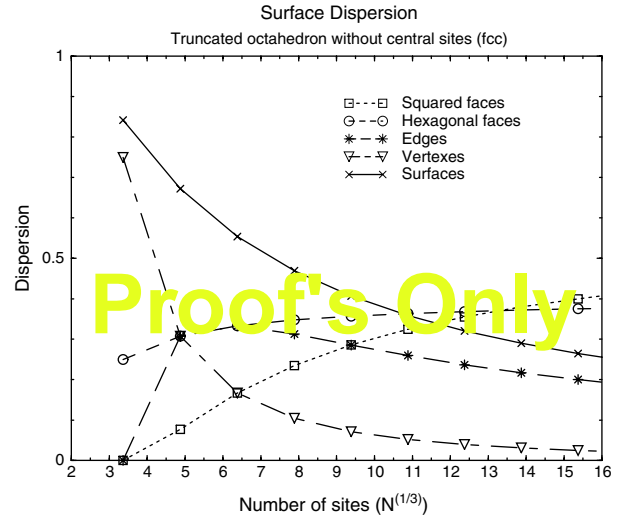
Figure 24. Dispersions due to surface sites of the truncated octahedron without a central site as a function of the cubic root of the cluster size.

vertexes ($V1$) of coordination 4 with sites of their own shell and of 4 with sites of exterior shells; and (2) 8 vertexes ($V2$) of coordination 1 toward sites of interior shells, 3 with sites of its own shell, and 4 with sites of exterior shells.

The number of first neighbors is found in Table 3, standard coordinates in Table 2, and the geometric characteristics of the decahedron are listed in Table 15, from which the dependence of geometric characteristics for the decahedron can be determined and are presented in Table 12. Surface dispersions originating from the different types of sites in the surface of the decahedron can also be shown graphically; Figure 31.

Based on Tables 3 and 14, it is possible to construct the expressions for the number of bonds for the different types of bonds in the dodecahedron, and are presented in Table 14 and their graphics in Figures 16–29.

Table 15. Particular expressions of the geometrical characteristics for the fcc without central site and dodecahedral structures.

|	OCTAS	OCTTS	DODE
N	$(16/3)v^2 + (2/3)v$	$(10/3)v^3 + 13v^2 + (47/3)v + 6$	$4v^3 + 6v^2 + 4v + 1$
N_σ	$16v^2 - 16v + 6$	$10v^2 + 16v + 6$	$12v^2 + 2$
$\mathscr{D}$	$3(16v^2 - 16v + 6)/(16v^3 + 2v)$	$3(10v^2 + 16v + 6)/(10v^3 + 39v^2 + 47v + 18)$	$(12v^2 + 2)/(4v^3 + 6v^2 + 4v + 1)$
N_S	—	$6(v - 1)^2$	—
R_S^p	—	$v(v + 2)/8$	—
R_S^i	—	$(v^2 - 1)/8$—	—
N_T	$8(2v - 3)(v - 1)$	—	—
R_T^m	A	—	—
N_H	—	$4v(v + 1)$	—
R_H^m	—	C	—
N_R	—	—	$12(v - 1)^2$
R_R^p	—	—	$v^2/4$
R_R^i	—	—	$(v^2 - 1)/4$
N_E	$24(v - 1)$	$24(v - 1)$	$24(v - 1)$
R_E^p	$v - 1$	$v/2$	$v - 1$
R_E^i	$v - 1$	$(v - 1)/2$	$v - 1$
$\mathscr{N}_{CO}$	$4(8v^3 - 24v^2 + 25v + 7)$	$2v(10v^2 + 9v - 1)$	$4(4v^3 - 6v^2 + 4v - 7)$
$\mathscr{N}_{CC}$	$48(v - 1)^2$	$6(5v^2 - 5v + 2)$	$24v(v - 1)$
$\mathscr{N}_{SS}$	$12(4v^2 - 4v + 1)$	$24v(v + 2)$	$4(6v^2 + 1)$
$\mathscr{N}_C$	$4(8v^3 - 11v + 40)$	$2v(10v^2 + 39v + 29)$	$8(2v^3 + 3v^2 - v - 3)$
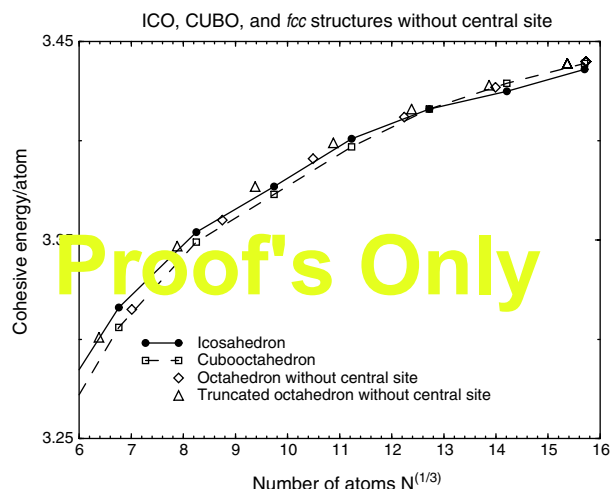
Figure 25. Cohesion energy per atom as a function of the square root of the number of atoms in the cluster for the octahedron and truncated octahedron with central site, type fcc.

2.6.2. EAM Applied to bcc Structures

The embedded atom method is applied, in the Foiles version and with the parameters of copper, to clusters with bcc structures to calculate the cohesion energy per atom, determining in this way the stability of the clusters. The results are compared with the ones from the icosahedrons and cubooctahedrons previously reported [28]. Figure 32 presents the cohesion energy graphic as a function of $N^{1/3}$ for dodecahedral clusters, for sizes from 300 to 3400 atoms. From Figure 32, it can be seen that the dodecahedrons ($\diamond$) compete in stability with the icosahedrons ($\bullet$) and cubooctahedrons ($\square$).

3. CLUSTERS AND NANOPARTICLES WITH PENTAGONAL SYMMETRY

3.1. Introduction

A cluster is defined as an aggregate of atoms; this can lead to clusters from two atoms (diatomic molecules), a lineal array of atoms, bidimensional, or three-dimensional arrays. This work presents the study of clusters with pentagonal symmetry, with sizes up to thousands of atoms in arrays of spherical or concentric layer types.
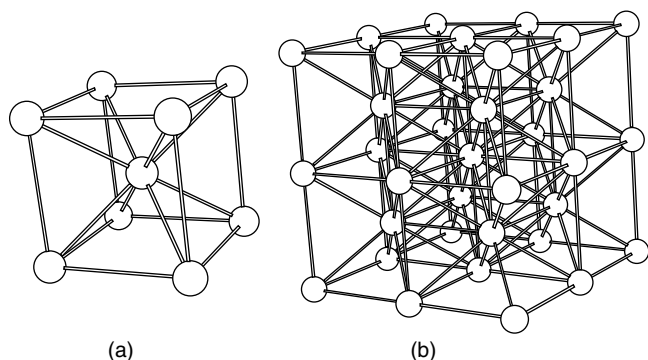
Figure 26. bcc structure of (a) 9 sites, and (b) 35 sites.
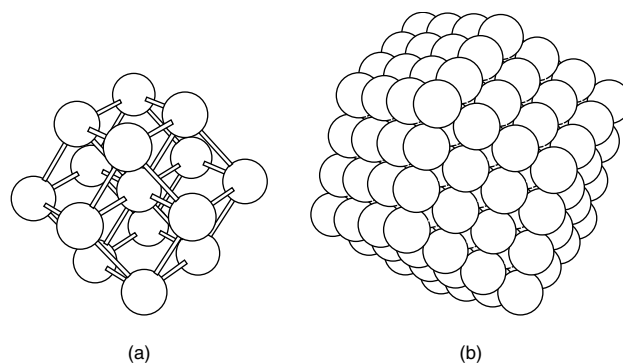
Figure 27. bcc dodecahedron of (a) order 1 with 15 sites, and (b) order 2 with 175 sites.

Arrays of linked atoms forming three-dimensional clusters are considered here as sites in geometric positions attached by the edges in such a way that faces of diverse forms are generated (triangular, squared, rombohedral, etc.). The distance between the sites is considered as the distance to first neighbors d_{NN}, which is normalized to one. There could be sites in the vertexes, edges, and faces, either in the surface or internals; also, there could be different types of sites, depending on their position and the number and type of neighbors in the geometric array. There also could be equivalent sites, which present the same geometric characteristics: to the same distance from the center of the geometric array, in the same type of site, and with the same number and type of neighbors.

From the bicaped hexahedron or decahedron, Figure 33(a), pentagonal symmetry structures can be obtained. Among the clusters with structures of pentagonal symmetry, the following structures are considered: decahedra with and without a central site, icosahedra, pentadecahedra, truncated decahedra (Marks decahedra), star-type decahedra, modified and developed decahedra, truncated icosahedra, and the *decmon*.
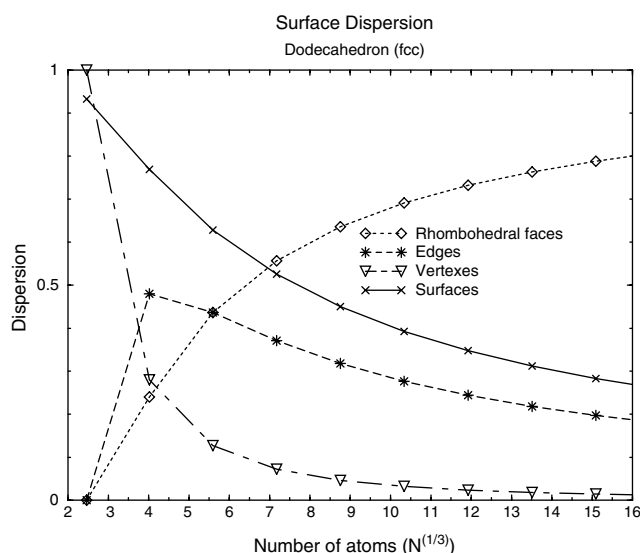

Figure 28. Dispersion due to surface sites of the dodecahedron as a function of the cubic root of the cluster size.
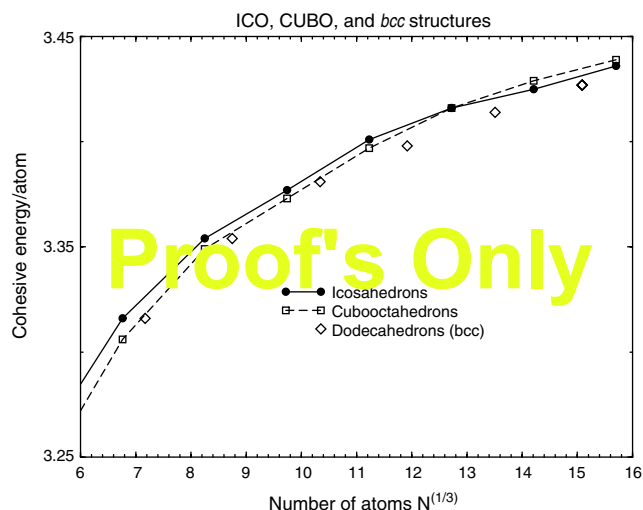
Figure 29. Cohesive energy per atom as a function of the cubic root of the number of atoms in the cluster for decahedron bcc type.

3.2. Decahedra

Decahedra are obtained from the bicapped hexahedra, and also from attaching two pentagonal-based pyramids from their bases and sharing their sites (which form the equator of the cluster), yielding geometrical bodies of 7 vertexes (2 at poles and 5 at equator), 15 edges (all from the same length, 5 at the equator), and 10 triangular equilateral faces; 5 of them converge on each pole, and by pairs, they form the edges of the equator. Decahedra can be without a central site, Figure 33(a) and (c), and with a central site, Figure 33(b), without losing the decahedral form. So, decahedra have the vertexes at the poles VP, vertexes at the equator VE, at the edges over the equator AE, edges at poles AP, and in triangular faces T. It has to be noticed that
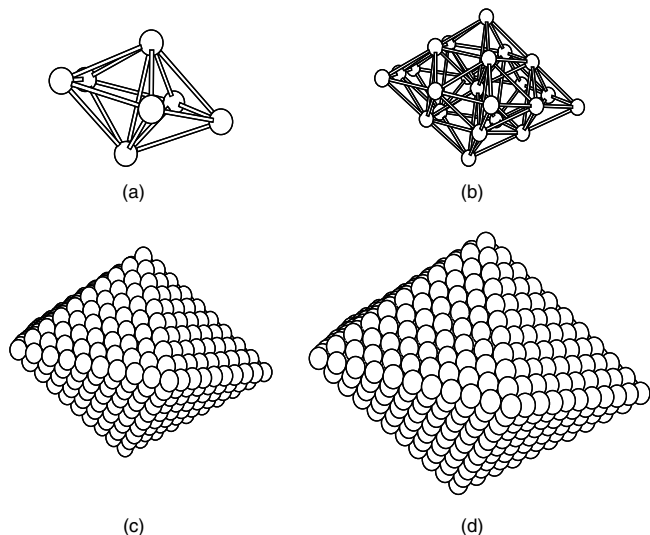
Figure 30. Decahedral polyhedrons. (a) Bilayered hexahedron or decahedron of 7 atoms of order 1, without central site. (b) Decahedron of 23 atoms of order 1 with central site. (c) Decahedron of 835 sites of order 5, without central site. (d) Decahedron of 1111 atoms of order 5 with central site.
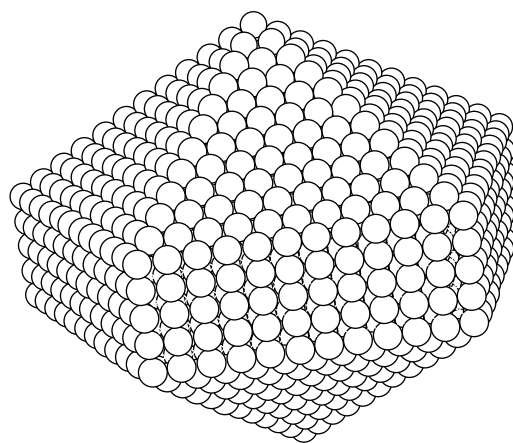

Figure 31. Pentadecahedron of 2766 atoms of order 65, obtained from a decahedron without a central site of order 6 with 5 layers in the waist, which means adding 4 SEC-type layers to the original decahedron.

coordination, that is, distribution to first neighbors (NN), is what makes the difference in each type of sites, although the total coordination is the same for all of the sites of the corresponding cluster. Table 16 presents the coordination of each site, for example, the poles (VP) have 4 first neighbors (NN) with sites at their same shell, 1 NN toward the inner shell, and 4 toward the exterior shell. The decahedron of order 1, without a central site, Figure 33(a), has only 7 vertexes in two layers; the one from order 2, Figure 33(c), is obtained from covering the one of order 1 with a shell of 47 sites distributed as follows: 7 V sites of two types, 30 A sites in three layers (10 sites of one type ant the equator), and 10 at triangular faces (sites T, one for each triangular face) in one single layer, for a total of 54 sites in the cluster. Decahedra of superior order are formed by coverage of this cluster of order 2 with successive shells of many layers in each one.

The decahedron with central site of order 1, Figure 33(b), has 15 sites A, one per edge, of two types, 5 sites of one type at the equator, and 7 sites V, a total of 22 sites and the central one in five layers. The second-order cluster results from the order 1 cluster covered by a shell of 82 sites distributed in 8 layers: 45 A sites in 5 layers, 30 T sites in one single layer, and 7 V sites in two layers, for a total of 105 sites in the cluster, and so on for cluster of superior order.
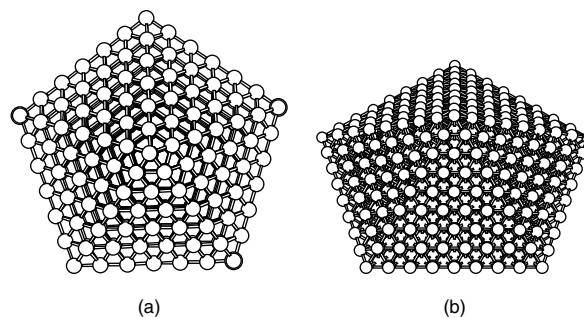

Figure 32. (a) Decahedron of 287 sites, of order 3, with a central site. (b) Decahedron of 609 sites, of order 4, with a central site.
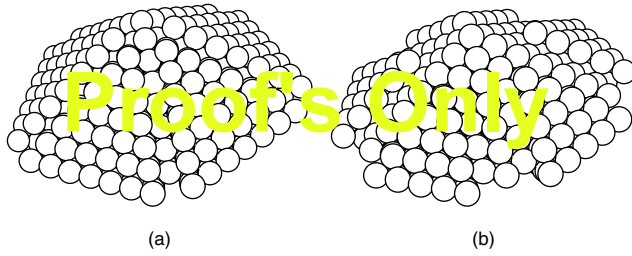
Figure 33. Decahedron of 609 sites of order 4 and (a) a single channel, and (b) a triple channel per edge converging to the pole, of 532 sites and 412 sites, respectively.

Table 17 presents the geometrical characteristics of decahedra with and without a central site. The first column, common for all decahedra, lists the cluster order v. This is followed by two groups of 9 columns each, which correspond to the decahedron with and without a central site. The first three columns of each group list the number of sites on each type of site in the cluster: triangular face (T) N_T, edge (A) N_A, and vertex (V) N_V. The two following columns show the number of sites per shell N_{SE}, and the total of sites in the plane just above the equator N_{tSE}, (the SE sites). The following two columns list the number of sites at the equator (sites EC) per shell N_{EC}, and in the whole cluster N_{tEC}; the joint between SE and EC sites form the SEC layer, which will be needed afterwards, and they both form a pentagonal flat layer. Finally, the two last columns of each group, the number of sites in the shell N_σ, and the total of sites in cluster N. Decahedra with (without) a central site have an odd (even) number of sites per edge, which is important for the star and truncated-type decahedra, detailed later.

From Table 17, it is observed that, for both decahedron types, the number of vertexes per shell is 7, 2 type VP, and 5 type VE; we can also obtain, for each type of decahedra, the dependence with the cluster order of the number of T sites, A sites, the number of sites in the layer at the equator, as well as the total sites in the shell (or of the surface), and from the total of sites over the equator, at the equator and in the decahedron. Such dependency is expressed in the following relations for the decahedra with a central site; it is to be noticed that, for $v = 1$, there are 11 sites at the equator because the central site is included:

$$N_A(v) = 15(2v-1) \begin{cases} N_{AP}(v) = 10(2v-1) \\ N_{AE}(v) = 5(2v-1) \end{cases}$$

$$N_T(v) = 20v^2 - 30v + 10$$

$$N_{SE}(v) = 10(v-1) + 5$$

Table 16. Coordination or number of first neighbors (NN) of the different types of sites in the decahedron with sites in external, the same one, and internal shell.

| Shell | Type of site | | | | |
	T	AE	AP	VE	VP
External	3	6	4	8	6
Same	6	6	6	4	5
Internal	3	0	2	0	1

$$N_{tSE}(v) = 5v^2$$

$$N_{EC}(v) = 10v$$

$$N_{tEC}(v) = 5v(v+1) + 1$$

$$N_\sigma(v) = 20v^2 + 2$$

$$N(v) = \frac{20}{3}v^3 + 10v^2 + \frac{16}{3}v + 1$$

and for decahedra without a central site,

$$N_A(v) = 30(v-1) \begin{cases} N_{AP}(v) = 20(v-1) \\ N_{AE}(v) = 10(v-1) \end{cases}$$

$$N_T(v) = 20v^2 - 50v + 30$$

$$N_{SE}(v) = 10(v-1)$$

$$N_{tSE}(v) = 5v(v-1) + 1$$

$$N_{EC}(v) = 5(2v-1)$$

$$N_{tEC}(v) = 5v^2$$

$$N_\sigma(v) = 20v^2 - 20v + 7$$

$$N(v) = \frac{20}{3}v^3 + \frac{v}{3}.$$

Note that from the expression for N_A, and from Figure 33(c) and (d), the number of AP and AE per edge is $2v-1$ [$2v-2$] for decahedra with (without) a central site.

If, instead of attaching the base of the two pentagonal base pyramids to form the decahedron, they are separated, two types of geometrical figures can be obtained, depending on the way the sites of the bases are connected: the pentadecahedron and the icosahedron.

3.3. Pentadecahedra

If the pentagonal pyramids which generate the decahedron when they are joined are separated, they are in a position in which the vertexes of the base of both can be attached by 5 edges (AC) perpendicular to the base, yielding 5 rectangular faces, which form the pentadecahedra, Figure 34, that is, a decahedron with a wide waist or a developed decahedron. Separation can be done by adding intermediate layers of type SEC (formed by a layer of sites SE and another of sites EC as mentioned previously). The number of SEC intermediate layers, and the length of the edges perpendicular to the bases, depend on the desired separation. For example, the pentadecahedron from Figure 34 has 5 layers in the waist; to obtain it, 4 layers of type SEC are added to the order 6 decahedron of 1442 sites without a central site, which results in edges $4d_{NN}$ long. It has to be noticed that, upon widening of the waist of a decahedron, from one equatorial layer to two equatorial layers, an SEC-type layer is added; when widening three equatorial layers, two SEC-type layers are added, that is, for each equatorial layer wanted to widen the decahedra waist, one type of SEC layer is added.

The pentadecahedra are polyhedra of 12 vertexes (2 poles and 10 in vertexes at the waist), 25 edges (20 of one type and 5 of the other type, which join the vertexes of the two pyramids, and whose length depends on the number of intermediate layers added), 10 equilateral triangular faces, and

Table 17. Geometric characteristics for the decahedra with and without central site. v is the order of the cluster, N_I con $I = T$, A, and V, is the number of sites I. Sites SE and EC are also listed, the number of sites in each shell N_σ, and in total N in the cluster.

	With central site									Without central site								
v	N_T	N_A	N_V	N_{SE}	N_{tSE}	N_{EC}	N_{tEC}	N_σ	N	N_T	N_A	N_V	N_{SE}	N_{tSE}	N_{EC}	N_{tEC}	N_σ	N
1	0	15	7	5	5	10	11	22	23	0	0	7	1	1	5	5	7	7
2	30	45	7	15	20	20	31	82	105	10	30	7	10	11	15	20	47	54
3	100	75	7	25	45	30	61	182	287	60	60	7	20	31	25	45	127	181
4	210	105	7	35	80	40	101	322	609	150	90	7	30	61	35	80	247	428
5	360	135	7	45	125	50	151	502	1111	280	120	7	40	101	45	125	407	835
6	550	165	7	55	180	60	211	722	1833	450	150	7	50	151	55	180	607	1442
7	780	195	7	65	245	70	281	982	2815	660	180	7	60	211	65	245	847	2289
8	1050	225	7	75	320	80	361	1282	4097	910	210	7	70	281	75	320	1127	3416
9	1360	255	7	85	405	90	451	1622	5719	1200	240	7	80	361	85	405	1447	4863
10	1710	285	7	95	500	100	551	2002	7721	1530	270	7	90	451	95	500	1807	6670

5 rectangular lateral faces (or squared, depending on the number of intermediate layers added) (Fig. 34). The number of sites in these pentadecahedra depends on the size of the original decahedron and how many intermediate layers are added; also, whether they are with and without a central site is considered, depending on the original decahedron from which they were generated. So, at the surface of the pentadecahedra, there are the same type and number of sites as in the decahedra, plus the N_{EC} sites added (because the N_{EC} are not at the surface), which are divided in sites type VE, sites AE, sites at vertical edges at the width of the waist AV, and in rectangular faces R. Table 18 presents the coordination of each type of site in the pentadecahedron. Notice that, upon comparison of Table 16, as expected, only the sites corresponding to the pentadecahedron are added, and those of the decahedron are not. Sites N_{SE} added, originally 5 AP sites, and the rest T sites (except for the pentadecahedron of order 11, without a central site) are converted in internal sites of coordination 12.

For pentadecahedron order, we can use $v\mu$, v for the decahedron order from which comes and μ for the number of layers at the waist, so regular decahedra would be pentadecahedra with $\mu = 1$. The number of layers of type SEC which are added to the decahedron referred to generate the pentadecahedron is $\mu - 1$, so that the number of sites added is equal to the sum of the total of sites SE and the total of EC sites of the corresponding decahedron, columns 6, 8, 15, and 17 of Table 1. So, in order to have a pentadecahedron of order 55 with a central site, one has to start with a

decahedron of order 5, 111 sites, and an additional 4 layers of type SEC of $125 + 151 = 276$ sites each, for a total of 1104 added sites and 2215 sites in the cluster.

The number of sites T, AP, and VP is the same as in the decahedron which originated from the pentadecahedron. The number of sites AE and VE is duplicated with respect to the original decahedron. The number of AV and R sites for the pentadecahedra with and without a central site is the same, and is presented in Table 18, which shows the geometric characteristics of the pentadecahedra with and without a central site, respectively; only some of μ values are presented. There are three groups of three, four, and five columns, respectively. In the columns of the first group are listed the quantities common to the two types of pentadecahedra: cluster order v and μ, and the number of sites AV, N_{AV}; for both polyhedra, in each following group, the geometric characteristics for each polyhedron are presented, those of the pentadecahedron both with and without

Table 18. Geometric characteristics for pentadecahedra. Generated from the corresponding decahedron of order v.

			With central site				Without central site			
v	μ	N_{AV}	N_R	N_{ag}	N_σ	N	N_R	N_{ag}	N_σ	N
1	1	0	0	0	22	23	0	0	7	7
	2	0	0	16	32	39	0	6	12	13
2	1	0	0	0	82	105	0	0	47	54
	2	0	0	51	102	156	0	31	62	85
	3	5	15	102	122	207	10	62	77	116
3	1	0	0	0	182	287	0	0	127	181
	2	0	0	106	212	393	0	76	152	257
	3	5	25	212	242	499	20	142	177	333
4	1	0	0	0	322	609	0	0	247	428
	2	0	0	181	362	790	0	141	282	569
	4	10	70	543	442	1152	60	423	352	851
5	1	0	0	0	502	1111	0	0	407	835
	2	0	0	276	552	1387	0	226	452	1061
	3	5	45	552	602	1653	40	452	497	1287
	5	15	135	1104	702	2215	120	904	587	1739

Note: μ is the number of equatorial layers in the cluster. Number of sites AV, N_{AV}, R sites N_R, of sites added N_{ag}, surface site N_σ, and of total sites N in the cluster of order $v\mu$. Notice that, for $\mu = 1$, values of Table 1 are obtained. Even when μ can have any value higher than zero, here only some values are presented.
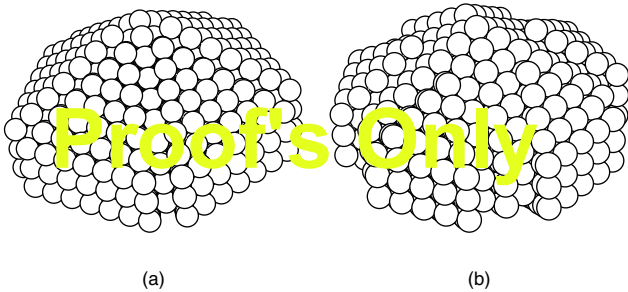

Figure 34. Decahedron of order 4 of 609 sites with central site, with (a) one single channel and (b) with a triple channel per edge converging to the pole, with three layers in the waist, of 874 sites and 714 sites, respectively.

a central site. A list of the number of R sites N_R, the number of sites added N_{ag}, of sites at the surface N_σ, and the total of sites N in the cluster of order $v\mu$ is given. Note that, for $\mu = 1$, the values from Table 16 are obtained.

From Table 18, the analytic expressions for the number of sites AV can be obtained as a function of μ and v:

$$N_{AV}(v, \mu) = 5(\mu - 2)$$

as well as the number of R sites, sites which are added, sites in the surface, and the total of sites for pentadecahedra with a central site:

$$N_R(v, \mu) = 5(2v - 2)(\mu - 2)$$

$$N_{ag}(v, \mu) = (\mu - 1)(10v^2 + 5v + 1)$$

$$N_\sigma(v, \mu) = 20v^2 + 2 + 10v(\mu - 1)$$

$$N(v, \mu) = \frac{20}{3}v^3 + 10v^2 + \frac{16}{3}v + 1$$
$$+ (10v^2 + 5v + 1)(\mu - 1)$$

and for pentadecahedra without a central site:

$$N_R(v, \mu) = 10(v - 2)(\mu - 2)$$

$$N_{ag}(v, \mu) = (\mu - 1)(10v^2 - 5v + 1)$$

$$N_\sigma(v, \mu) = 20v^2 - 20v + 7 + 5(2v - 1)(\mu - 1)$$

$$N(v, \mu) = \frac{20}{3}v^3 + \frac{v}{3} + (10v^2 + 5v + 1)(\mu - 1).$$

3.4. Modified Decahedra

In a certain decahedron, with or without a central site, the number of sites per edge increases in 2 sites per shell increased. For example, in the decahedron of 287 sites of order 3 with a central site, Figure 35(a), in the surface shell, there are 5 sites in each edge, and in the one of order 4,
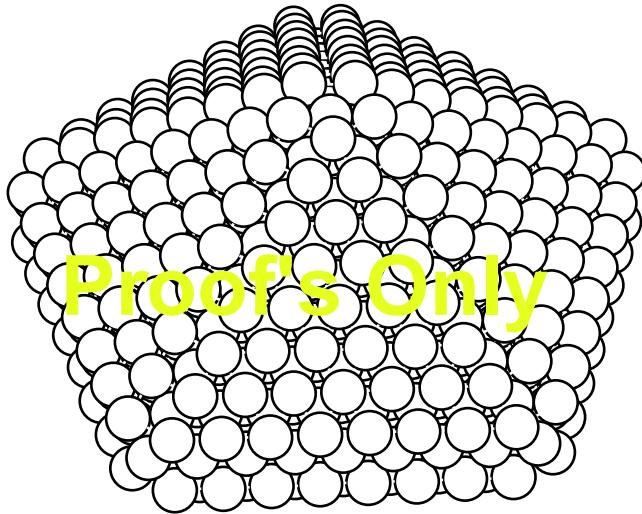
there are 609 sites, Figure 35(b); there are 7 sites per edge. The decahedron modification can be done in two ways: (1) as channels at the surface, and (2) as surface reconstruction. Besides, modified decahedra can be obtained, adding *SEC*-type layers in order to widen the waist of the decahedra.

3.4.1. Decahedra with Additional Faceting (*Channels at Twin Boundaries*)

When suppressing surface sites from the edges converging in the poles (*AP* sites) and from all of the vertexes in a decahedron, a one-channel decahedron is obtained; for example, from the decahedron of 609 sites of order 4 with a central site [Fig. 35(b)], a decahedron of 532 sites is obtained with one channel convergent to the pole, Figure 36(a), eliminating 77 sites. These result in a polyhedron formed by a decahedron of order 3 with triangular faces covered with sites corresponding to the decahedron of order 4, in a way that some surface sites that were T type are now type A. If, now, the following edges (which were type T sites) are eliminated from the surface, a triple-channel decahedron of 412 sites is obtained; 120 sites were eliminated [Fig. 36(b)]. It can be continued in this way until the desired number of channels is reached. The construction of the first channel, eliminating vertexes and AP edges from the surface, in other words, remains with a coordination lower than 12, which implies that there are free bonds. Type VP sites from the internal decahedron have two free bonds, sites VE have three, and sites AP have four. So, surface sites are not only the difference between surface sites and the ones that were eliminated, but the interior decahedron sites are added which have a coordination lower than 12.

Table 19 lists geometrical characteristics for the decahedra, with and without a central site, modified with surface channels. v is the original cluster order. The only characteristics presented are for an $n = 1$, a single channel and 2, a
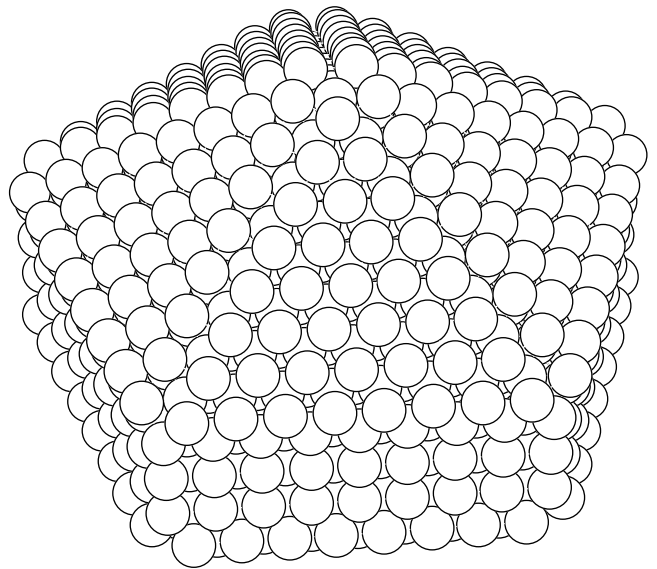

Figure 35. Decahedron of order 4 with 609 sites and with a central site, with 360 sites aggregated for surface reconstruction for a total of 969 sites.

Figure 36. Decahedron with a central site of order 4 (609 sites), with surface reconstruction (969 sites) and three equatorial layers (two layers SEC of 181 sites each one) for a total of 1331 sites in the polyhedron.

Table 19. Geometric characteristics of decahedra with and without a central site, modified with surface channels.

		With central site							Without central site						
v	n	N_{el}	N_{SE}	N_{tSE}	N_{EC}	N_{tEC}	N_σ	N	N_{el}	N_{SE}	N_{tSE}	N_{EC}	N_{tEC}	N_σ	N
2	1	37	10	15	15	26	62	68	27	5	6	10	15	27	27
3	1	57	20	40	25	56	162	230	47	15	26	20	40	107	134
	2	137	10	30	15	46	122	150	107	5	16	10	30	67	74
4	1	77	30	75	35	96	302	532	67	25	56	30	75	227	361
	2	197	20	65	25	86	262	412	167	15	46	20	65	187	261
5	1	97	40	120	45	146	482	1014	87	35	96	40	120	387	748
	2	257	30	110	35	136	442	854	227	25	86	30	110	347	608

Note: v is the cluster order. Here are presented only characteristics for $n = 1$ and 2 channels. The number of eliminate sites are listed N_{el}, the number of sites SE and EC per shell and in total, and the number of sites in the surface and in total in the final cluster.

triple channel. Eliminating the sites for the channel sin the decahedron affects the number of sites *SE* and *EC* of the original decahedron. Table 5 lists the number of sites that are eliminated N_{el}, the number of sites *SE* and *EC*, per shell and in total, and the number of sites at the surface and in total in the final cluster. The number of sites *SE* and *EC* is needed in order to generate the decahedra with channels and developed, as was done for the pentadecahedron.

From Table 19 are deduced the analytic expressions for the number of sites eliminated in a decahedron in order to obtain the decahedron with channels, the number of *SE* and *EC* sites, and the number of sites in the surface and the number of total sites in the cluster, which are presented next for the decahedron with a central site and a simple channel:

$$N_{el} = 20v - 3$$
$$N_{SE} = 10(v - 1)$$
$$N_{tSE} = 5v^2 - 5$$
$$N_{EC} = 10v - 5$$
$$N_{tEC} = 5v(v + 1) - 4$$
$$N_\sigma = 20v^2 - 18$$
$$N = \frac{20}{3}v^3 + 10v^2 - \frac{44}{3}v + 4$$

for the decahedron with a central site and a triple channel:

$$N_{el} = 60v - 43$$
$$N_{SE} = 10v - 20$$
$$N_{tSE} = 5v^2 - 15$$
$$N_{EC} = 10v - 15n$$
$$N_{tEC} = 5v(v + 1) - 14$$
$$N_\sigma = 20v^2 - 58$$
$$N = \frac{20}{3}v^3 + 10v^2 - \frac{164}{3}v + 44$$

and for the decahedron without a central site and a simple channel:

$$N_{el} = 20v - 13$$
$$N_{SE} = 10v - 15$$
$$N_{tSE} = 5v(v - 1) - 4$$
$$N_{EC} = 10(v - 1)$$
$$N_{tEC} = 5v^2 - 5$$
$$N_\sigma = 20v^2 - 20v - 13$$
$$N = \frac{20}{3}v^3 - \frac{59}{3}v + 13.$$

For the decahedron without a central site and a triple channel,

$$N_{el} = 60v - 73$$
$$N_{SE} = 10v - 25$$
$$N_{tSE} = 5v(v - 1) - 14$$
$$N_{EC} = 10v - 20$$
$$N_{tEC} = 5v^2 - 15$$
$$N_\sigma = 20v^2 - 20v - 53$$
$$N = \frac{20}{3}v^3 - \frac{179}{3}v + 73.$$

In the same way used to generate the pentadecahedra, by modifying the decahedra, the new type of decahedra can be obtained (Fig. 37). In order to do this, a layer of type *SEC* is added for each layer desired to increase the waist of the decahedron with channels. Table 5 lists the number of sites *SE* and *EC*, which are used to construct Table 20 for the decahedra with channels and developed.

When adding layers to widen the waist, the number of sites *AE* and *VE* is duplicated with respect to the original polyhedron, and different type *AV* and *R* sites are generated, as happened with pentadecahedra, and the number of sites is the same. The number of sites added N_{ag}, of which
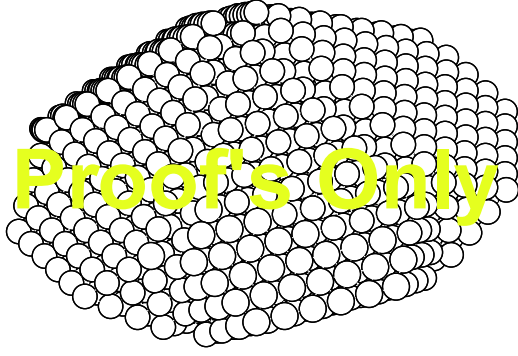
Figure 37. Truncated decahedron of 1372 sites of order 63, without a central site.

$N_{\sigma ag}$ are added to the surface for μ equatorial layers for the polyhedron with a central site and a single channel, is

$$N_{ag} = (\mu - 1)(10v^2 + 5v - 9)$$

$$N_{\sigma ag} = (\mu - 1)(10v - 5).$$

With a central site and a triple layer,

$$N_{ag} = (\mu - 1)(10v^2 + 5v - 39)$$

$$N_{\sigma ag} = (\mu - 1)(10v - 15).$$

Without a central site and a single channel,

$$N_{ag} = (\mu - 1)(10v^2 - 5v - 9)$$

$$N_{\sigma ag} = (\mu - 1)[10(v - 1)].$$

With a central site and a triple channel,

$$N_{ag} = (\mu - 1)(10v^2 - 5v - 39)$$

$$N_{\sigma ag} = (\mu - 1)(10v - 20).$$

3.4.2. Modified Decahedra with Surface Reconstruction

Modification of surface reconstruction of a decahedron is obtained if each triangular face of the decahedron proceeds as follows: a triangular face is obtained exactly as the one from the original decahedron; it is transported outwards to the same distance as the one between parallel triangular faces, $0.7953d_{NN}$, which is the height of a tetrahedron with a base of $1.05d_{NN}$ from one side and the other sides of $1.0d_{NN}$, then in a parallel way is shifted to the waist to a distance of $0.606d_{NN}$, which is 2/3 of the height of the equilateral triangle of $1.05d_{NN}$ from one side, until the generated sites coincide with the triangle centers of the original triangular face, and finally, the complete edge of the waist is eliminated. Figure 38 shows an example of a decahedron of 287 sites of order 3, to which 21 sites are added per face; this is 210 sites in total, for a total of 497 sites. It should be noted that it seems that a decahedron with a surface channel is obtained, although the sites which seem to form the channel are at a distance of $1.13d_{NN}$, while in a decahedron with a simple channel, they are at $1.63d_{NN}$. This is why, in this modification, a long bond is considered, and the AP sites of the interior decahedron do not form part of the surface. In fact, the surface of the resulting polyhedron is formed by the added sites and the sites VE, VP, and AE of the internal decahedron, which are those which also can be considered as a surface because they remain with free bonds.

It should be noted that the planes above the equator and the sites in the plane of the equator of the original decahedron are not modified. The characteristics of these polyhedra are presented in Table 21. v is the original cluster order, N_{ag} is the number of sites added, N_σ is the number of sites in the surface, and N is the total number of sites in the cluster.

From Table 21, it is possible to obtain the analytic expressions as a function of the order of the original cluster for the

Table 20. Geometric characteristics for the decahedron with and without a central site, modified with surface channels and with added layers in the waist.

| | | | | \multicolumn{6}{c}{With central site} | | | | | | \multicolumn{6}{c}{Without central site} | | | |
| | | | | \multicolumn{3}{c}{One channel} | | | \multicolumn{3}{c}{Two channels} | | | \multicolumn{3}{c}{One channel} | | | \multicolumn{3}{c}{Two channels} | |
v	μ	N_{AV}	N_R	N_{ag}	N_σ	N	N_{ag}	N_σ	N	N_R	N_{ag}	N_σ	N	N_{ag}	N_σ	N
2	1	0	0	0	62	68	—	—	—	0	0	27	27	—	—	—
	2	0	0	41	77	109	—	—	—	0	21	37	48	—	—	—
	3	5	15	82	92	150	—	—	—	10	42	47	69	—	—	—
3	1	0	0	0	162	230	0	122	150	0	0	107	134	0	67	74
	2	0	0	96	187	326	66	137	226	0	66	127	200	36	77	110
	3	5	25	192	212	422	132	152	302	20	132	147	266	72	87	146
4	1	0	0	0	302	532	0	262	412	0	0	227	361	0	187	261
	2	0	0	171	337	703	151	287	563	0	131	257	492	101	207	362
	4	10	70	513	407	1045	453	337	865	60	393	317	754	303	247	564
5	1	0	0	0	482	1014	0	442	854	0	0	387	748	0	347	608
	2	0	0	266	527	1280	236	477	1100	0	216	427	964	186	377	794
	3	5	45	532	572	1546	472	512	1346	40	432	467	1180	372	407	980
	5	15	135	1064	662	2078	944	582	1838	120	864	547	1612	744	467	1352

Note: v is the cluster order, μ is the number of equatorial layers. Only the characteristics for $n = 1$ and 2 channels are presented. Notice that for $\mu = 1$ Table 5 values are obtained. Although μ can take any value higher than zero, here are only presented some values.
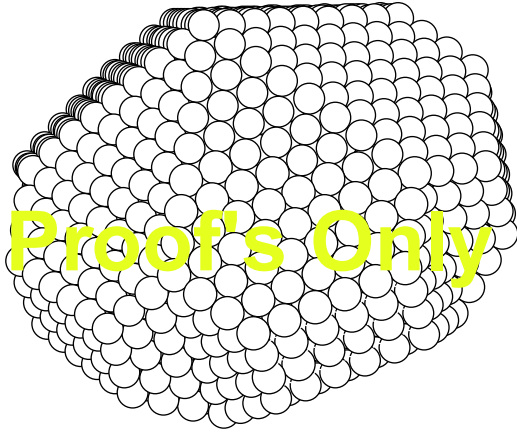
Figure 38. Truncated decahedron without a central site of order 63 with four equatorial layers, for a total of 2230 sites.

different characteristics listed here, and they are presented next for the polyhedron with a central site:

$$N_{ag} = 20v^2 + 10v$$

$$N_\sigma = 20v^2 + 20v + 2$$

$$N = \frac{20}{3}v^3 + 30v^2 + \frac{46}{3}v + 1,$$

and without central site:

$$N_{ag} = 20v^2 - 10v$$

$$N_\sigma = 20v^2 - 3$$

$$N = \frac{20}{3}v^3 + 20v^2 - \frac{29}{3}v.$$

Alternatively, it is possible to generate other decahedra with surface reconstruction. For this, simply add one *SEC*-type layer for each layer wanted to increase the waist of the decahedron with channels. Table 2 presents the sites of type *SE* and *EC* of the original decahedron, used to construct Table 22 for the decahedra with surface reconstruction and developed.

When adding the layers to widen the waist of the sites *AE* and *VE* of the original decahedron, they duplicate and generate the sites of type *AV* and *R*, as occurred with the pentadecahedra, and the number of sites is the same. The number of added sites N_{ag} from which $N_{\sigma ag}$ are added to

Table 21. Geometric characteristics for decahedra with and without a central site, modified with surface reconstruction.

	With central site			Without central site		
v	N_{ag}	N_σ	N	N_{ag}	N_σ	N
2	100	122	205	60	77	114
3	210	242	467	150	177	331
4	360	402	969	280	317	708
5	550	602	1661	450	497	1285

Note: v is the cluster order. The number of added sites N_{ag}, surface sites N_σ and total sites N in the cluster are listed.

Table 22. Geometric characteristic for decahedra with and without a central site modified with surface reconstruction and added layers in the waist.

			With central site				Without central site		
v	μ	N_{AV}	N_R	N_{ag}	N_σ	N	N_R	N_{ag}	N_σ	N
2	1	0	0	0	122	205	0	0	77	114
	2	0	0	51	142	256	0	31	92	145
	3	5	15	102	162	307	10	62	107	176
3	1	0	0	0	242	497	0	0	177	331
	2	0	0	106	272	603	0	76	202	407
	3	5	25	212	302	709	20	152	227	483
4	1	0	0	0	402	969	0	0	317	708
	2	0	0	181	442	1150	0	151	352	859
	4	10	70	343	522	1512	60	453	422	1161
5	1	0	0	0	602	1661	0	0	497	1285
	2	0	0	276	652	1937	0	226	542	1511
	3	5	45	552	702	2213	40	452	587	1737
	5	15	135	1104	802	2765	120	904	677	2189

Note: v is the cluster order, μ is the number of equatorial layers. Notice that, for $\mu = 1$, Table 8 values are obtained. Although μ can take any value higher than zero, here are presented only some values.

the surface for μ equatorial layers for the polyhedron with a central site is

$$N_{ag} = (\mu - 1)[10v^2 + 5v + 1]$$

$$N_{\sigma ag} = (\mu - 1)(10v),$$

and without a central site:

$$N_{ag} = (\mu - 1)[10v^2 - 5v + 1]$$

$$N_{\sigma ag} = (\mu - 1)[5(2v - 1)].$$

3.5. Truncated Decahedra (Marks Decahedra)

These result from the adequate elimination of some sites of a certain decahedron. The resulting geometry is a figure of 22 vertexes (of three types), 40 edges (of 4 types, 15 from the original decahedron, but shorter, and 25 which are generated by elimination of the adequate sites), 10 pentagonal faces (triangular faces from the original decahedron are converted to irregular pentagons), and 10 equilateral triangular faces (at the equator and joint by pairs) (Fig. 39).

The adequate elimination of sites is equivalent to eliminating the end sites of the edges which converge in the vertexes of the equator of the corresponding decahedron. Notice that in, each elimination, the equatorial edges lose two sites, while the edges which converge also toward the poles only lose one; this causes edges converging to the poles to be larger than the equatorial ones, but shorter then the ones from the original decahedron.

In the first step, $n = 1$, the equator vertexes from the equator of the exterior shell are eliminated, the last shell, 5 sites. In the second step, $n = 2$, two sites per equatorial edge are eliminated, and one of the rest of the edges; 20 sites of the previous stage are converted into 25. In the third step, $n = 3$, the step of the edges of the last shell is repeated, 20 sites, plus two sites of each triangular face, 20 sites; besides,
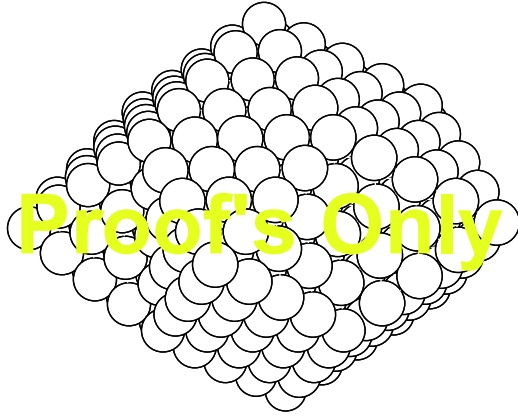
Figure 39. Star-type decahedron of order 4.

in one shell before the last, the interior decahedron, the equator vertexes are eliminated, 5 more sites are needed in order to obtain 40 sites to be eliminated in this step, and there is a complete total of 70 eliminated sites in three steps, and so on, for $n < v$ because $N_{AE} = 5(2v - 1)$ $[= 5(2v - 2)]$ for decahedra with (without) a central site; for $v = n - 1$, there are only 3 (2) sites AE; see Table 23.

Table 23 lists the truncated decahedra, resulting from decahedra with and without a central site, respectively. The order of the truncated decahedron consists of two numbers corresponding to the first and second columns of Table 23; the first column is the order of the decahedron generated v, and the second column is the number of steps n needed to eliminate the adequate sites, or is half of the sites eliminated from each edge at the equator; $n = 1$ means that only the vertexes at the equator are eliminated, the first step in the elimination process. The third column lists the total number of sites eliminated from the original decahedron to obtain the truncated decahedron of order vn, $N_{(-)}$; in the

Table 23. Truncated decahedron constructed from a certain decahedron of order v, with and without a central site.

| Order | | | With central site | | | | Without central site | | | |
| | | | | Sites in | | | | Sites in | | |
v	n	$N_{(-)}$	AE	sobrec	EC	Total	AE	sobrec	EC	Total
1	1	5	1	5	6	18				
2	1	5	3	20	26	100	2	11	15	49
3	1	5	5	45	56	282	4	31	40	176
	2	25	3	40	46	262	2	26	30	156
4	1	5	7	80	96	604	6	61	75	423
	2	25	5	75	86	584	4	56	65	403
	3	70	3	65	71	539	2	46	50	358
5	1	5	9	125	146	1106	8	101	120	830
	2	25	7	120	136	1086	6	96	110	810
	3	70	5	110	121	1041	4	86	95	765
	4	150	3	95	101	961	2	71	75	685
6	1	5	11	180	206	1828	10	151	175	1437
	2	25	9	175	196	1808	8	146	165	1417
	3	70	7	165	181	1763	6	136	150	1372
	4	150	5	150	161	1683	4	121	130	1292
	5	275	3	130	136	1558	2	101	105	1167

Note: n is the half of sites eliminated from each equator edge.

fourth (eighth), the number of sites per equatorial site AE remaining in the originals are presented (taking into account that in these sites are included the two new vertexes VE) per edge, for the polyhedron with a central site (without a central site) ($n = 1$ is the number of sites in edges in the original decahedron); finally, the fifth, sixth, and seventh columns (ninth, tenth, and eleventh) present the number of sites SE and EC and the total in the resulting truncated decahedron with a central site (without a central site). For example, the truncated decahedron without a central site of order 63, Figure 38, is generated from the decahedron with a central site of order 6 (1442 sites, 10 sites per edge, 151 sites SE, and 180 sites EC), and eliminates the 5 sites VE, 4 sites AE of each one of the equatorial edges of the surface, 2 sites AP from each edge toward the poles and the 5 VE sites from the immediate interior shell, so the truncated decahedron of order 63 has 6 sites per equatorial edge; 70 sites are eliminated, and it has a total of 136 sites SE, 150 sites EC, and 1372 in total.

The number of eliminated sites, the third column of Table 23, is the same for the two polyhedra, with and without a central site, and depends only on the number of steps n given, and is obtained by

$$N_{(-)} = \frac{5}{6}n(n + 1)(2n + 1).$$

Expressions for the number of sites SE, sites EC, and in total for the truncated decahedra with a central site are

$$N_{SE} = 5(v^2 - n + 1)$$
$$N_{EC} = 5(v^2 + v - n) + 1$$
$$N = \frac{20}{3}v^3 + 10v^2 + \frac{16}{3}v + 1 - \frac{5}{6}n(n + 1)(2n + 1)$$

and for the truncated decahedra without a central site are

$$N_{SE} = 5(v^2 - v - n + 1)$$
$$N_{EC} = 5(v^2 - n)$$
$$N = \frac{20}{3}v^3 + \frac{v}{3} - \frac{5}{6}n(n + 1)(2n + 1).$$

The truncated decahedron is a polyhedron formed by 22 vertexes, joined by 22 vertexes, attached by 40 edges, forming 10 pentagonal faces and 10 triangular. Vertexes are of three types: VP, VE, V', VP (2 vertexes), and are the same as in the original decahedron; VE and V' (10 vertexes each) result by pairs from elimination of the original VE and from elimination of sites from AE and AP; sites V' are found to be the end of the edges that converge toward the poles, that is, the edges AP join sites VP and V'. Edges are of 4 types: the original AP edges (10 edges) and AE (5 edges), but the shorter AT (20 edges) and AV' (5 edges) which make up the triangular faces (10 faces) formed upon elimination of the equatorial sites; the edges AV' join the vertexes V' by pairs, and the edges AT join sites VE and V'. So, any truncated decahedron will have vertex sites of type VP, VE, V', edge type AP, AE, AT, AV', and face type CT and CP. The number of VP sites is 2, of V' is 10, and of VE is also 10. The number of remaining sites is variable, and is listed in Table 24 for the truncated decahedra with and without a

Table 24. Geometric characteristics of truncated decahedra with and without a central site. Number of surface sites for each type of site in the polyhedron, and number of total sites in the surface and in the cluster.

		With central site								Without central site							
v	n	N_{AP}	N_{AE}	N_{AT}	$N_{AV'}$	N_{CP}	N_{CT}	N_σ	N	N_{AP}	N_{AE}	N_{AT}	$N_{AV'}$	N_{CP}	N_{CT}	N_σ	N
2	1	20	5	0	0	30	0	77	100	10	0	0	0	10	0	42	49
3	1	40	15	0	0	100	0	177	282	30	10	0	0	60	0	122	176
	2	30	5	20	5	80	0	162	262	20	0	20	5	40	0	107	156
4	1	60	25	0	0	210	0	317	604	50	20	0	0	150	0	242	423
	2	50	15	20	5	190	0	302	584	40	10	20	5	130	0	227	403
	3	40	5	40	10	150	10	277	539	30	0	40	10	90	10	202	358
5	1	80	35	0	0	360	0	497	1106	70	30	0	0	280	0	402	830
	2	70	25	20	5	340	0	482	1086	60	20	20	5	260	0	387	810
	3	60	15	40	10	300	10	457	1041	50	10	40	10	220	10	362	765
	4	50	5	60	15	240	30	422	961	40	0	60	15	160	30	327	685

central site. The number of surface sites is also listed as well as the total sites of the polyhedron. Columns 1 and 2 correspond to the order of the cluster v and n, respectively. Columns 3–8 (11–16) correspond to sites AP, N_{AP}, A_E, N_{AE}, AT, N_{AT}, AV', $N_{AV'}$, CP, N_{CP}, and CT, N_{CT}, respectively, and the two last columns to the surface sites N_σ and the total of sites N for truncated decahedra with (without) a central site.

From Table 25, it is possible to deduct the analytic expressions for the number of sites of the different types of sites as a function of the order of the truncated decahedron; the resulting expressions, common for the polyhedra with and without a central site, but depending on the number of steps made for the elimination of the sites, are N_{AT}, $N_{AV'}$, and N_{CT}:

$$N_{AT} = 20(n-1)$$
$$N_{AV'} = 5(n-1)$$
$$N_{CT} = 5(n-2)(n-1),$$

Table 25. Geometric characteristics for the decahedra with and without a central site, modified with surface reconstruction and added layers in the waist.

		With a central site					Without a central site			
v	μ	N_{EV}	N_{RF}	N_{ag}	N_σ	N	N_{RF}	N_{ag}	N_σ	N
2	1	0	0	0	122	205	0	0	77	114
	2	0	0	51	142	256	0	31	92	145
	3	5	15	102	162	307	10	62	107	176
3	1	0	0	0	242	497	0	0	177	331
	2	0	0	106	272	603	0	76	202	407
	3	5	25	212	302	709	20	152	227	483
4	1	0	0	0	402	969	0	0	317	708
	2	0	0	181	442	1150	0	141	352	849
	4	10	70	543	522	1512	60	423	422	1131
5	1	0	0	0	602	1661	0	0	497	1285
	2	0	0	276	652	1937	0	226	542	1511
	3	5	45	552	702	2213	40	452	587	1737
	5	15	135	1104	802	2765	120	904	677	2189

Note: v is the cluster order, μ is the number of equatorial layers in the polyhedron. Notice that for $\mu = 1$ Table 24 values are obtained. Although μ can take any value higher than zero, here only some values are presented.

The expressions for the other types of sites are as follows: for the one with a central site:

$$N_{AP} = 10(2v-1) - 10n$$
$$N_{AE} = 5(2v-1) - 10n$$
$$N_{CP} = 10(2v-1)(v-1) - 10n(n-1)$$
$$N_\sigma = 20v^2 - 5n^2 + 2$$

and without a central site:

$$N_{AP} = 20(v-1) - 10n$$
$$N_{AE} = 10(v-1) - 10n$$
$$N_{CP} = 10(2v-3)(v-1) - 10n(n-1)$$
$$N_\sigma = 20v^2 - 20v - 5n^2 + 7.$$

3.5.1. Modified Truncated Decahedra

The same method used to generate pentadecahedra is used here. Intermediate layers can be added to the truncated decahedra in order to obtain polyhedra with 15 lateral faces, 5 rectangular, and 10 trapezoidal (before triangular) (Fig. 40).
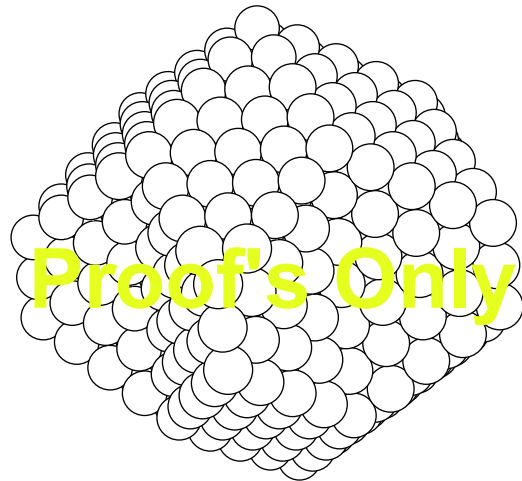
Figure 40. Star-type decahedron of order 4 and three equatorial layers added, with 661 sites.

This means that a layer of *SEC* type is added per each layer wanted to widen the polyhedron, so the polyhedron of Figure 9 has 4 equatorial layers; this means that 3 *SEC* layers were added. So, in a developed truncated decahedron, there will be the same sites as in one without development, except for the *CT* sites, triangular face, which convert into sites, *TR* trapezoidal face, and the sites generated when adding the *SEC* layers, sites in the rectangular faces *R* and in the vertical edges *AV*, joining the *VE* sites which are duplicated. The number of sites that will be added depends on the number of equatorial layers that the polyhedron will have, $N_{SE} + N_{EC}$ sites from the original truncated decahedron are added per each layer to widen them. It is to be noticed that, in this case, the *SE* sites corresponding to *AV'* and *AT* sites will be added to the surface also, that is, they will not remain internal, along with the *EC* sites. Table 26 lists the number of sites of the different types of sites in the truncated decahedron with and without a central site and developed.

When adding *SEC* layers to grow the truncated decahedron, the number of sites *VP*, *AP*, *AT*, *V'*, and *CP* are not modified, while the number of sites *VE* and *AE* are duplicated, sites *AV'* increase, and sites *CT* are converted to *TR*, and they increase with respect to the original truncated decahedron. Sites *R* and *AV* appear. From Table 26, it is possible to obtain the analytic expressions for the different number of sites in the developed truncated decahedron. The number of sites *AV'*, *AV*, and *TR* is common for the two polyhedra with and without a central site, that is, they only depend on n and μ, and their analytic expression is the following:

$$N_{AV'} = 5(n + \mu - 2)$$
$$N_{AV} = 10(\mu - 2)$$
$$N_{TR} = 5(n - 1)(n + 2\mu - 4).$$

And the expressions for the other types of sites, for the one with a central site, are

$$N_R = 5(2v - 2)(\mu - 2)$$
$$N_{ag} = (\mu - 1)(10V^2 + 5v - 10n + 6)$$
$$N_\sigma = 10v(2v - 1) - 5n(n + 7) + 5\mu(2n + 2v - 1)$$

and without a central site,

$$N_R = 10(v - 2)(\mu - 2)$$
$$N_{ag} = (\mu - 1)(10v^2 - 5v - 10n + 5)$$
$$N_\sigma = 20v(v - 1) - 10n(n + 1) + 5\mu(2n + v - 1) + 12.$$

Table 26. Geometric characteristics for developed truncated decahedra. Constructed from truncated decahedra of order $v\mu$, with and without a central site.

					With central site				Without central site			
v	n	μ	N_{TR}	N_{AV}	N_R	N_{ag}	N_σ	N	N_R	N_{ag}	N_σ	N
2	1	1	0	0	0	2	77	100	0	0	42	49
		2	0	0	0	46	45	146	0	26		75
3	1	1	0	0	182	287	0	127	181			

Note: μ is the number of equatorial layers. Notice that, for $\mu = 1$, Table 10 values are obtained. Although μ can take any value higher than zero, here are only presented some values.

The total number of sites is equal to the total number of sites in the original decahedron plus the N_{ag} sites.

3.6. Star-Type Decahedra

If the method to obtain a truncated decahedron is applied to a decahedron without a central site, which has an odd number of edges, it could be possible to eliminate all of the sites from the equatorial edges, except one, obtaining the star-type decahedron, named after the shape it represents (Fig. 41). For this decahedron, the equator edges from the original decahedron are practically eliminated, with one site remaining which converts to a vertex. The edges toward the poles are reduced to a half. The resulting figure has 17 vertices, 30 edges, 10 rhombohedral-shaped faces, and 10 lateral triangular faces (over the equator and joint in pairs). The types of sites present are the same as in the truncated decahedron, although the *CP* sites, pentagonal faces, change to *CR* sites, rhombohedral faces. The number of *VP* sites is 2, of *V'* is 10, and of *VE* is 5; the number of sites *AP*, *AT*, and *AV'* per edge is the same, not the number of edges of each type.

The analytic expressions for the star-type decahedra are presented next:

$$N_{AP} = 10(v - 1)$$
$$N_{CR} = 10(v - 1)^2$$
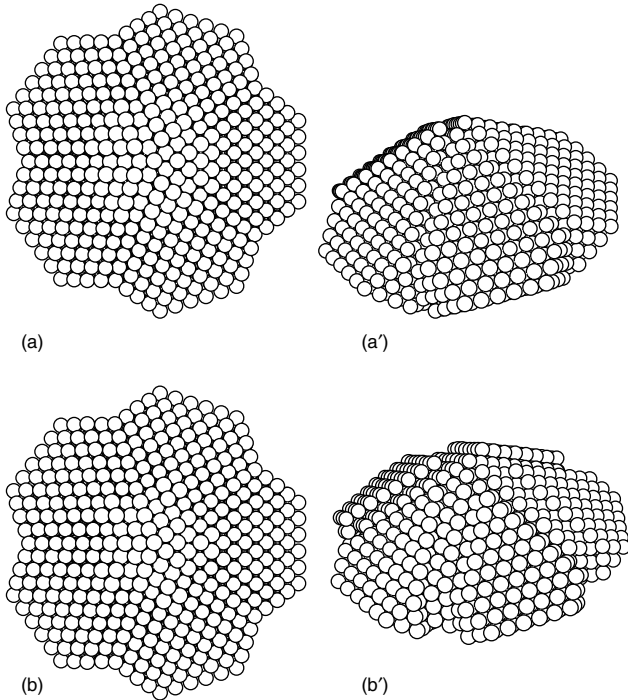$$N_{AT} = 20(v - 1)$$
$$N_{CT} = 5(v - 2)(v - 1)$$
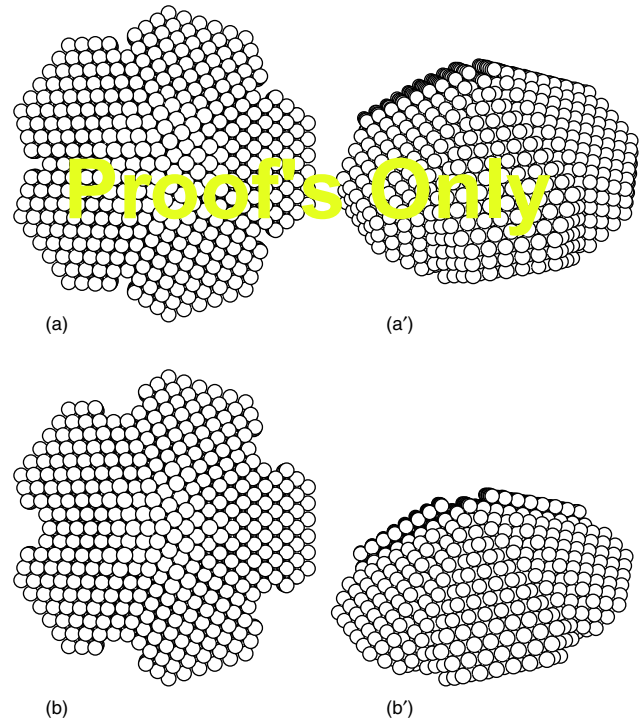
Figure 41. Truncated decahedron without central site of order 74 with (a) one single channel and 2032 sites, and (b) a triple channel and 1822 sites, eliminating *AP*, *VP*, *AV*, and *V'* sites. [(a') and (b') are lateral views of superior (a) and (b) views, respectively.]

$$N_{AV'} = 5(v - 1)$$

$$N_\sigma = 15v^2 + 2$$

$$N = \frac{5}{2}v(v+1)(2v+1) + 2v + 1.$$

To these decahedra, it is possible to add intermediate layers. The resulting figure has 10 trapezoidal lateral faces (which were triangular), and besides the 10 rhombohedral, 5 edges more (Fig. 42). When adding layers of type *SEC*, the number of sites VP, AP, AT, V', and CR are not modified, while the number of sites AE and VE are duplicated; the number of sites AV' increases, and the CT sites, triangular face, change to TR, trapezoidal face. Besides, sites AV appear. Analytical expressions for the number of sites for the modified sites are presented next:

$$N_{AV'} = 5(v + \mu - 2)$$

$$N_{TR} = 5(v - 1)(v + 2\mu - 4)$$

$$N_{AV} = 5(\mu - 2)$$

$$N_{ag} = (\mu - 1)[5v(v + 1) + 1]$$

$$N_\sigma = 5(v - 1)(3v + 2\mu + 1) + 10\mu + 7$$

$$N = .$$

The total number of sites is equal to the total number of sites in the original star-type decahedron plus the N_{ag} sites.

(a)   (a′)

(b)   (b′)

Figure 42. Truncated decahedron without central site of order 74 with (a) one single channel and 2047 sites, and (b) a triple channel and 1857 sites, eliminating AP, VP, and V' sites. [(a′) and (b′) are lateral views of superior (a) and (b) views, respectively.]

3.7. Additional Truncations in Decahedra

Just as in the decahedra, it is possible to add or eliminate sites to obtain modified structures of all of the types of decahedra previously described to obtain new structures. This is achieved by eliminating the sites on the edges which converge to a pole in a truncated decahedron, for example, the one of order 74 without a central site with 2139 sites; a truncated decahedron with one channel per edge converging to a pole is obtained, Figure 43(a), of 2047 sites, having an elimination of 92 sites, sites AP, VP, AV, and V'. If only the sites AP, VP, and V' are eliminated, Figure 44(a), a polyhedron of 2032 sites is obtained. If, now, the following edges are eliminated, the result is a truncated decahedron with a triple channel of 1877 sites; 170 sites were eliminated, [Fig. 43(b)], and also, it is possible to eliminate only the sites at edges without eliminating the AV sites [Fig. 44(b)]. This process can continue until obtaining the desired number of channels. It seems more convenient not to eliminate the AV sites because, when eliminating them, more abrupt holes are originated, so the ones of Figure 43 will be studied.

The expressions for the number of sites eliminated from a truncated decahedron with a single channel and with a central site is

$$N_{el} = 20v - 5\mu - 3.$$

For a triple channel,

$$N_{el} = 10(2v - \mu - 3),$$

without a central site and a simple channel,

$$N_{el} = 20v - 5\mu - 13,$$

and a triple channel,

$$N_{el} = 10(4v - \mu - 5).$$

Elimination of only the AP, VP, and V' does not affect the number of SE and EC sites from the original polyhedron, while upon elimination of the sites AV, they do modify. With this, it is possible to add the layers of type *SEC* to obtain truncated decahedra with channels and developed [Fig. 45(a) and (b)]. Table 27 lists also these polyhedra. The number of sites added is equal to the added in the developed truncated decahedra.

(a)   (b)
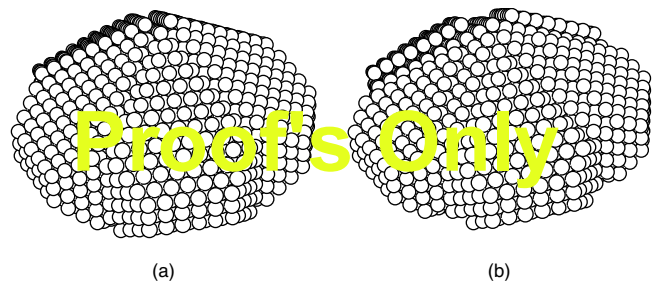
Figure 43. Truncated decahedron without central site of order 74 with (a) one single channel, and (b) with a triple channel and three layers in the waist.
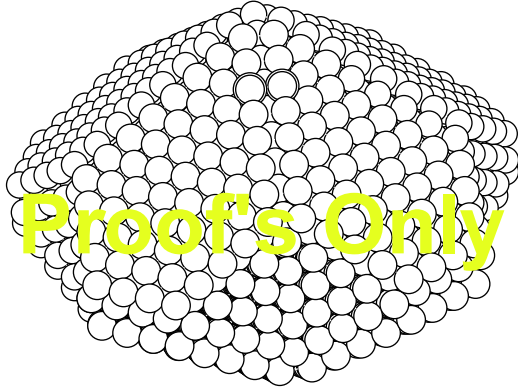
Figure 44. Truncated decahedron with surface reconstruction.

Another modification of a truncated decahedron with surface reconstruction, as explained for the decahedron, can be achieved by shifting the pentagonal face outwards and to the waist, eliminating then the sites AE, VE, AT, and V', which reflects in adding N_{ag} sites (Fig. 46). Table 28 lists the geometrical characteristics of the truncated decahedra modified by surface reconstruction. For the truncated decahedron with a central site are added

$$N_{ag} = 10[2v^2 + v - 2 - (\mu - 1)(\mu + 2)],$$

and without a central site

$$N_{ag} = 10[(2v - 3)(v + 1) - (\mu - 1)(\mu + 2) + 1].$$

When adding the sites for the surface reconstruction, the number of sites SE and EN is not affected. So, layers of type SEC can be added to obtain truncated decahedra with surface reconstruction and developed.
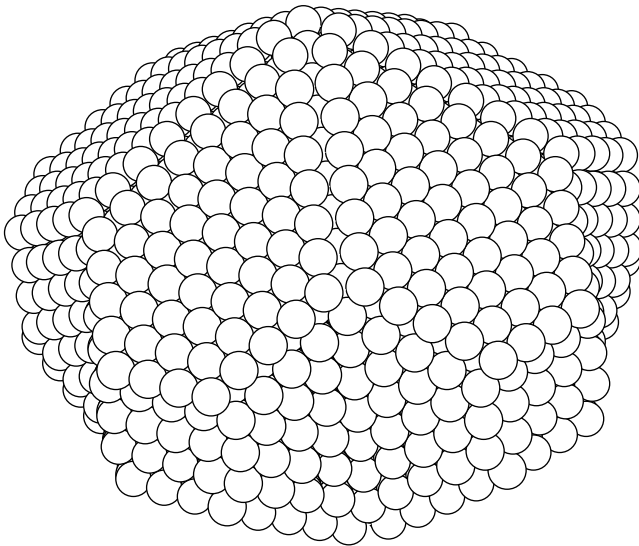
Figure 45. Truncated decahedron with surface reconstruction and with three SEC layers.

3.8. Icosahedra

The icosahedron (ICO) is a geometric figure with a central site, 12 vertexes, connected with 30 edges, and formed by 20 triangular faces; Figure 47 shows a 561 icosahedron. From this figure, it can be seen that the icosahedron can also be considered as two pentagonal pyramids with a rotation of 36° of one with respect to the other, and with intermediate layers, to adequately join the vertexes of both pyramids. Each icosahedric cluster presents a certain number of sites, but distributed in different layers, which are formed by equivalent sites: sites at the same distance from the origin, which have the same environment, and the same type of neighbors. Sites in the ICO are localized in triangular faces (T), edges (A), and vertexes (V). The order-1 ICO is formed by one central site and one first shell with only one layer of 12 vertexes. The second-order ICO is formed by the addition of one shell formed by 42 sites, to complete 55 sites, distributed in two layers: one layer of 30 sites A, and a second layer of 12 sites V. When adding a third shell of 92 sites, the ICO of third order of 147 sites is completed; the added sites are distributed in three layers: one of 20 sites T, one more of 60 sites A, and the third of 12 sites V. And successively, complete shells are added, forming clusters of order v.

The geometric characteristics of the ICO are listed in Table 29, to clusters of order 10. The first column lists the order of the cluster v. The following columns list the number of sites in each type of site in the cluster. Next is the number of sites of each type of site or the layers of each type of site. Finally, the number of sites in the shell and in the total of sites in the cluster is given. From this table, it is possible to obtain the dependence on the cluster order v from the total number of sites N, on the number of surface sites N_σ, the number of sites T, N_T and of sites A, N_A, as well as the number of layers of sites T, R_T, and sites A, R_A.

$$N = \frac{10}{3}v^3 + 5v^2 + \frac{11}{3}v + 1$$

$$N_\sigma = 10v^2 + 2$$

$$N_T = 10(v - 1)(v - 2)$$

$$N_A = 30(v - 1)$$

$$R_T^m = \begin{cases} \sum_{\alpha=1}^{m/2}(3\alpha + a) + \sum_{\alpha=1}^{(m/2)-1} 3\alpha; & m \\ & \begin{cases} v = 3m + a \\ a = -1, 0, 1 \end{cases} \\ \frac{1 + a}{1 + |a|} + \sum_{\alpha=1}^{(m-1)/2}(6\alpha + a); & m \end{cases}$$

$$R_A = \begin{cases} \dfrac{v}{2}; & v \\ \dfrac{v - 1}{2}; & v \end{cases}$$

Table 27. Truncated decahedron modified with one single channel and a triple channel, eliminating sites *VP*, *AP*, *V'*, and *AV'*.

v	n	N_{el}	N_{tSE}	N_{tEC}	N	N_{el}	N_{tSE}	N_{tEC}	N	N_{el}	N_{tSE}	N_{tEC}	N	N_{el}	N_{tSE}	N_{tEC}	N
2	1	32	15	26		30	15	16		22	6	15		10	6	5	
3	1	52	40	56		70	40	46		42	26	40		50	26	30	
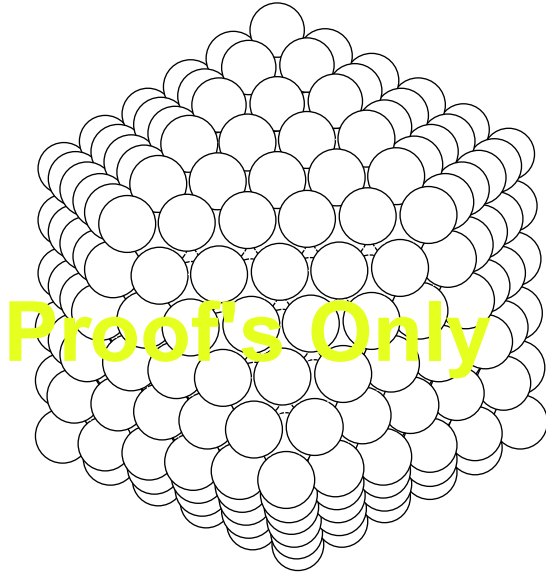
Figure 46. Icosahedron.

Table 28. Geometric characteristics for decahedra with and without a central site, modified with surface reconstruction.

	With central site			Without central site		
v	N_{ag}	N_σ	N	N_{ag}	N_σ	N
2	100	122	205	60	77	114
3	210	242	497	150	177	331
4	360	402	969	280	317	708
5	550	602	1661	450	497	1285

Note: v is the cluster order. Listed are the number of sites added N_{ag}, sites in the surface N_σ, and the total of sites N in the cluster.
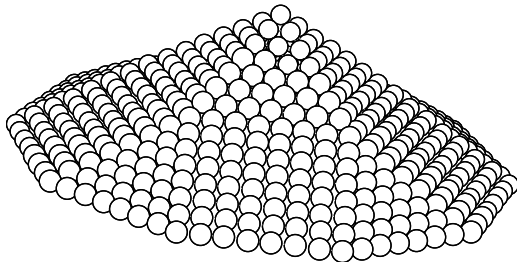
Figure 47. Decmon-type pyramid.

3.9. Decmon-Type Polyhedra

In contrast with previous polyhedra, decmon polyhedra are based on a decmon-type pyramid, which is constituted by 16 vertexes joined by 30 edges which form 15 faces: 5 rectangular type (100) and 10 triangular of type (111), 5 of which are equilateral and 5 isosceles, Figure 48. The 5 equilateral triangular faces (*TE*) have *m* sites per side, and each side of length $1.05(m-1)d_{NN}$, where d_{NN} is the distance to the first neighbors; the 10 isosceles triangle faces (*TI*) have *n* sites per side, two sides of length $(n-1)d_{NN}$ and one of length $1.05(n-1)d_{NN}$; the 10 rectangular faces (*R*), with $m \times n$ sites, have sides $1.0(n-1)d_{NN}$ and $1.05(m-1)d_{NN}$.

Equal sides of faces *TI* coincide with the sides of faces *R*, and the different side forms part of the equator along with one of the sides of *R* faces. Faces *TE* coincide with the pole, and have a common side; also, each face has a common face with one *R* face. The angle between the planes of *R* and *TE* faces is 190.66°, and between *R* and *TI* faces is 161.94°. The 16 vertexes (*V*) are of three types: 1 pole, where the 5 *TE* faces converge, 5 where the three types of faces (*V*3) converge, and 10 at the equator, and where an *R* and a *TI* face converge (*V*4). These vertexes are joined by 30 edges (*A*) of 5 types: 5 of length $1.05(m-1)$, between *TE* faces and which converge at the poles and join the *VP* and *V*3 vertexes (*AE*); 5 of length $1.05(m-1)$, between *TE* and *R* faces and join vertexes *V*3 (*A*3); 10 of length $1.0(n-1)$ between *TI* and *R* faces and join vertexes *V*3 and *V*4 (*A*34); and 10 at the equator, 5 of them of length $1.05(m-1)$ of one *R* (*AR*) face and 5 of length $1.05(n-1)$ of one *TI* (*AI*) face, which joins *V*4 vertexes. Based on the decmon pyramid, many polyhedra can be obtained: the

Table 29. Geometrical characteristics for icosahedra.

	Sites at			Layers of			Layers of		Sites at	
v	T	A	V	T	A	V	en v	Total	en v	Total
1	0	0	12	0	0	1	1	1	12	13
2	0	30	12	0	1	1	2	3	42	55
3	20	60	12	1	1	1	3	6	92	147
4	60	90	12	1	2	1	4	10	162	309
5	120	120	12	2	2	1	5	15	252	561
6	200	150	12	3	3	1	7	22	362	923
7	300	180	12	4	3	1	8	30	492	1415
8	420	210	12	5	4	1	10	40	642	2057
9	560	240	12	7	4	1	12	52	812	2869
10	720	270	12	8	5	1	14	66	1002	3871

Note: v is the cluster order; T, A, and V are the type of sites in the icosahedron, triangular face, edge, and vertex, respectively. Listed is the number of sites of each type of site, the number of layers of each site, and the number of layers and sites in each shell and in the entire cluster.
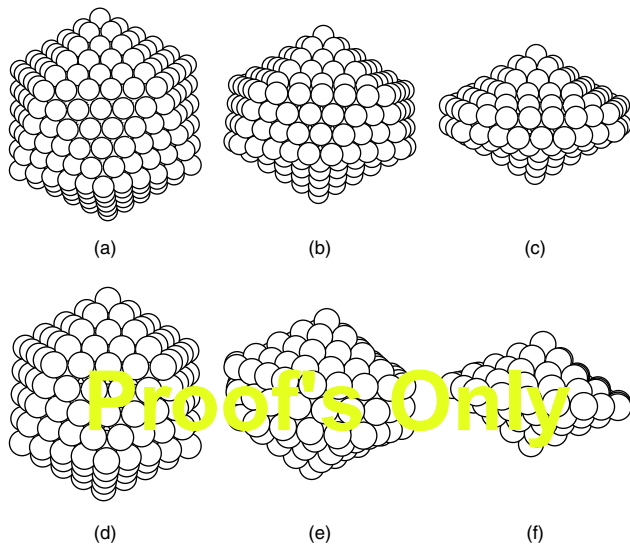
Figure 48. (a) Icosahedron I_h of 561 atoms. (b) Truncated icosahedron TI_h of 409 atoms. (c) TI_h of 257 atoms. (d) I_h of 309 atoms. (e) TI_h of 207 atoms. (f) TI_h of 105 atoms.

truncated icosahedron, the decmon, and the decmon with intermediate aggregated layers.

3.9.1. Decmon Icosahedra

The truncated icosahedron or icosahedron of decmon type is a polyhedron obtained upon adequate truncation and in a symmetric way of an icosahedron (however, they can be truncated asymmetrically also). An asymmetric truncation of an icosahedron is done in the following manner: surface sites forming a cover with a pentagonal pyramid shape over a vertex, yielding a decmon-type pyramid, with rectangular faces and a side with a length of d_{NN}. In order to perform a symmetrical truncation, first a cover like that previously presented has to be eliminated, but from the vertex diagonally opposite. The following truncations have to be done by elimination of sites which form a pyramid-shaped cover of decmon type. Figure 49 shows two icosahedra with their corresponding truncations. Figure 49(a) [Fig. 14(d)] shows a 561 (309) site icosahedron that, upon truncation, yields the 409 (207) sites TI_h (observe in this one the decmon-type pyramid); Figure 49(b) [Fig. 49(e)]
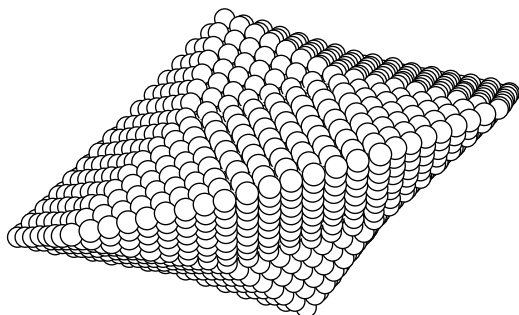
Figure 49. Decmon-type polyhedron.

which, when truncated, again yields the 257 (105) sites TI_h, Figure 49(c) [Fig. 49(f)]. From this figure, it can be observed that it is possible to obtain the TI_h of two different kinds: (1) the TI_{ha} [Fig. 49(f)], and (2) the TI_b [Fig. 49(b), (c), (e)].

3.9.2. Truncated Icosahedra TI_{ha}

As shown in Figure 49(f), it is formed by 22 vertexes, joined by 50 edges, forming faces of three types: rectangular, R type (110), and two triangular of type (111), one equilateral (TE) and the other isosceles (TI). Also, from this figure, it can be noticed that the TI_{ha} can be formed by attaching two decmon-type pyramids, with TI faces coinciding with TI faces at the equator or waist.

3.9.3. Truncated Icosahedra TI_{hb}

As shown in Figure 49(b), (c), and (e), it is formed by 32 vertexes, joined by 80 edges of I order to form 50 faces: 10 vertexes, 30 edges, and 20 faces more than TI_{ha}. The 10 vertexes form one plane, and are of equator type from TI_{ha}, and the 20 edges connect the vertexes from the two planes forming the 20 extra faces of trapezoidal type Tr, now having the waist of the TI_{hb}.

TI_h are characterized by three numbers (m, n, r) where m (n) $[r]$ is the number of sites in one edge between faces TE, $(R$ and $TI)$ $[Tr]$, including vertexes; for example, in Figure 49(f), there is TI_{ha} (3, 3, 1), and in Figure 49(b), (e), and (f), there are the TI_{hb} (5, 2, 4), (4, 3, 2), and (4, 2, 3). It is clear that, based on this notation, to the icosahedra corresponds an $m = r$ and an $n = 1$; for example, (6, 1, 6) and (5, 1, 5) from Figure 49(a) and (d), respectively. From Figure 49, it can be seen also that TI_{ha} results from complete truncation (when there is only one or two edge sites from the original icosahedron) of an icosahedron with an odd number of sites in the edges.

By truncation of an icosahedron, only some TI_h are obtained, and upon truncation of another icosahedron, others are obtained; in each truncation, a certain number of sites are eliminated, but the same number in each truncation. Table 30 presents some of the geometric characteristics of TI_h. The first column shows the order of the icosahedron from where the v comes, the second column shows the number of truncations done n_t, n, the third column shows the three characteristic numbers, in the fourth column is the number of sites eliminated from the original icosahedron n_-, in the fifth column the number of sites remaining in the surface N_σ is shown, and in the sixth column, the total number of sites in TI_h, N is shown. So, for example, the TI_h (5, 3, 3) comes from the icosahedron of order 6, to which 424 sites were eliminated in two truncations, yielding a TI_h of 499 sites, of which 242 are at the surface.

From Table 30, it can be seen that the maximum number of truncations is $v/2$ $[(v-1)/2]$, the minimum value of $m+n+r$ is $(v+3)$ $[(v+4)]$, of m is $v/2+1[(v+1)2+1]$, and of r is 1 [1]; the maximum n value is $(v/2+1)$ $[(v-1)/2+1]$ for v even (odd); besides, the maximum values for $m+n+r$ are $(2v+3)$, of m and r is $v+1$, and the minimum value of

Table 30. Geometric characteristics for truncated icosahedra TI_{ha}.

v	n_t	mnr	n_-	N_σ	N
1	0	2,1,2	0	12	13
2	0	3,1,3	0	42	55
	1	2,2,1	32	22	23
3	0	4,1,4	0	92	147
	1	3,2,2	62	62	85
4	0	5,1,5	0	162	309
	1	4,2,3	102	122	207
	2	3,3,1	204	82	105
5	0	6,1,6	0	252	561
	1	5,2,4	152	202	409
	2	4,3,2	304	152	257
6	0	7,1,7	0	362	923
	1	6,2,5	212	302	711
	2	5,3,3	424	242	499
	3	4,4,1	636	182	287

Note: n_t is the number of truncations made.

n is 1 for all v. For n_-, N_σ, and N, there are the following expressions:

$$n_- = 2n_t\left[1 + \frac{5v(v+1)}{2}\right]$$

$$N_\sigma = (N_\sigma)_{\text{ico}} - 10v$$
$$= 10v^2 - 10v + 2$$

$$N = (N)_{\text{ico}} - n_-$$
$$= \frac{10}{3}v^3 - 5v^2 + \frac{11}{3}v - 1 - 2n_t\left[1 + \frac{5v(v+1)}{2}\right].$$

3.9.4. Decmon Polyhedra

A decmon polyhedra, Figure 50, is very similar to TI_{ha}; it has the same number of vertexes, edges, and faces, and the same type of sites. Also, it can be constructed by two decmon-type pyramids. The difference is that, at the equator or at the waist, faces TI have TI layers, and R have R faces.

The lengths of decmon edges, even when they are of three sizes, are related to the m and n of the decmon pyramid, characterizing each particular decmon. mn can be considered as the order of the decmon (decmon mn), and the values taken by m and n are not limited. m and n are the number of edges AE and $A34$, respectively. Indeed, every decmon is formed by centered shells in one decmon of an order in which: (1) $m = 1$ and $n = 1$, (2) $m > 1$ and $n = 1$,
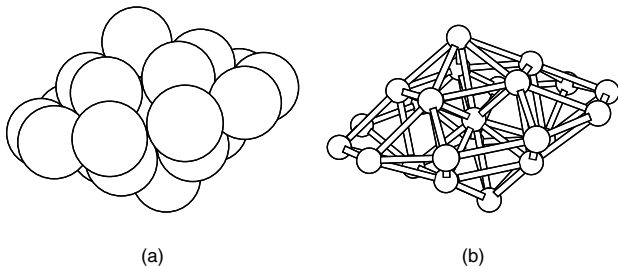
or (3) $m = 1$ and $n > 1$, which are the smallest. For example, decmon of Figure 15 is of order 67, decm67, which in turn is a decm56 + one shell, decm56 is a decm45 + one shell, decm45 is a decm34 + one shell, decm34 is a decm23 + one shell, and decm23 is decm12 + one shell, decm12 being the smallest of this family.

Decmon of order 11 (decm11) is the smallest of all decmons, and the edges at the equator are all the same; Figure 51. It only has sites in vertexes, and is centered in one site, having a cluster of 23 sites. There is a decmon family mm, based on decm11, and the possible decmons to be created are decm22, decm33, decm44, decm55, and so on.

The geometric characteristics of a decahedra-type decmon of order mm are listed in Table 31. The first column lists the m value, the four following columns list the number of sites in each type of site, rectangular sites R, in triangular faces T, in edges A, and in vertexes V. It should be clear that T sites include TE and TI sites, which in number are equal. Besides, the 5 types of edges are included in A, corresponding 1/5 to each of AE and AR, 1/10 to AC, and another to $A34$ and 2/5 to AI. Vertexes are always 22, and from the three kinds already mentioned, 2 poles, 10 $V3$, and 10 $V4$. The following three groups of two columns list the number of sites in the plane above the equator, at the equator, and for the number of sites in clusters, for each shell and in total. Figure 52 shows the decmon for $m = 4$ and of 609 atoms.

From Table 31, it can be seen that, for a decmon of order m, the dependency with m values of the number of sites in a rectangular face N_R, triangular face N_T, edges N_A, surface N_σ, and total N is given by the following expressions:

$$N_R = 10(m-1)^2$$
$$N_T = 10(m-1)(m-2)$$
$$N_{AC} = 50(m-1)$$
$$N_\sigma = 20m^2 + 2$$
$$N = \frac{20}{3}m^3 + 10m^2 + \frac{16}{3}m + 1.$$

Also, expressions for the number of sites SE and EC can be calculated for each m, N_{SE}, N_{EC}, and total N_{tSE} and N_{tEC}:

$$N_{SE} = 10(m-1)$$
$$N_{tSE} = 5(m^2 - m + 1)$$
$$N_{EC} = 10m$$
$$N_{tEC} = 5m(m+1) + 1.$$

Figure 50. Decmon-type decahedron of order 11. In (b), the sizes of the atoms of (a) were reduced to more clearly observe the squared and triangular faces by bondings to first neighbors, and to show that this is a polyhedron with a central site.
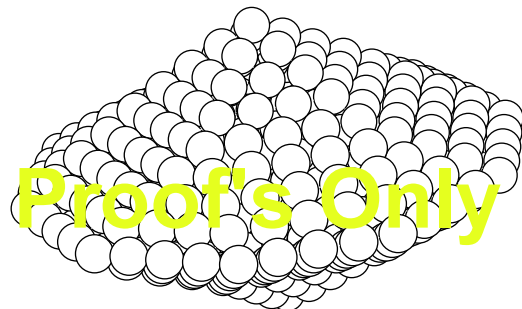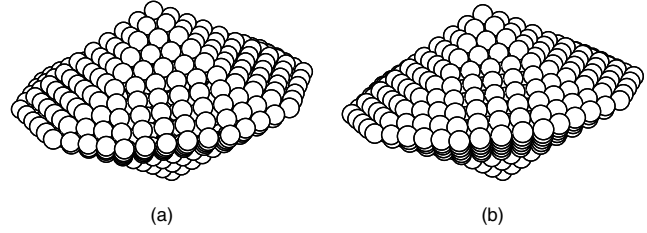

Figure 51. Decmon-type decahedron of order 44, decm44, of 609 sites.

Table 31. Geometric characteristics for decmons of family of order *mm* based on decmons of order 11, decm11.

m	R	Sites at T	A	V	sobrec m	Total	Equator m	Total	Sites Total
1	0	0	0	22	5	5	10	11	22	23
2	10	0	50	22	10	15	20	31	82	105
3	40	20	100	22	20	35	30	61	182	287
4	90	60	150	22	30	65	40	101	322	609
5	160	120	200	22	40	105	50	151	502	1111
6	250	200	250	22	50	155	60	211	722	1833
7	360	300	300	22	60	215	70	281	982	2815
8	490	420	350	22	70	285	80	361	1281	4096
9	640	560	400	22	80	365	90	451	1622	5718
10	810	720	450	22	90	455	100	551	2002	7720

The next family decmon size, following the decmon family *mm*, is the decmon family *mn*, with $n = m + 1$ or $n = m - 1$, and based on the decm12 and decm21, respectively. Decm12 and decm21 have the same number of sites, a total of 54, although decm21 is more elongated toward the poles; Figure 53. Decm12 has 20 sites in edges $A34$ and 5 in AI, while decm21 has 10 sites in edges AE, 10 in $A3$, and 5 in AR, and both are centered in a decahedron of 7 sites, regular for decm12 and more elongated toward the poles for decm21. From decm12, other decm can be generated: decm23, decm34, decm45, decm56, and so on. From decm21, the decm generated are decm32, decm43 decm54, decm65, and so on.

The geometric characteristics of decmon-type decahedra, of order *mn*, with $m = n - 1$ and $m = n + 1$, are listed in Table 32. The first two columns list the *m* and *n* values, and in the following 10 columns, the number of sites of each type of site, which considers only the sites in rectangular faces R, equilateral triangular faces TE, isosceles triangular faces TI, of two types of edges, AC and AL and in vertex V. It should be clear that sites in AC (AL) include sites AE, AR, and AC (AI and $A34$), corresponding (2/5) to AE, (2/5) to $A3$, and (1/5) to AR (4/5 to AI and 1/5 to $A34$). The vertexes are always 22, and come from the three types already mentioned. The number of sites R and V is common for the two decmon *mn* families, with $m = n - 1$ and $m = n + 1$, while the number of sites TE and TI, AC and AL are interchanged. Columns 8–11 correspond to the interchange of values of *m* and *n*; this is what happens with decmon families of order *mn* with $m = n + 1$. The following three groups of two columns list the number of sites in the plane

(a) (b)
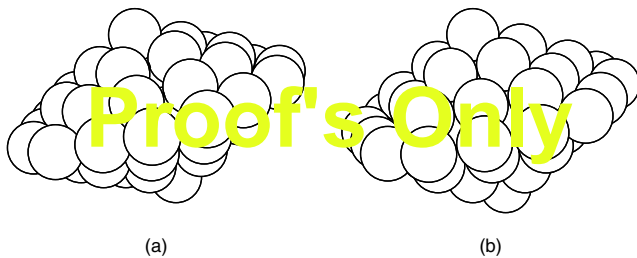
Figure 52. Decmon-type decahedra of 54 sites and (a) order 12, (b) order 21.

(a) (b)

Figure 53. Decmon-type decahedron of 835 sites of (a) order 45, decm45, and (b) order 54, decm54.

above the equator (sobrec), at the equator, and the numbers of sites in the cluster, per shell and in total; these values are common to the *m* and *n* values, and are interchanged. Figure 54 shows decmons of order 45 and 54, of 835 atoms.

The *mn* decmon families, with $m = n - 1$ and $m = n + 1$, follow in size the ones of decmon of order *mn*, with $m = n - 2$ and $m = n + 2$, and are based on decm13, and decm31, respectively.

The decm13 and decm31 decmon have the same number of sites, 105 in total, although decm31 is more elongated toward the poles; Figure 55. Decm13 has 40 sites in edges $A34$, 10 in AI, and 10 in faces TI, while decm31 presents 20 sites in edges AE, 20 in $A3$, 10 in AR, and 10 in faces TE, and both are centered at a decahedron of 23 sites with a central site, regular for the decm13 and more elongated toward the poles for the decm31. From the decm13, it is possible to generate the decm24, decm35, decm46, decm57, and so on. From decm 31, it is possible to obtain the decm42, decm53, decm64, decm75, and so on. The geometrical characteristics of the decahedra-type decmon of order *mn*, with $m = n - 2$ and $m = n + 2$, are listed in Table 33, with the same indications for the columns as in Table 32. Figure 56 shows the 1111 atoms decmon of order 46 and 64.

From Tables 31–33, it is deduced that, for a decmon order *mn*, the dependency on the *m* and *n* values of the number of sites in rectangular face N_R sites in the equilateral triangular face N_{TE} of sites in an isosceles triangular face N_{TI} of sites in the edge type AC (AE, $A3$, and AR), N_{AC}, of sites in the edge type AL (AI and $A34$), N_{AL}, and of sites in the surface N_σ is given by the following expressions:

$$N_R = 10(m - 1)(n - 1)$$
$$N_{TE} = 5(m - 1)(m - 2)$$
$$N_{TI} = 5(n - 1)(n - 2)$$
$$N_{AC} = 25(m - 1)$$
$$N_{AL} = 25(n - 1)$$
$$N_\sigma = 5(m + n)2 + 2.$$

Also, it is possible to obtain the number of sites in the immediate superior plane over the equator for each *m* and *n*, N_{SE} and in total N_{tSE}, and in the equator N_{ec} and N_{tec} for the number of sites in the surface and the number of sites

Table 32. Geometric characteristics for decmon of the family of order mn, with $m = n - 1$ and $m = n + 1$, based on the decmon of order 12, decm12, and of order 21, decm21.
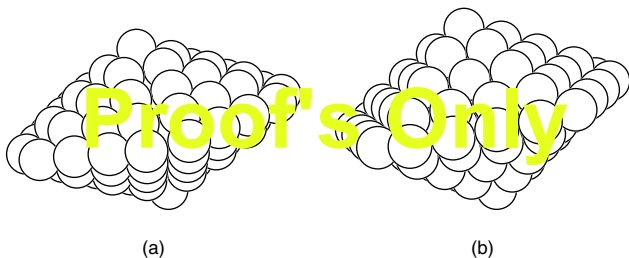
| Order | | | Sites at | | | | | | | | | Sites sobrec | | Sites equator | | Sites at | |
m	n	R	TE	mn TI	AC	AL	TE	TI	nm AC	AL	V	mn	Total	mn	Total	mn	Total
1	2	0	0	0	0	25	0	0	25	0	22	10	11	15	20	47	54
2	3	20	0	10	25	50	10	0	55	25	22	20	31	25	45	127	181
3	4	60	10	30	50	75	30	10	75	50	22	30	61	35	80	247	428
4	5	120	30	60	75	100	60	30	100	75	22	40	101	45	125	407	835
5	6	200	60	100	100	125	100	60	125	100	22	50	151	55	180	607	1442
6	7	300	100	150	125	150	150	100	150	125	22	60	211	65	245	847	2289
7	8	420	150	210	150	175	210	150	175	150	22	70	271	75	320	1127	3416
8	9	560	210	280	175	200	280	210	200	175	22	80	351	85	405	1447	4863
9	10	720	280	360	200	225	360	280	225	200	22	90	441	95	500	1807	6670
10	11	900	360	450	225	250	450	360	250	225	22	100	541	105	605	2207	8877

for each m and n and in total for the decmon for each combination of m and n used here. For $m = n$,

$$N_{se} = 10(m - 1)$$
$$N_{tse} = 5(m^2 - m + 1)$$
$$N_{ec} = 10m$$
$$N_{tec} = 5m(m + 1) + 1$$
$$N_{\sigma} = 20m^2 + 2$$
$$N = \frac{20}{3}m^3 + 10m^2 + \frac{16}{3}m + 1.$$

For $n = m \pm 1$,

$$N_{se} = 10m$$
$$N_{tse} = 5m(m + 1) + 1$$
$$N_{ec} = 10m + 5$$
$$N_{tec} = 5m(m + 2) + 5$$
$$N_{\sigma} = \begin{cases} 20m^2 + 20m + 7, & \text{for } (+) \\ 20m^2 - 20m + 7, & \text{for } (-) \end{cases}$$
$$N = \begin{cases} \frac{20}{3}m^3 + 20m^2 + \frac{61}{3}m + 7, & \text{for } (+) \\ \frac{20}{3}m^3 + \frac{1}{3}m, & \text{for } (-). \end{cases}$$

For $n = m \pm 2$,

$$N_{se} = 10m + 5$$
$$N_{tse} = 5m(m + 2) + 5$$
$$N_{ec} = 10(m + 1)$$
$$N_{tec} = 5m^2 + 6m + 11$$
$$N_{\sigma} = \begin{cases} 20m^2 + 40m + 22, & \text{for } (+) \\ 20m^2 - 40m + 22, & \text{for } (-) \end{cases}$$
$$N = \begin{cases} \frac{20}{3}m^3 + 30m^2 + \frac{136}{3}m + 23, & \text{for } (+) \\ \frac{20}{3}m^3 - 10m^2 + \frac{16}{3}m - 24, & \text{for } (-). \end{cases}$$

3.9.5. Modified Decmon

To obtain decmon-type decahedra, widened with extra layers, the same procedure is followed as with the decahedrons, separating the decmon as two pyramids with parallel bases, making the vertexes coincide, and adding layers of type *SEC*; Figure 57. The obtained figure has 10 regular lateral faces besides the ones previously mentioned, and 10 more edges.

4. SYNTHESIS OF NANOPARTICLES

Metal clusters have been formed in a supersonic beam; this method to prepare colloidal metals in nonaqueous media was first reported by the group of Andres at Purdue University [30–32]. A supersonic beam source was used; this

(a) (b)

Figure 54. Decmon-type decahedra of (a) order 13, and (b) order 31.

(a) (b)
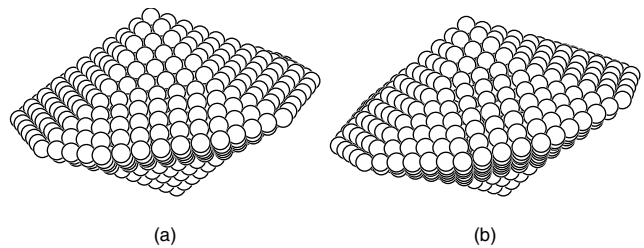
Figure 55. Decmon-type decahedron of 1111 sites of (a) order 46, decm46, and (b) order 64, decm64.

Table 33. Geometric characteristics for decmon of families of order *mn*, with $m = n - 2$ and $m = n + 2$, based on decmon of order 13, decm13 and of order 31, decm31.

| Order | | | | Sites at | | | | | | | | | Sites sobrec | | Sites equator | | Sites at | |
| | | | | *mn* | | | | *nm* | | | | | | | | | | |
m	*n*	*R*	*TE*	*TI*	*AC*	*AL*	*TE*	*TI*	*AC*	*AL*	*V*	*mn*	Total	*mn*	Total	*mn*	Total
1	3	0	0	10	0	50	10	0	50	0	22	15	20	20	31	82	105
2	4	30	0	30	25	75	0	0	75	25	22	25	45	30	61	182	287
3	5	80	10	60	50	100	60	10	100	50	22	35	80	40	101	322	609
4	6	150	30	100	75	125	100	30	125	75	22	45	125	50	151	502	1111
5	7	240	60	150	100	150	150	60	150	100	22	55	180	60	211	722	1833
6	8	350	100	210	125	175	210	100	175	125	22	65	245	70	281	982	2815
7	9	480	150	280	150	200	280	150	200	150	22	75	320	80	361	1282	4097
8	10	630	210	360	175	225	360	210	225	175	22	85	405	90	451	1622	5719
9	11	800	280	450	200	250	450	280	250	200	22	95	500	100	551	2002	7721
10	12	990	360	550	225	275	550	360	275	225	22	105	605	110	661	2412	10143

instrument produces metal clusters with a controlled mean diameter in the range of 1–20 nm in size. Once the clusters have nucleated, the cluster aerosol is directed through a spray chamber to be placed in contact with a fine spray of organic solvent and surfactant.

However, conceptually, the simplest method of preparing colloidal metals is the condensation of atomic metal vapor into a dispersing medium [33]. Given the high oxidation potential of most atomic metals (for example, the oxidation potential for atomic gold is −1.5 V), the use of water as the diluent's phase can be ruled out, so exclusively inert organic liquids are going to be used in this procedure. Since the activation energy for the agglomeration of metal atoms is very low, the possibility for competing molecular complex formation processes which have higher activation energies can be mitigated by operating at low temperatures.

The use of metal vapors cocondensed with organic vapors to prepare colloidal metals in nonaqueous media was first reported by Roginski and Schalnikoff in 1927 [34], some 50 years before the recent wave of activity in metal vapor chemistry. The organosols were prepared at reduced pressure by the evaporation of relatively volatile metals such as cadmium, lead, and thallium, and a subsequent cocondensation of these with the vapors of organic diluents such as benzene and toluene on a liquid air-cooled cold finger. After cocondensation was complete, a colloidal suspension of the

metal was obtained by warming up the frozen matrix and collecting the liquid (Fig. 58).

A new metal vapor synthesis system for the preparative scale cocondensation of metal vapors with aerosols of organic liquids was recently achieved by Bradley's group [35]. The use of aerosol overcomes one limitation of the other methods, in which the organic diluent must be either volatile or has a liquid range which extends to a temperature low enough to reduce its vapor pressure to a useful value. The aerosol droplets, ca. 1 μm in diameter, are generated by feeding the organic liquid (neat liquid, polymer solutions, solutions of nonvolatile ligands) into an ultrasonic atomizing nozzle from which they fall onto a rotating plate cooled to 77 K in a vacuum chamber, as shown in Figure 2. Vapors of one or more metals, obtained by simultaneous sputtering from metal or alloy targets, are then cocondensed with the aerosol. This results in the formation of a frozen organometallic matrix, which is then warmed up to allow the aggregation of the metal atoms. The resulting colloid solution is removed from the reactor under helium atmosphere for characterization and further studies.

In the 1980s, several research groups in Japan prepared metal particles of Al, Mg, Mn, Be, Te, Fe, Pb, Co, Ni, Cd, Ag, In, Pd, and Au by these method [36–45]. The work most
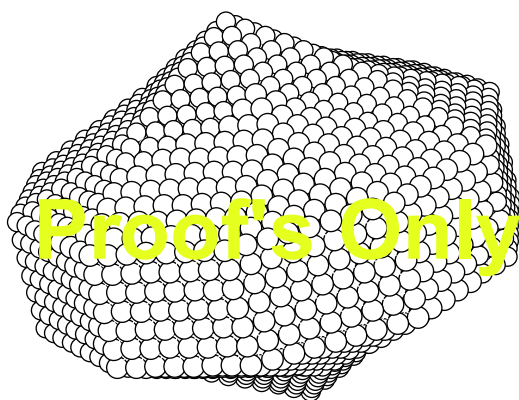
Figure 56. Decmon-type decahedron of order 78 with 6 intermediate layers added.
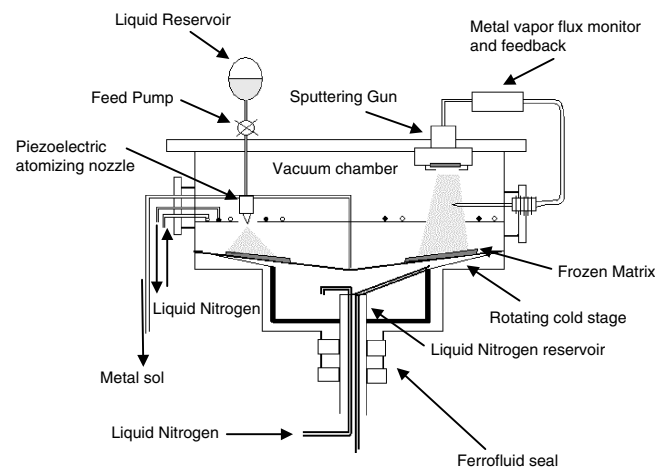
Figure 57. Schematic of sputtering source metal vapor/aerosol for metal colloid preparation (after design of from Bradley [35]).
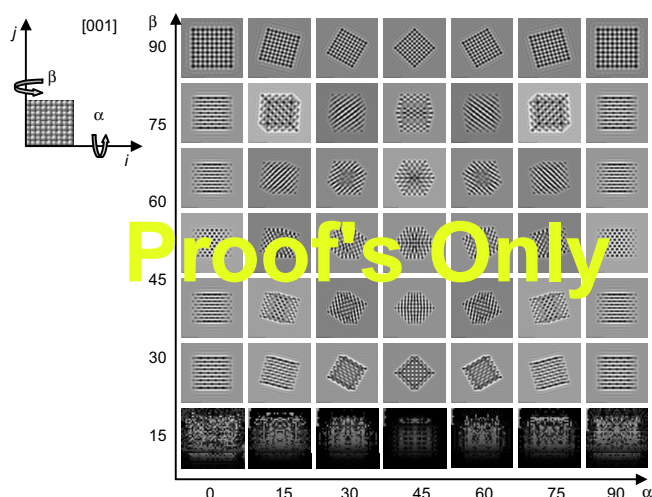
Figure 58. Simulation of HREM images of a cubooctahedral particle in different orientations with respect to the electron beam.

recently performed was by Uyeda in 1991 [46]. This study demonstrated the feasibility of producing films of almost any metal or semiconductor by metal vapor deposition in a noble gas high-pressure atmosphere.

Another method to produce nanoparticles is the bioreduction method. Several researchers established that live and nonlive biologic systems such as algae have the ability to absorb metal ions from solutions through their cell walls and various cellular constituents [47, 48]. Studies have shown that algae are able to bind gold ions from aqueous solutions and form colloidal particles on their surfaces, yet the mechanisms have not been fully understood [49–53]. Several plants have been studied for their unique biochemical ability to accumulate metal compounds over extended periods. In fact, plant species such as *Douglas-fir* and *rye grass* are utilized as biological indicators of geologic gold deposits [54, 55]. Some other plants such as Indian mustard have been utilized for phytomining; the accumulation of valuable metals comes from low concentrations in soils by plants [56, 57]. Furthermore, Lujan and co-workers reported that a purple color, similar to "Purple of Cassius," resulted when aqueous Au(III) was reacted with the biomaterials in their study, indicating the formation of gold colloids [58–60]. Plants may possess a unique natural chemical stabilization mechanism that allows the formation of nanoparticles. In addition, the plant biomaterials may be isolated for a more thorough study of the colloidal information mechanisms. Therefore, by taking advantage of the naturally occurring compounds found within the plant systems, a novel method may be found to generate similarly sized stable metal colloids. While consistency in nanoparticle size and shape is important to many materials, differences in nanoparticle synthesis may also lead to changes in particle conformation and spatial arrangement, which may provide better nanoscopic building blocks to form new raw materials with distinctly different properties than their macroscaled counterparts.

Recently, it was shown that live plants can uptake metal solutions and produce nanoparticles [61]. This approach is very promising for further developments in nanotechnology.

All of the particles reported in the present work were produced by the methods described above.

A third way to prepare metal nanoparticles is the colloidal methods discussed in the Introduction. In the original Brust et al. reaction [13], the addition of dodecanethiol to the organic-phase $AuCl_4^-$ (1:1 molecule), followed by reduction with BH_4^-, led to dodecanethiolate protected Au clusters having a 1–3 nm range of core diameters:

$$AuCl_4^- (\text{toluene}) + RSH \longrightarrow (-AuSR^-)_n (\text{polymer})$$

$$(-AuSR^-)_4 + BH_4 \longrightarrow Au_x (SR)_y.$$
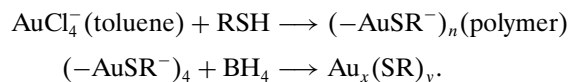
Subsequent reports have shown that a wide range of alkanethiolate chain lengths ($C3–C24$) [62], ω-functionalized alkanethiolates, and dialkyl disulfides [63] can be employed in this same protocol. An example of a passivated nanoparticles formula is $Au_{145}(S(CH_2)_5CH_3)_{50}$.

Pt, Rh, and Pd salts can be used following the same method. One of the possible reactions is

$$AuCl_4^- (\text{toluene}) + PtCl^- + R - SH$$
$$\longrightarrow (-Au_x Pt_y SR^-)_n (\text{polymer})$$
$$(-Au_x Pt_y SR^-)_4 + BH_4 \longrightarrow Au_x Pt_y (SR)_z.$$
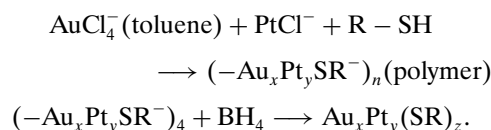
The details of these reactions have not been completely understood; however, the behavior of the reaction is consistent with a nucleation-growth-passivation process: (1) larger thiol: gold mole ratios give smaller average nanoparticle metal core sizes [64, 65], (2) fast reductant addition and cooled solutions produce smaller, more monodisperse nanoparticles [66, 67], and (3) quenching the reaction immediately following reduction produces higher abundances of very small core sizes (≤ 2 nm).

The Schiffrin reaction tolerates considerable modification with regard to the protecting ligand structures. While alkanethiolate passivated nanoparticles (a) are nonpolar, highly polar ligands (b–d) can yield water-soluble passivated nanoparticles in modified synthesis. Nanoparticles passivated with arenethiolate [68–71] (e–g) and (γ–mercaptopropyl) trimethyloxysilane ligands (h) have also been prepared. Sterically bulky ligands tend to produce smaller Au core sizes (relative to alkanethiolate-passivated nanoparticles prepared using equal thiol/$AuCl_4^-$ ratios), suggesting a steric connection (as yet unproven) with the dynamics of core passivation [72].

The core metal of passivated nanoparticles can also be modified. Alloy nanoparticles with Au/Ag, Au/Cu, Au/Ag/Cu, Au/Pt, Au/Pd, and Au/Ag/Cu/Pd cores [73] have been reported.

It is well known for the case of bare particles that noncrystallographic structures are formed in many cases, these being predominantly icosahedral and decahedral. In other cases, fcc, bcc, or single twinned particles are also produced. Extensive literature is found on shape observations and the kinetic growth conditions in which the different types of particles are produced [74–86].

5. TEM AND SIMULATIONS OF IMAGES OF NANOPARTICLES

5.1. Introduction

Since its inception in the 20th century, electron microscopy has developed into a powerful tool for scientific research. Indeed, the use of electron microscopy has facilitated many fundamental discoveries. This technique has itself been subject to constant evolution thanks to unceasing design efforts in the scientific and manufacturing transmission electron microscopy (TEM) community. The advances in this field have been characterized by a series of quantum leaps in technology. For instance, the double condenser lens and tilting stages revolutionized the study of defects in metals in the late 1950s and early 1960s. The high lattice resolution achieved in the 1970s, along with improvements in vacuum methods and lens control, produced a less complicated instrument, capable of achieving rapid results with minimal training. Consequently, the TEM gained enormous popularity in the materials community. In the second half of the 1980s, a new quantum leap was realized by the achievement of atomic resolution on a routine basis. Microscopes with a point resolution of 0.17 nm coupled with spectacular advances in diffraction theory led to many fine examples of materials characterization. In the 1990s, another quantum leap occurred with the introduction of highly coherent field emission electron sources and electron loss analyzers. Combined with X-ray analysis, this established the TEM as a powerful analytical machine. For the first time, images, diffraction, and spectroscopy could be obtained from a single instrument. The TEM has become a standard instrument for many scientific fields. During the second half of the 1990s, the substantial increase in the number of papers published in *Physical Review Letters* containing electron microscopy studies attests to this fact. Other important developments include the introduction of electron holography and dark field images produced using incoherently scattered electrons (*Z* contrast).

The next quantum leap in electron microscopy will be produced by the introduction of aberration correctors for the objective lens and STEM lens-forming system, and by the development of monochromators for the incident beam. These techniques will undoubtedly usher in a new era for TEM. Improved point resolution of 0.007 nm, an increased information limit, enhanced energy resolution, and improved stages using MEMS technology will allow 3-D reconstruction of amorphous materials such as glasses. Refined X-ray techniques will facilitate chemical analysis essentially at the single atom level. Still more exciting, Cs-corrected microscopes will allow more space in the objective lens gap, thus making it possible to construct stages for the *in situ* examination of materials at atomic resolution and analysis with atomic accuracy [87]. The most recent developments in TEM coincide with the emergence of nanotechnology [88], and because the TEM probe size is ideal for nanoscale studies, it is clear that advanced TEM will be a major instrument in subsequent nanotechnological developments. The TEM will also be fundamental in areas of rapid development such as advanced materials research, biotechnology, and microelectronics. The automation of modern TEM has led to applications in semiconductor fabrication processes, and energy filtering will permit the study of polymers and biological materials with unprecedented accuracy.

Transmission electron microscopy is one of the most important techniques to study nanoparticles. The resolution of the TEM is well below the size of most of the particles and in the order of magnitude of the metal–metal bonds. There are several papers which have explained in a very detailed way the electron microscopy methods to study nanoparticles. We will not discuss in this chapter dynamical diffraction methods, but we rather refer the reader to those publications [89–92].

Images were obtained using a JEOL 2010-FEG microscope, with a resolution of 0.19 nm and a tilting possibility of ±30°, and a JEOL 4000EX with a resolution of 0.17 nm. HREM images of nanoparticles were obtained at the first optimum defocus (Scherzer focus) or at the second optimum defocus condition, resulting in images of atomic columns as black (first maximum) or white (second maximum) dots. Molecular Dynamics software was used to build theoretical models of the particles. Simulated images were obtained using the Simula TEM software of the Institute of Physics at UNAM, which is especially adequate for studying nanoparticles with noncrystallographic symmetries. A comparison of experimental and simulated data will allow us to interpret the experimental images.

In general, in order to recognize a nanoparticle in a nonambiguous fashion, it is necessary to obtain a tilting sequence of HREM. Figure 59 illustrates the changes in contrast when the orientation of the particle is changed with respect to the electron beam. This case corresponds to a cubooctahedral particle. This image illustrates a remarkable difference between nanoparticles and large crystals. In the latter case, the image will be very sensitive to tilting, and will disappear with small tilts. The nanoparticle, on the other hand, always shows images despite the large angle of tilting. In many cases, the images correspond to pseudolattice images. Considerable caution should be taken when analyzing fringe images of nanoparticles. The images out of a low-index direction do not necessarily reflect a structural feature.
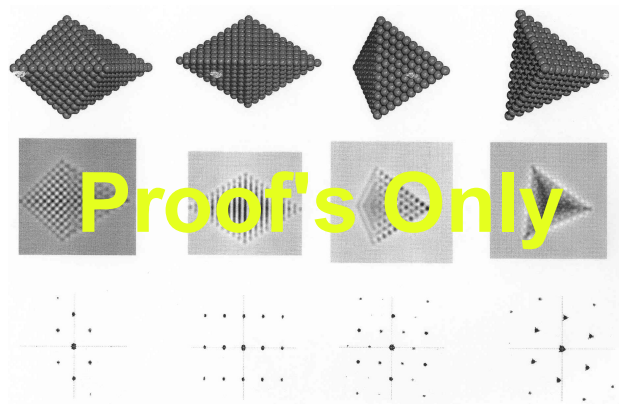

Figure 59. Models of an fcc pyramid formed by two tetrahedra. Observe their contrast in the second row and their diffraction pattern in the third row.

In diffraction terms, the finite size of the nanoparticles in real space results in rel rods in reciprocal space. The Ewald sphere will always cut the reciprocal space points despite the angle.

5.2. fcc Particles

The fcc particles are straightforward to identify. Figure 60 illustrates the contrast produced by an fcc by a pyramid formed by two tetrahedrons and their diffraction pattern (which in most instances is identical to the FFT of the image). Experimental examples of a pyramidal and of a tetrahedral particle are shown in Figure 61.

5.3. Decahedral Particles

Very important cases to consider are the images produced by pentagonal particles, such as the one shown in Figure 62.

Typical TEM images of pentagonal particles are shown in Figure 63. The fivefold symmetry of the FFT can be observed. However, these patterns are a combination of the diffraction patterns of different portions of the particle, as shown in Figure 64. This indicates that the overall structure of the particle has a fivefold symmetry, but this is not the result of fivefold symmetry in each portion of the particle. Because of that, it is more correct to consider that the particle has a pseudofivefold symmetry. This is in sharp contrast with the case of quasicrystals [93].

It should be remembered that another important effect in the images observed in a TEM is due to the defocus condition which can change the image significantly. Figure 65 illustrates this effect for the case of a regular decahedron. In this case, the calculations were made for a JEOL 4000 microscope. As is known from image theories [94], there

Figure 61. Bright field image of a pentagonal gold particle.

are two defocus conditions in which the image represents the true atomic columns which correspond on the figure to −40.5 nm (black atoms) and −70.2 nm (white atoms). If another defocus is used, the image does not necessarily reflect the atomic positions, but useful information still can be obtained. For instance, a defocus of −35.5 increases the grain boundary contrast, and the nature of the interfaces can be examined. At an even lower defocus of −20.5 nm, the pentagonal particle structure is reflected on the image. An experimental example of a pentagonal particle showing well-defined atomic resolution is shown in Figure 66. In this case, some of the twin boundaries are incoherent. An example of the structure formed at a defocus condition below the optimum value is shown in Figure 67.

A commonly observed type of pentagonal particle corresponding to a rounded shape and the respective model of the particle are shown in Figure 68(a) and (b), respectively. A complete set of images at different tilting angles is shown in Figure 69. Obtaining different images at different tilting angles and referring to this sequence should be enough data to fully identify the structure of that particle.

Figure 60. Bright field images of: (a) pyramidal particle, (b) tetragonal particle, (c) FFT of (b), (d) diffraction pattern of (b).
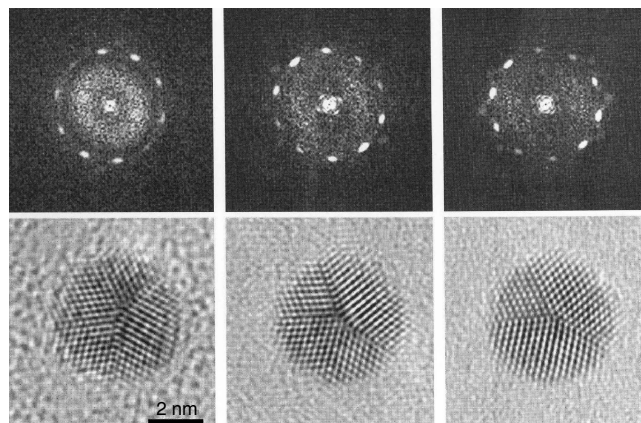
Figure 62. High-resolution images showing atomic contrast of ∼2 nm pentagonal gold nanoparticles and their corresponding FFT showing the fivefold symmetry.
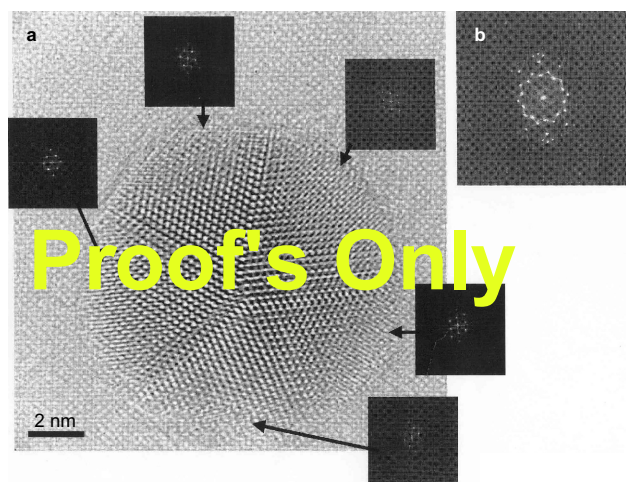
Figure 63. (a) Pentagonal particle showing the FFT of different sections. (b) Overall FFT.

In the previous sections, we described a new type of pentagonal structure that was described originally by Montejano [95] and was termed a decmon type of particle. This type of structure belongs to a more general family of decahedral nanoparticles, which includes the truncated decahedron (Marks) [96], the pancake structure of Koga and Sugarawa [97], and the truncated icosahedron of Ascencio et al. [98].

A tilting sequence for three different decmon structures is shown in Figures 70–72. We also include the calculation a 64-order pentadecahedron in Figure 73. An experimental example of this type of particle is shown in Figure 74. This image corresponds to a dark field taken in a weak beam condition. In this case, a continuous set of thickness fringes is expected. However, because of the decmon shape, a pentagonal profile is formed at the center of the particle.

Another experimental example is shown in Figure 75(a). The particle marked by an arrow can be identified using a model with surface reconstruction, as shown in Figure 75(b).
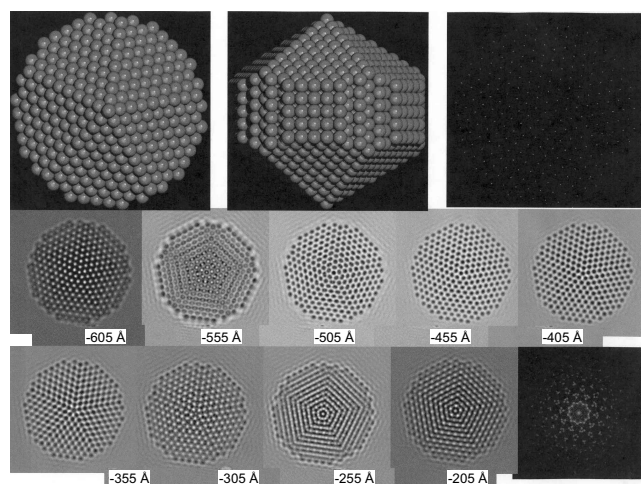
Figure 64. Effect of defocus on TEM images. Calculations made for a truncated decahedron and for a JEOL 4000 microscope.
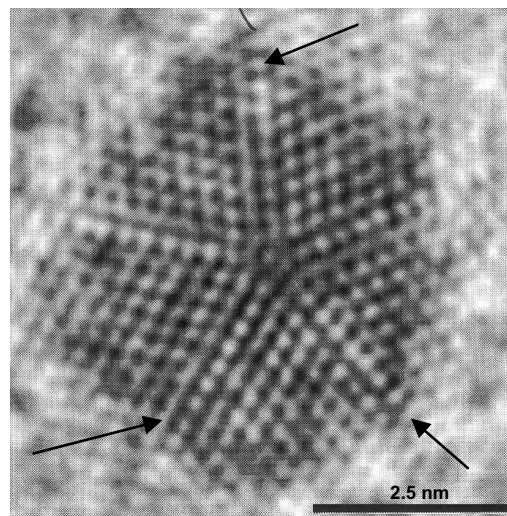
Figure 65. HREM image of a pentagonal particle, showing incoherent twin boundaries indicated by arrows.

We have found that surface reconstruction particles are formed very frequently when the sample approaches the equilibrium condition. For instance, the particle in Figure 75(a) was obtained after heating the sample with an electron beam and allowing recrystallization. In this process, the total surface energy of the nanoparticle will tend to be a minimum. There are several ways to achieve this surface energy minimization. Marks described truncations on the decahedron structure [96] that result in a more stable structure. However, the energy landscape has many structures with similar energy. Another possibility is to introduce faceting along the twin boundaries of the decahedra, resulting in the structure shown in Figure 76(a). If images are formed at the Scherzer condition, the channels can be visualized [Fig. 76(b)], in contrast to the case of the regular decahedron. We have described these particles previously in this chapter.

A full map of images for these channeled structures as a function of the tilting angle for the optimum defocus is shown in Figure 77(a) and (b). This type of decahedron is often observed in larger particles, as shown in Figure 78.
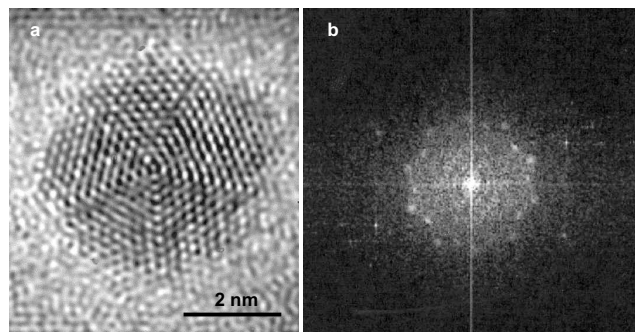
Figure 66. (a) High-resolution image of a pentagonal particle with a defocus below the optimal value. (b) Corresponding FFT indicating the fivefold symmetry.
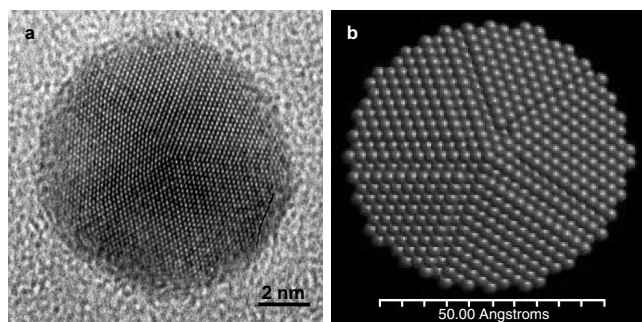
Figure 67. Pentagonal particle with rounded shape. (a) HREM image. (b) Model of particle.
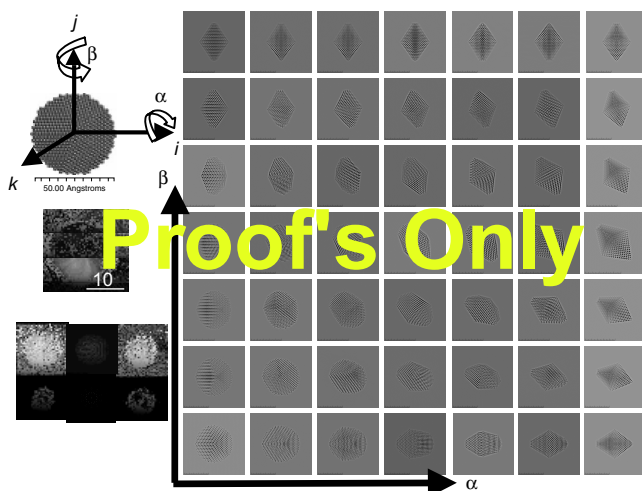
Figure 68. Images of a pentagonal particle obtained as a function of the tilting angles α and β. The origin of the coordinate system indicates a 0, 0 position, and the range of the angles is 90°. The model and typical bright field and HREM image (including FFT) are shown in the left portion of the figure.
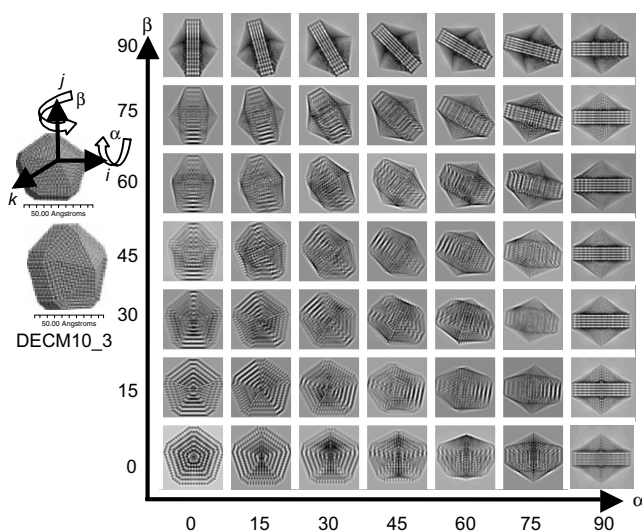
Figure 69. HREM images calculated for a decmon 10 structure shown in the left portion of the figure. The rotation angles α and β go from 0 to 90°.
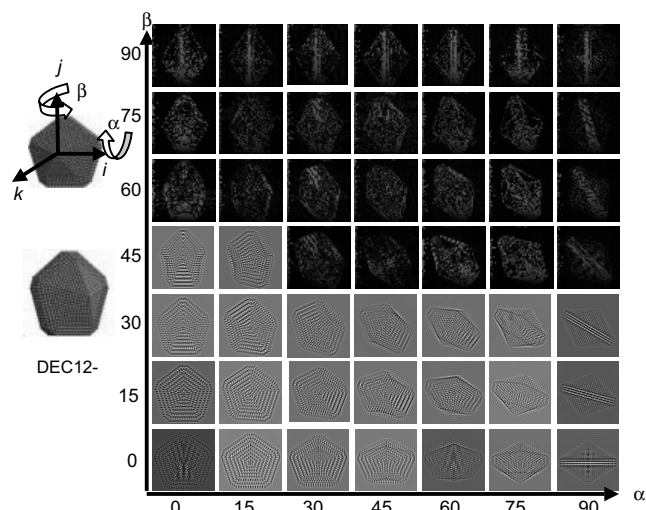
Figure 70. HREM images calculated for a decmon 12 structure shown in the left portion of the figure. The rotation angles α and β go from 0 to 90°.

Another very interesting possibility has been suggested by molecular dynamic simulations of Chushak and Bartell [99] and other group [100]. This work indicates that, in the twin boundaries, a stacking fault is formed. In other words, the *ABC* stacking will be converted to *ABAB* stacking in the boundary region.

A different situation corresponds to the structure reported in Figure 46. In this case, the stacking is altered only in the last layer of the packing. This is illustrated in Figure 79 in which a regular stacking in a unit of the decahedra is altered in the surface. In other words, the *ABCA* sequence becomes *ABCB*. In Figure 79, each layer is illustrated in a different color. The yellow atoms correspond to the surface sites. We have found experimentally that this type of decahedron is very stable, especially at small sizes.
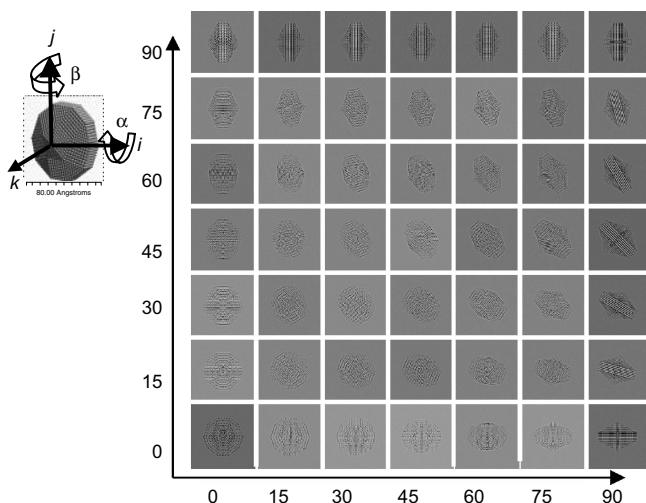
Figure 71. HREM images calculated for a decmon structure with less degree of truncation, as the model shown in the left portion of the figure. The rotation angles α and β go from 0 to 90°.
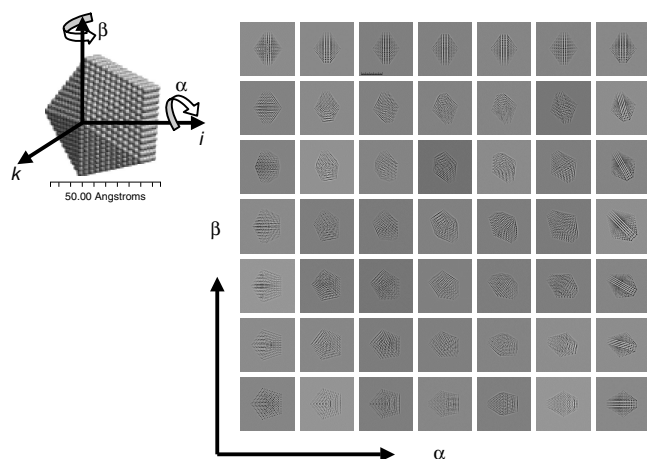
Figure 72. HREM images calculated for a pentadecahedral structure as the model shown in the left portion of the figure. The rotation angles α and β go from 0 to 90°.
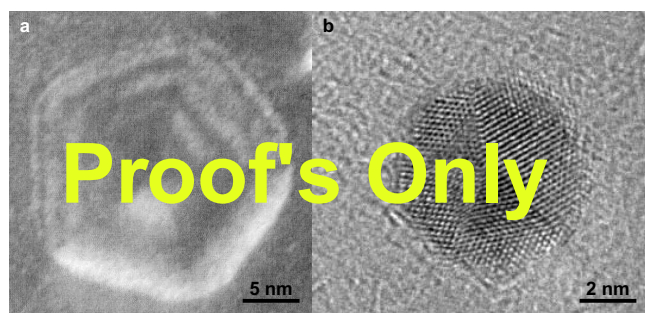
Figure 73. (a) A weak multibeam dark field image of a decmon type of decahedron obtained in a gold particle synthesized by bioreduction. (b) An HREM image of a decmon-type particle.
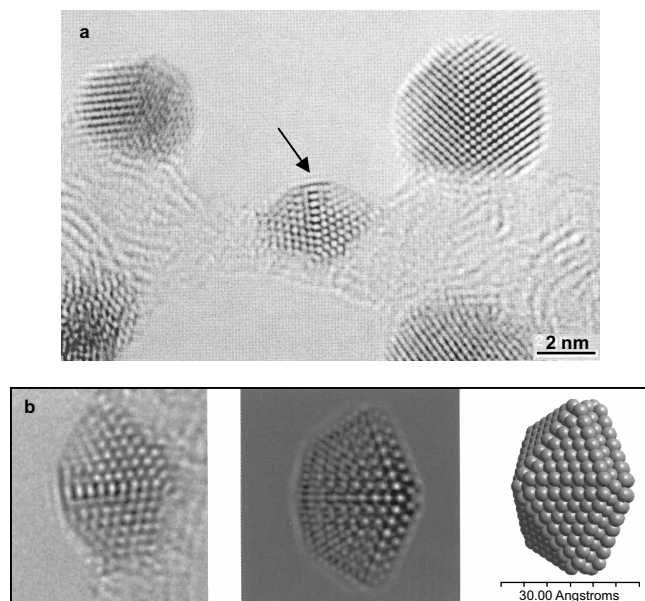
Figure 74. Analysis of a decmon-type particle supported on a thin portion of a carbon film (indicated by an arrow). (a) TEM Image. (b) Identification of particle using a model with surface reconstruction.
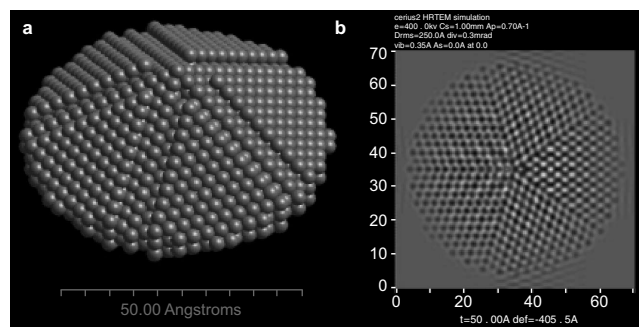
Figure 75. (a) Model of decahedron showing faceting along the twin boundaries. (b) Simulated TEM image of a decahedron in Scherzer condition, where the channels can be observed.
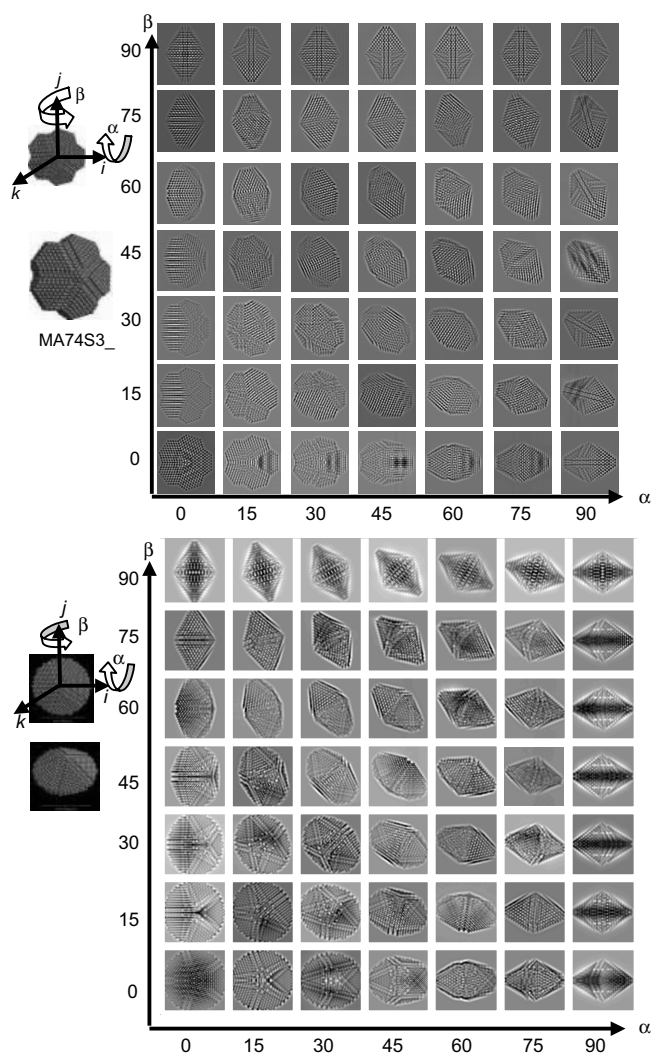
Figure 76. (a) Map of images for the truncated decahedron as function of the tilting angle for the optimum defocus. (b) Map of images for the decahedron in Figure 75(a) as function of the tilting angle for the optimum defocus.
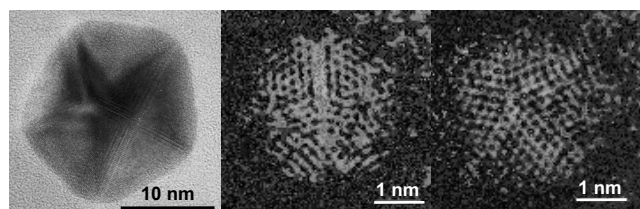
Figure 77. (a) Bright field image of a large particle produced by biore-duction showing a typical contrast of channels in the twin boundaries in the interface. (b) and (c) show the high-resolution image of deca-hedral shape in which the contrast at the boundaries does not change with defocus, and can be explained by the model of interface channels discussed in the theoretical section.

The contrast of this particle is very peculiar, and is shown in Figure 80 for a different defocus. In this case, the boundaries show a very strong contrast at all defo-cus conditions. This provides a practical way to distinguish this particle from other types of decahedra which, under some focus conditions, can produce boundary contrast, as shown before. The contrast of the boundaries will be very strong, as shown in Figure 80. This type of particle is often observed experimentally in nanoparticles with sizes ~1.5 nm, as shown in Figure 81(a), or when two metals are present. Figure 81(b) and (c) show the HREM image of a particle of Au–Pd at 50%–50% in which, in many places, it is possible to observe the surface atom vacancy. In general, it can be said that the central atom vacancy is a unique feature of this type of particle.
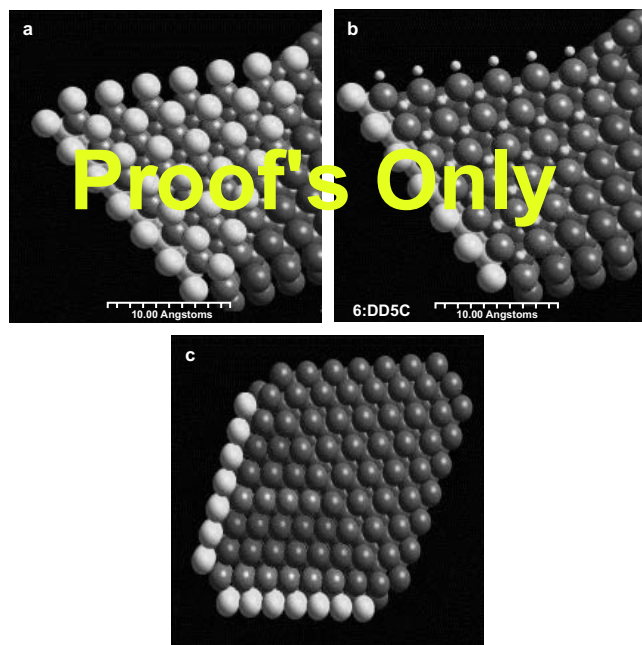
Figure 78. (a) Packing of atoms in a decahedron showing a stacking fault in the last atomic layer. Different colors correspond to differ-ent layers of the packing sequence, and the *ABCA* sequence becomes *ABCB*. (b) Another view of the same packing, in which the surface atoms are drawn in a smaller size. (c) Side view of the resulting stricture in which a missing atom in the center can be observed.
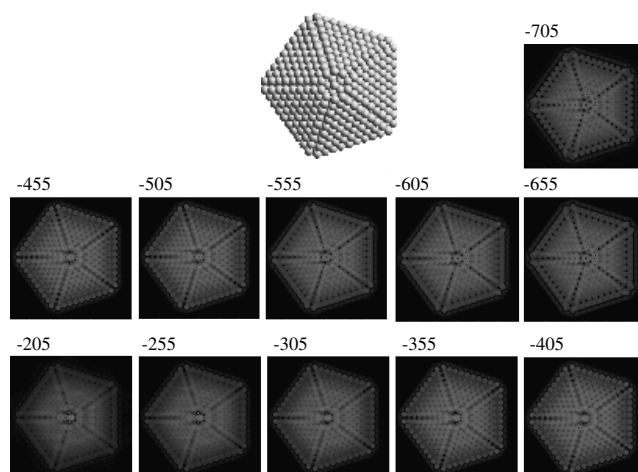
Figure 79. Sequence of simulated images of a decahedron particle with a missing atom in the center (fivefold site) as the result of surface reconstruction. The image is calculated at a different defocus.

Finally, in some cases, an irregular or asymmetric deca-hedral shape is produced. This was described by Uppenbrik and Wales [101], and most likely is the result of the kinetics of growth; a typical example is shown in Figure 82. When the particles grow larger, some special shapes are seen, as indicated in Figure 83.

5.4. Icosahedral Particles

One of the most frequently observed particles at small sizes corresponds to the icosahedral structure. A typical TEM image of these particles is shown in Figure 84. The profile is typically hexagonal in the threefold orientation.

The most common images are in the two- and threefold orientation. The calculations of these images are shown in Figure 85, and are consistent with previous calculations [102]. Experimental images of a gold icosahedral particle in a threefold orientation and a twofold orientation are pre-sented in Figure 86(a), (b) and (c), (d) including the FFT, which indicates the symmetry. A less commonly observed orientation is the fivefold. This is probably due to the fact that, under flat surfaces, particles will be tilted until one tri-angular face (111) becomes in contact with the substrate. This results in most cases in a twofold orientation.

However, when the particles are around 1–2 nm, it is pos-sible to observe the fivefold orientation more frequently.
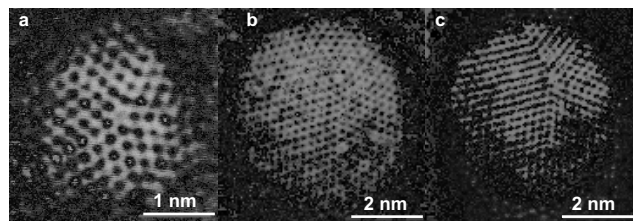

Figure 80. Decahedral particles, in which a defect was formed in the last layer of atoms. Notice that the particle in (a) does not have a central atom in the fivefold site. The particles in (b) and (c) correspond to an Au–Pd system, and atom vacancies in several sites are observed.
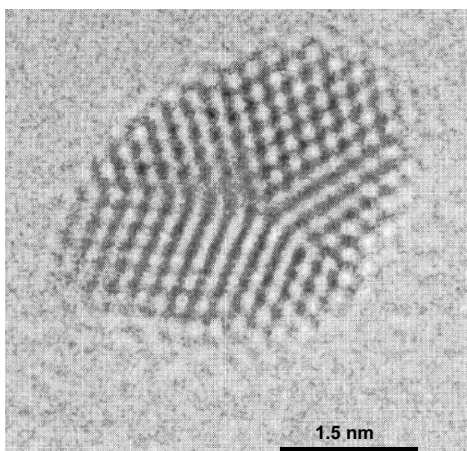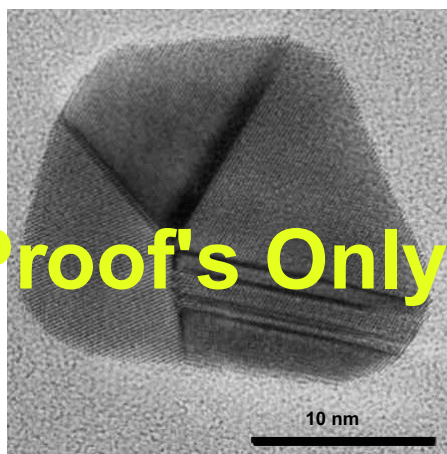
Figure 81. Distorted decahedral particle.

Figure 82. Large irregular decahedral particle grown from a distorted decahedral particle.
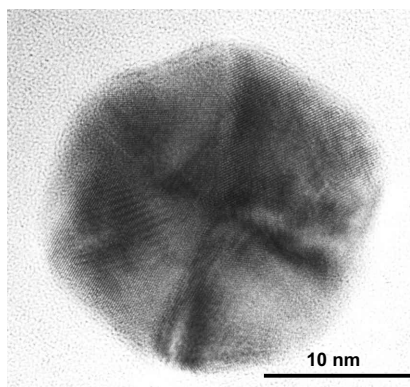

Figure 83. Bright field of an icosahedral gold particle showing a typical hexagonal profile.
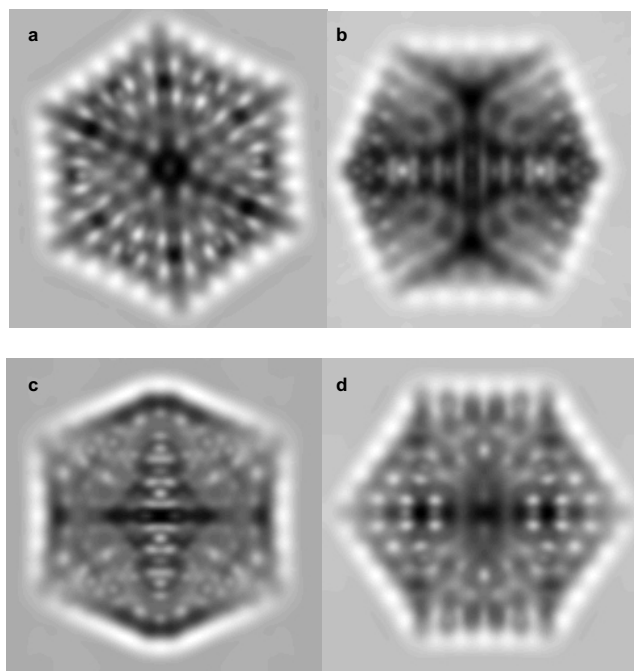

Figure 84. Calculated images of HREM icosahedral particles at (a) threefold orientation, and (b)–(d) different twofold orientations.
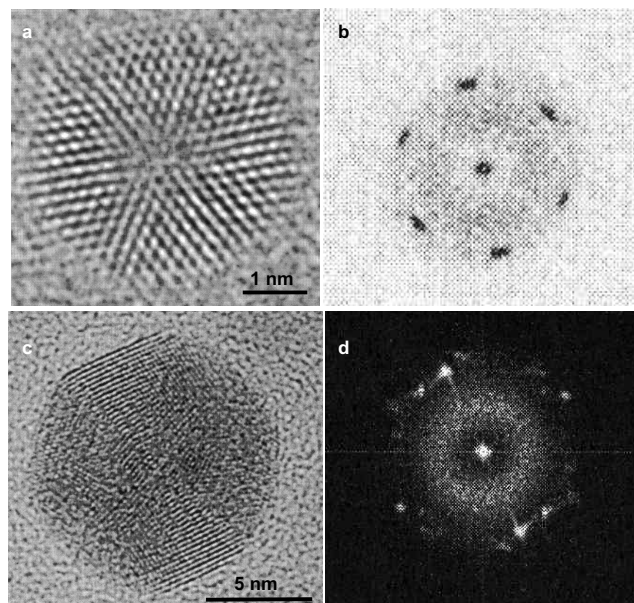

Figure 85. Experimental images of icosahedral particles and their corresponding FFT. (a), (b) Threefold orientation. (c), (d) Twofold orientation.

Figure 88. (a) Model for a double icosahedron obtained by molecular dynamics. (b) Simulated image. As can be seen, one part of the structure is a fivefold orientation, and the other one is at fivefold orientation.
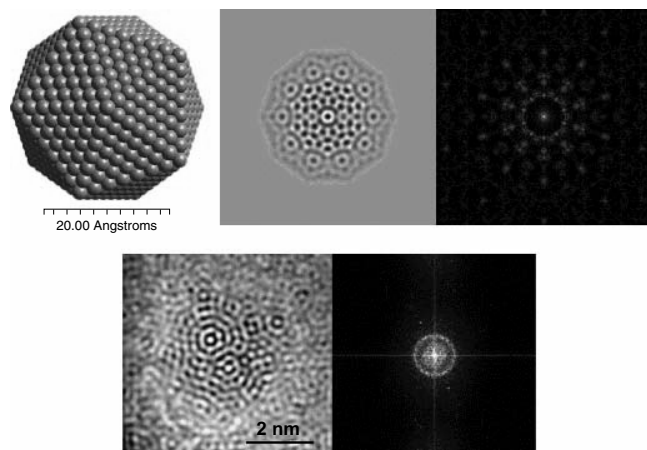
Figure 86. Model and image simulations of an icosahedral particle in fivefold symmetry (upper portion) and experimental images for a gold particle in the lower part. In both cases, we include the FFT.

This is probably due to truncations on the surface in contact with the substrate. An example of this contrast and an experimental example are shown in Figure 87.

When a bimetallic particle is synthesized, the frequency of the icosahedral particle increases, particularly at the smallest sizes [103].

corresponds to a minimum in the total energy, and has been observed experimentally by Hofmeister's group [104].

5.6. Surface Faceting in Nanoparticles

In many cases, the particles can present a surface faceting, especially when they are annealed or heated *in situ*. This faceting is relevant since it can be related to the catalytic activity of the particles; an example is shown in Figure 90. The presence of steps will increase the particle curvature, yielding an almost spherical particle. We have observed that faceting results in (110) and (112) faces.

5.5. Single Twinned and Complex Particles

Twinning is a very general phenomenon which might happen in the very early stages of growth, and does not necessarily result in a decahedral or icosahedral particle. In many cases, we can observe a pyramidal particle with a single twin. This particle is shown in Figure 88.

We have observed particles down to 1.5 nm in size which present single twins. Therefore, is it safe to assume that, in some cases, twinning proceeds in the very early stages of growth. However, when the particles grow to larger sizes, coalescence can occur, leading to a more complex type of particles. We have found by molecular dynamics that a double icosahedral structure can be produced very often. In this structure, we have two interpenetrating icosahedra to form a double icosahedron, as shown in Figure 89. This structure
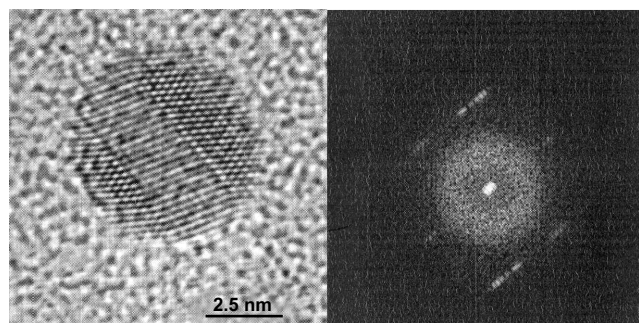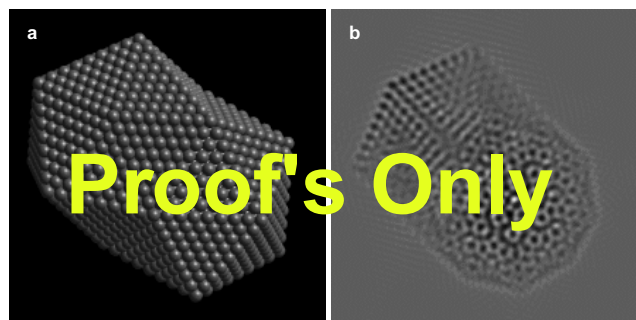
6. CONCLUSIONS

We have made a systematic description of the most significant geometries which are formed in nanoparticles. We have calculated the number of different atomic sites and growth characteristics of the nanoparticles. It has been shown that the models correspond closely with the experimental HREM and diffraction data.

New types of particles have been described in this work, which correspond to a new family of decahedral structures.

We expect that, as the field advances and new synthesis routes for particles ~1 nm are developed, all of the predicted clusters will be observed.

This work also illustrates the richness of the crystallography of nanoparticles and clusters. Unlike the bulk materials, fivefold symmetry in nanoparticles produces a very rich landscape of structures.
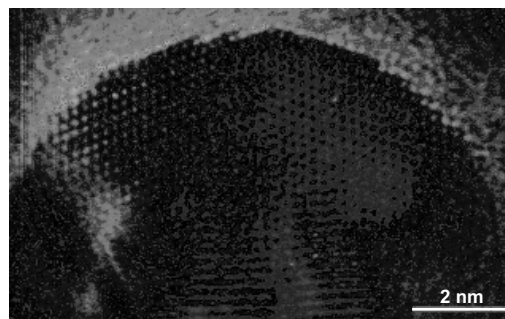

Figure 87. HREM image of a single twin particle and its corresponding FFT.

Figure 89. HREM image of a gold particle showing surface faceting.

GLOSSARY

ACKNOWLEDGMENTS

REFERENCES

1. M. Gross, "The Nanoworld, Miniature Machinery in Nature and Technology," p. 254. Plenum Trade, New York and London, 1999.
2. H. S. Nalwa, "Handbook of Nanostructured Materials and Nanotechnology," pp. 1–4. Academic, San Diego, 2000.
3. S. Sugano and H. Koizumi, "Microcluster Physics." Springer-Verlag, 1998.
4. S. a. P. Das-Sarma, "Perspectives in Quantum Hall Effects," p. 430. Wiley, New York, 1997.
5. H. L. Stormer, *Solid State Commun.* 107, 617 (1998).
6. H. Grabert, "Single Charge Tunneling," p. 335. Plenum, New York, 1992.
7. M. H. Dvoret, D. Esteve, and C. Urbina, *Nature* 547 (1992).
8. R. C. Ashoori, *Nature* 413 (1996).
9. A. P. Alivisatos, *Science* 933 (1996).
10. A. Rosen, Nanostructured Materials Made from Self-Assembled Particles, Chalmers University of Sweden, 2000.
11. H. Haberland, "Clusters of Atoms and Molecules I and II: Solvation and Chemistry of Free clusters, Embedded, Supported and Compressed Cluster," p. 412. Springer-Verlag, Berlin, New York, 1994.
12. W. A. de Heer, *Rev. Mod. Phys.* 65, 611 (1993).
13. M. Brust, M. Walker, D. Bethel, D. Schiffrin, and R. Whyman, *J. Chem. Soc.* 801 (1994).
14. A. C. Templeton, M. J. Hostetler, E. K. Warmoth, S. Chen, C. M. Hartshorn, V. M. Krishnamurty, M. D. E. Forbes, and R. W. Murray, *J. Am. Chem. Soc.* 120, 4845 (1998).
15. R. Whetten, T. Khoury, M. Alvarez, S. Murthy, I. Vezmar, Z. L. Wang, P. W. Stephens, C. L. Cleveland, W. D. Luedtke, and U. Landman, *Adv. Mater.* 8, 428 (1996).
16. T. G. Schaaff, M. N. Shafigullin, J. T. Khoury, I. Vezmar, R. L. Whetten, W. Cullen, P. N. First, C. Gutierrez-Wing, J. Ascencio, and M. Jose-Yacaman, *J. Phys. Chem. B* 101, 7885 (1997).
17. D. V. Leff, L. Brandt, and J. Heat, *Langmuir* 12, 4723 (1996).
18. S. L. Logunov, T. S. Ahmadi, M. A. El-Sayed, J. T. Khoury, and R. L. Whetten, *J. Phys. Chem.* 101, 3713 (1997).
19. C. J. Kiely, J. Fink, M. Brust, D. Bethell, and D. J. Schiffrin, *Nature* 396, 444 (1998).
20. A. Mews, A. V. Kadavanich, U. Banin, and A. P. Alivisatos, *Phys. Rev. B* 53, 13242 (1996).
21. H. Bonnemann, W. Brijoux, R. Brinkmann, R. Fretzen, T. Joussen, R. Koppler, B. Korall, P. Neiteler, and J. Richter, *J. Molec. Catal.* 86, 129 (1994).
22. Z. L. Wang, *Adv. Mater.* 10, 13 (1998).
23. B. Korgel and D. Fitzmaurice, *Phys. Rev. B* 59, 14191 (1999).
24. H. Bonnemann and R. M. Richards, *Eur. J. Inorg. Chem.* 2455 (2001).
25. S. Ino and S. Ogawa, *J. Phys. Soc. Jpn.* 22, 1365 (1967).
26. S. Ogawa, S. Ino, T. Katar, and H. Ota, *J. Phys. Soc. Jpn.* 21, 1963 (1966).
27. T. P. Martin, *Phys. Rep.* 273, 199 (1996).
28. J. M. Montejano, *J. Cluster Sci.* 5, 287 (1994).
29. J. M. Montejano-Carrizales, M. P. Iñiguez, and J. A. Alonso, *J. Cluster Sci.* 5, 287 (1994).
30. R. Andres, J. Bielefeld, J. Henderson, D. Janes, V. Kolagunta, C. Kubiak, W. Mahoney, and R. Osifchin, *Science* 273, 1690 (1996).
31. D. Janes, V. Kolagunta, R. Osifchin, J. Bielefeld, R. Andres, J. Henderson, and C. Kubiak, *Superlatt. Microstruct.* 18, 275 (1995).
32. R. Osifichin, W. Mahoney, R. Andres, J. Henderson, C. Kubiak, and R. Dominey, *Superlatt. Microstruct.* 18, 283 (1995).
33. J. R. Blackborow and D. Young, "Metal Vapor Synthesis." Springer-Verlag, New York, 1979.
34. S. Roginsky and A. Schalnikoff, *Kolloid Z.* 43, 67 (1927).
35. Bradley in "Clusters and Colloids: From Theory to Applications" (G. Schmid, Ed.). VCH, Weinheim, 1994.
36. K. Kimoto, *J. Phys. Soc. Jpn.* 9, 762 (1953).
37. H. Morimoto, *J. Phys. Soc. Jpn.* 13, 1015 (1958).
38. K. Mihama and Y. Yasuda, *J. Phys. Soc. Jpn.* 21, 1166 (1966).
39. T. Hayashi, T. Ohno, Yatsuya, and R. Uyeda, *Japanese J. Appl. Phys.* 16, 705 (1977).
40. K. Kimoto and I. Nishida, *Japanese J. Appl. Phys.* 6, 1047 (1967).
41. K. Kimoto and I. Nishida, *J. Phys. Soc. Jpn.* 22, 940 (1967).
42. T. Okazaki, *Japanese J. Appl. Phys.* 27, 2037 (1988).
43. N. Wada, *Japanese J. Appl. Phys.* 8, 551 (1969).
44. R. Uyeda, in "Phys.-Math. Society." Japan, 1942.
45. A. Tasaki, S. Tomiyama, S. Iida, and R. Uyeda, *Japanese J. Appl. Phys.* 4, 707 (1965).
46. R. Uyeda, *Progr. Mater. Sci.* 35, 1 (1991).
47. J. Chang and J. Huang, *Biotech. Progr.* 14, 735 (1998).
48. D. W. Darnall, B. Greene, M. T. Henzl, M. J. Hosea, R. A. McPherson, and J. Sneddon, *Environ. Sci. Technol.* 20, 206 (1986).
49. D. W. Darnall, B. Greene, and J. L. Gardea-Torresdey, *BioHydroMetall.* 487 (1988).
50. A. V. Pethkar and K. M. Paknikar, *J. Biotech.* 63, 121 (1998).
51. N. Kuyucak and B. Volesky, *Biorecovery* 1, 189 (1989).
52. N. Kuyucak and B. Volesky, *Precious Metals* 211 (1986).
53. M. J. Hosea, B. Greene, R. A. McPherson, M. T. Henzl, M. D. Alexander, and D. W. Darnall, *Inorgan. Chem. Acta* 161 (1986).
54. J. A. Erdman, B. F. Leonard, and D. M. Mckown, A Case for Plants in Exploration: Gold in Douglas-Fir at the Red Mountain Stockwell, U.S. Department of the Interior Geological Survey, Yellow Pine District, ID, 1985, p. 85.
55. K. C. Jones and P. J. Peterson, *Biogeochem.* 7, 3 (1989).
56. C. W. Anderson, R. R. Brooks, A. Ciarucci, C. J. LaCoste, M. Leblanc, B. H. Brobinson, R. Simcock, and R. B. Stewart, *J. Geochem. Explor.* 67, 407 (1999).
57. A. L. Kovalebskii and O. M. Kovalevskaya, *Appl. Geochem.* 4, 369 (1989).
58. J. R. Lujan, D. W. Darnall, P. C. Stark, G. D. Rayson, and J. L. Gardea-Torresdey, *Solvent Extract. Ion Exchange* 12, 803 (1994).
59. J. L. Gardea-Torresdey, K. J. Tiemann, J. G. Parsons, G. Gamez, and M. Yacaman, *Adv. Environ. Res.* 00, 1 (2001).
60. J. R. Peralta, J. L. Gardea-Torresdeay, K. J. Tiemann, E. Gomez, S. Arteaga, E. Rascon, and J. G. Parsons, *Bull. Environ. Contam. Toxicol.* 66, 727 (2001).
61. J. L. Gardea-Torresdey, J. G. Parsons, E. Gomez, J. Peralta-Videa, H. Troiani, P. Santiago, and M. J. Yacaman, *Nano Lett.* 2, 397 (2002).
62. M. J. Hostetler, J. E. Wingate, C. J. Zhong, J. E. Harris, R. W. Vachet, R. M. Clark, J. D. Londono, S. J. Green, J. J. Stokes, G. D. Wignall, G. L. Glish, M. D. Porter, N. D. Evans, and R. W. Murray, *Langmuir* 14, 17 (1998).

63. L. A. Porter, Jr., D. Ji, S. Westcott, M. Graupe, R. Czernuszewicz, N. Halas, and T. Lee, *Langmuir* 14, 7378 (1998).

64. D. V. Leff, P. C. Ohara, J. R. Heat, and W. M. Gelbart, *J. Phys. Chem.* 99, 7036 (1995).

65. M. Hostetler, S. Green, J. Stokes, and R. Murray, *J. Am. Chem. Soc.* 118, 4212 (1996).

66. M. Alvarez, J. Khoury, T. Schaaff, M. Shafigullin, I. Vezmar, and R. L. Whetten, *Chem. Phys. Lett.* 266, 91 (1997).

67. R. S. Ingram, M. Hostetler, and R. Murray, *J. Am. Chem. Soc.* 119, 9175 (1997).

68. P. Buning, B. Humbel, A. Philipse, and A. Verklej, *Langmuir* 18, 3921 (1997).

69. S. Chen and K. Kimura, *Langmuir* 15, 686 (1999).

70. S. R. Johnson, S. D. Evans, S. Mahon, and A. Ulman, *Langmuir* 13, 51 (1997).

71. M. Brust, D. Bethell, D. Schiffrin, C. Kiely, and L. Novel, *Adv. Mater.* 7, 795 (1995).

72. A. Templeton, M. Hostetler, C. Craft, and R. Murray, *J. Am. Chem. Soc.* 120, 1906 (1998).

73. Srnová-Sloufová, F. G. A. Lednický, and J. Gemperlová, *Langmuir* 16, 9928 (2000).

74. M. J. Yacaman, K. Heinemann, and H. Popa, *Crit. Rev. Sol. Stat. Mater.* 10, 243 (1983).

75. K. Yagi, "High Resolution Electron Microscopy and Associated Techniques," p. 568. Oxford, 1988.

76. K. Yagi, K. Takanayagi, K. Kobayashi, and G. Honjo, *J. Cryst. Growth* 28, 117 (1975).

77. M. Jose-Yacaman, J. A. Ascencio, H. B. Liu, and J. L. Gardea-Torresdey, *J. Vac. Sci. Technol. B* 19, 1091 (2001).

78. Z. L. Wang, "Characterisation of Nanophase Materials." Wiley-VCH, 2000.

79. S. A. Harfenist, Z. L. Wang, R. L. Whetten, I. Vezmar, and M. Alvarez, *Adv. Mater.* 9, 817 (1997).

80. J. Spiller Metois and J. A. Venables, *Philos. Mag.* 46, 1015 (1982).

81. M. Gillet, *Surf. Sci.* 67, 139 (1977).

82. L. D. Marks, "The Structure of Small Silver Particles." Cambridge University Press, 1980.

83. M. J. Yacaman, and J. M. Domínguez, *J. Catal.* 213 (1980).

84. Z. L. A. Wang, T. S., and M. A. El-Sayed, *Surf. Sci.* 380, 302 (1996).

85. M. José-Yacaman, J. A. Ascencio, H. B. Liu, and J. Gardea-Torresday, *J. Vac. Sci. Technol. B* 19, 1091 (2001).

86. S. Giorgio and J. Urban, *Appl. Phys. Lett.* 52, 1467 (1988).

87. See papers in "Nanoscale characterization of materials," *MRS Bull.* 22, ?? (1997).

88. Papers in "Handbook of Nanostructured Materials and Nanotechnology" (H. Singh Nalwa, Ed.), Vols. 1–5. Academic, London, 1999.

89. J. A. Ascencio, C. Gutierrez-Wing, M. E. Espinosa, M. Marin, S. Tehuacanero, C. Zorrilla, and M. Jose-Yacaman, *Surf. Sci.* 396, 349 (1998).

90. E. J. Kirkland, "Advanced Computing in Electron Microscopy." Plenum, New York, 1998.

91. Z. L. Wang, "Elastic and Inelastic Scattering in Electron Diffraction and Imaging." Plenum, New York, 1995.

92. L. D. Marks, *Rep. Prog. Phys.* 57, 603 (1994).

93. "Extended Icosahedral Structures" (M. V. Jaric and D. Gratias, Eds.). Academic, 1987.

94. O. Krivanek, in "High Resolution Electron Microscopy" (P. Busec, J. Cowley, and L. Eyring, Eds.). Oxford University Press, 1988.

95. J. M. Montejano, Institute of Physics, University of San Luis Potosi, internal report and personal communication, 2000.

96. L. D. Marks, *J. Cryst. Growth* 61, 556 (1984).

97. K. Koga and K. Sugawara, *Surf. Sci.* 529, 23 (2003).

98. J. Ascencio, M. Perez, and M. Jose-Yacaman, *Surf. Sci.* 447, 73 (2000).

99. Y. Chushak and L. S. Bartell, *Eur. Phys. J. D* 16, 43 (2001).

100. K. Manninen and M. Manninen, *Eur. Phys. J. D* 20, 243 (2002).

101. J. Uppenbrik and D. J. Wales, *J. Chem. Phys.* 96, 8520 (1992).

102. J. Urban, H. Sack-Kongehl, and K. Weiss, *Z. Phys. D* 28, 247 (1993).

103. D. Lu and K. Tanaka, *Surf. Sci.* 409, 283 (1998).

104. S. A. Nepijko, H. Hofmeister, H. Sack-Kongehl, and R. Schlogl, *J. Cryst. Growth* 312, 129 (2000).